International
Progress Report

IPR-01-14

Äspö Hard Rock Laboratory

Fractographic characterization by quantitative microscopy of the excavation disturbance caused by boring of the experimental full scale deposition holes in the research tunnel at Olkiluoto

Prof. Modesto Montoto
Dr. Angel Rodriguez Rey
Dr. Angel Martínez Nistal
Mr. Ildefonso Díez Sarriá

University of Oviedo

November 1999

Svensk Kärnbränslehantering AB
Swedish Nuclear Fuel
and Waste Management Co
Box 5864
SE-102 40 Stockholm Sweden
Tel 08-459 84 00
+46 8 459 84 00
Fax 08-661 57 19
+46 8 661 57 19

Äspö Hard Rock
Laboratory

Report no.	No.
IPR-01-14	F19K
Author	Date
Montoto, Rodriguez Rey, Martínez Nistal, Díez Sarriá	00-03-31
Checked by	Date
Christer Svemar	
Approved	Date
Christer Svemar	02-01-28

Äspö Hard Rock Laboratory

Fractographic characterization by quantitative microscopy of the excavation disturbance caused by boring of the experimental full scale deposition holes in the research tunnel at Olkiluoto

Prof. Modesto Montoto
Dr. Angel Rodriguez Rey
Dr. Angel Martínez Nistal
Mr. Ildefonso Díez Sarriá

University of Oviedo

November 1999

Keywords: Excavation disturbance, Microfractography, Crack specific surface, Crack orientation, Crack aperture, Quantitative microscopy, Stereology, Digital image analysis, Confocal laser scanning microscopy, Scanning electron microscopy

ABSTRACT

The microfractography developed in the rock-walls of the experimental full scale deposition holes drilled in the Research Tunnel at Olkiluoto (Finland) has been analysed using quantitative microscopy.

The evaluation of the penetration depth of an epoxy based sealant applied to the rock-walls and the fractographical characterisation of the disturbed zone in their mineralogical and textural rock framework were the main goals of this study. The following parameters were evaluated from the external to the internal (less disturbed zone): crack specific surface, crack orientation, crack aperture and crack volume percentage; the different procedures used for their evaluation are explained.

Different microscopical techniques were applied: polarising microscopy, reflected light fluorescence microscopy, confocal laser scanning microscopy and scanning electron microscopy (secondary and backscattered electron detectors); the information contained in the so obtained images has been quantified using stereology and digital image analysis techniques. All the fractographic studies have been carried out on so called "vertical sections" normal to the walls of the drilled holes; for avoiding artefacts the corresponding microscopical sections were prepared using non standard procedures.

The obtained results evidence that the most disturbed zone is surprisingly restricted to the outer 1.5-2 mm and less generalised fissured zones can be observed up to a depth of about 3-4 mm. The penetration depth of the epoxy based sealant reaches a maximum depth of 2-3 mm. The wider cracks (> 5.5 μm) of the new developed microfractographic network are mainly parallel to the outer surface and represents less than the 10 % of the total crack population; the most abundant, those narrower than 5.5 μm, show less regular orientations. The crack specific surface, Sv, ranges between 0.06 m^{-1} in the outer zone to about 0.02 m^{-1} at 2-3 mm; at "greater depths", 5-6 mm, Sv falls very fast and keeps at relatively low values (between 0.005 and 0.01 m^{-1}).

SAMMANFATTNING

Mikrosprickbildningen i de fullskaliga deponeringshålens väggar i forskningstunneln i Olkiluoto, Finland, har analyserats med hjälp av kvantitativ mikroskopi.

Undersökningens huvudsyften var utvärdering av inträngningsdjupet hos en epoxybaserad tätningssubstans som anbringats på bergväggarna samt grafisk sprickkarakterisering av den störda zonen med avseende på mineralogi och textur. Följande parametrar bestämdes från den yttre till den inre (minst påverkade) delen av störda zonen: specifika sprickarean, sprickorienteringen, sprickvidden och procentuella sprickvolymen; de olika förfarandena som användes för utvärdering förklaras i rapporten.

Olika mikroskopimetoder användes: polarisationsmikroskopi, fluorescensmikroskopi med reflekterat ljus, konfokal laserscanningsmikroskopi och scanningmikroskopi (med elektrondetektorer av sekundär och backscattertyp). Bildinformationen har kvantifierats med hjälp av stereoteknik och digital bildanalys. Alla sprickstudier har gjorts på s.k. "vertikala sektioner" vinkelrätt mot borrhålsväggarna. För undvikande av artefakter har motsvarande snitt för mikroskopi framställts med icke konventionell teknik.

De erhållna resultaten gav det överraskande beskedet att djupet hos den mest störda zonen begränsas till 1.5 till 2 mm medan viss, men mindre, störning konstaterades till 3-4 mm djup. Epoxysubstansens inträngningsdjup var 2-3 mm. De nybildade sprickorna med störst vidd (>5.5 mikrometer) befanns i huvudsak vara orienterade parallellt med hålväggen och representera mindre än 10 % av hela sprickmängden. Den specifika sprickarean, Sv, var mellan 0.06 m^{-1} i störzonen till 2-3 mm djup och 0.02 m^{-1} på djupet 5-6 mm. Sv minskade snabbt
med ytterligare ökande avstånd från hålväggen och varierade här mellan 0.005 och 0.01 m^{-1}.

CONTENTS

1 INTRODUCTION

1.1 Objective

The objective of this study is the analysis of micro fracturing developed in five rock samples numbered D5, D11.1, D12, D13 and D15 provided by Consulting Engineers Saanio & Riekkola (Finland) from the rock-walls of the experimental full scale deposition holes drilled in the Research Tunnel at Olkiluoto (Finland). The specimens D5, D12, D13 and D15 were previously impregnated with a green epoxy based sealant.

The main goals are focused on:

a) Evaluation of the penetration depth of the epoxy based sealant.
b) Characterisation of the micro fracturing in the disturbed zone.

1.2 Instrumentation

a) Sample preparation

1) Flat slabs and thin sections

- Grinding machines: Logitech LP-30 (2), Discoplan TS
- Ultrasoniccleaner
- Heating plates: Selecta S-157 (2), Thermoline 1900
- Vacuum pumps: Edwards ED-50, Speedvac, Telstar S4/30.

2) Rock surface polishing

- Polishing machines: Planopol V with an automatic driven arm "PDM Force", Struers DP-7, DP-9 and DP-10
- Ultrasonic cleaners: Selecta Ultrasons, Bransonic 12
- Oven
- Vacuum pumps.

b) Microscopes

1) Scanning Electron Microscopes: SEM-Philips XL30 (with secondary and back scattered electrons detectors), Jeol 6100 (with secondary and back scattered electrons detectors; EDAX) combined with a Microanalysis Link EXL-1000 with detector PENTAFET.

2) Confocal Laser Scanning Microscope: Bio-Rad MRC-600 Laser Scanning Confocal Imaging System (Bio-Rad Laboratories) equipped with: a Kripton-Argon laser source (488, 568 and 647 nm) and attached to an Olympus inverted microscope IMT-2. The standard Bio-Rad COMOS software was used to record the image in a PC with an Intel 486/DX2 (66 MHz) processor, 16 Mb RAM memory, 768x512x16 bits

frame store, 110 Mb hard disk and 128 Mb optical disk drive. The Confocal Assistant 4.02 software (by Todd Clark) was used to convert the "pic" Bio-Rad image file format to the standard "tiff" format.

c) Image analysis

Performed in a Leica Q500MCP (Leica Cambridge Ltd.) with an Intel Pentium (200 MHz) processor, 32 Mb RAM, 1,2 Gb hard disk, frame grabber 720x512x24 bits and a 4 Mb Matrox Millennium graphic card, using the Leica Qwin-Pro 2.2 software package. With this software a new image analysis routine has been developed to quantify the used crack parameters.

d) Stereology

For the estimation of crack specific surface (Sv) by stereology, a grid with points and cycloid lines has been used.

1.3 Methodology

1.3.1 Introduction

The methodology applied for this microfractographic analysis combine techniques for the observation and quantification of the new formed cracks in their mineralogical and textural rock framework.

According to the main goals and the peculiarities of the provided samples, the most efficient procedures were specifically designed. Basically, the following aspect were taken into consideration: a) the problems implied with sample preparation and artifacts, b) the microscopical techniques to be used and c) the stereological and digital image analysis techniques.

Therefore, the general procedure applied to this study is based on: a) use of the most appropriate microscopy for a fast and easy mineralogical and fractographical identification, b) adequate magnification for an easy observation and measurement of cracks wider than 1 μm, c) number and size of images to sample in each thin section, d) appropriate stereological grids and e) implementation of specific software for image processing.

The rock-forming components and the epoxy based sealant have been imaged under different microscopical techniques: polarising microscopy, reflected light fluorescence microscopy, confocal laser scanning microscopy and scanning electron microscopy (secondary electron and backscattered electron detectors) (Figure 1). The information contained in the so obtained images has been quantified, according to our experience in similar applied studies, using stereology and digital image analysis techniques. More details on these aspects of quantitative microscopy in fissured crystalline rocks can be found in Menéndez (1992) and Martinez-Nistal (1993).

"Profiles" of images from the drilled hole border to the internal (less disturbed) zone were obtained; for quantitative microscopy purposes the image coordinates in those profiles were referred to columns and rows (Figure 2). The wall of the hole border is always contained in the image corresponding to the first row of each column.

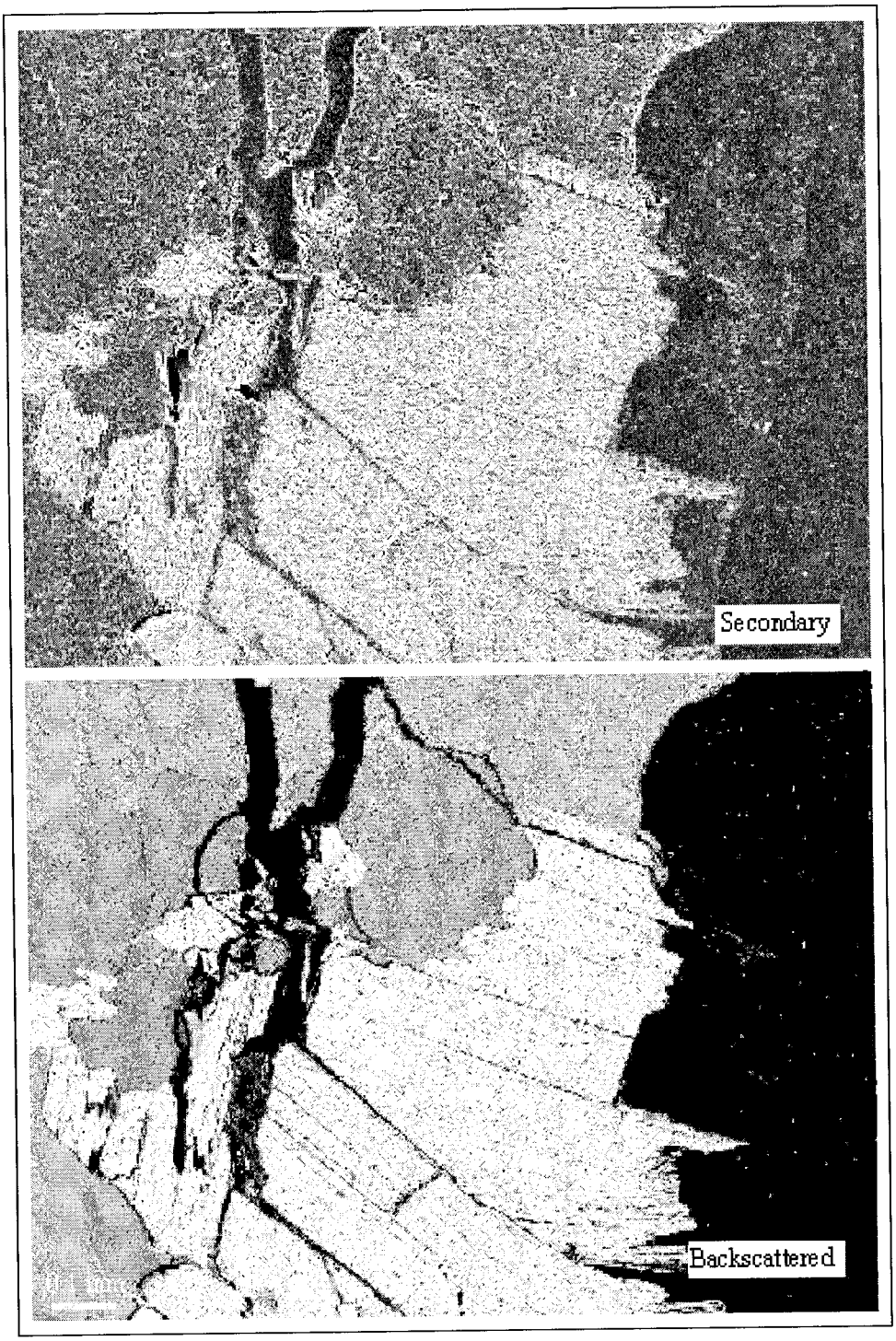

Figure 1. *For an easier identification of the rock-forming components, scanning electron microscopy (secondary electron and backscattered electron detectors) is used.*

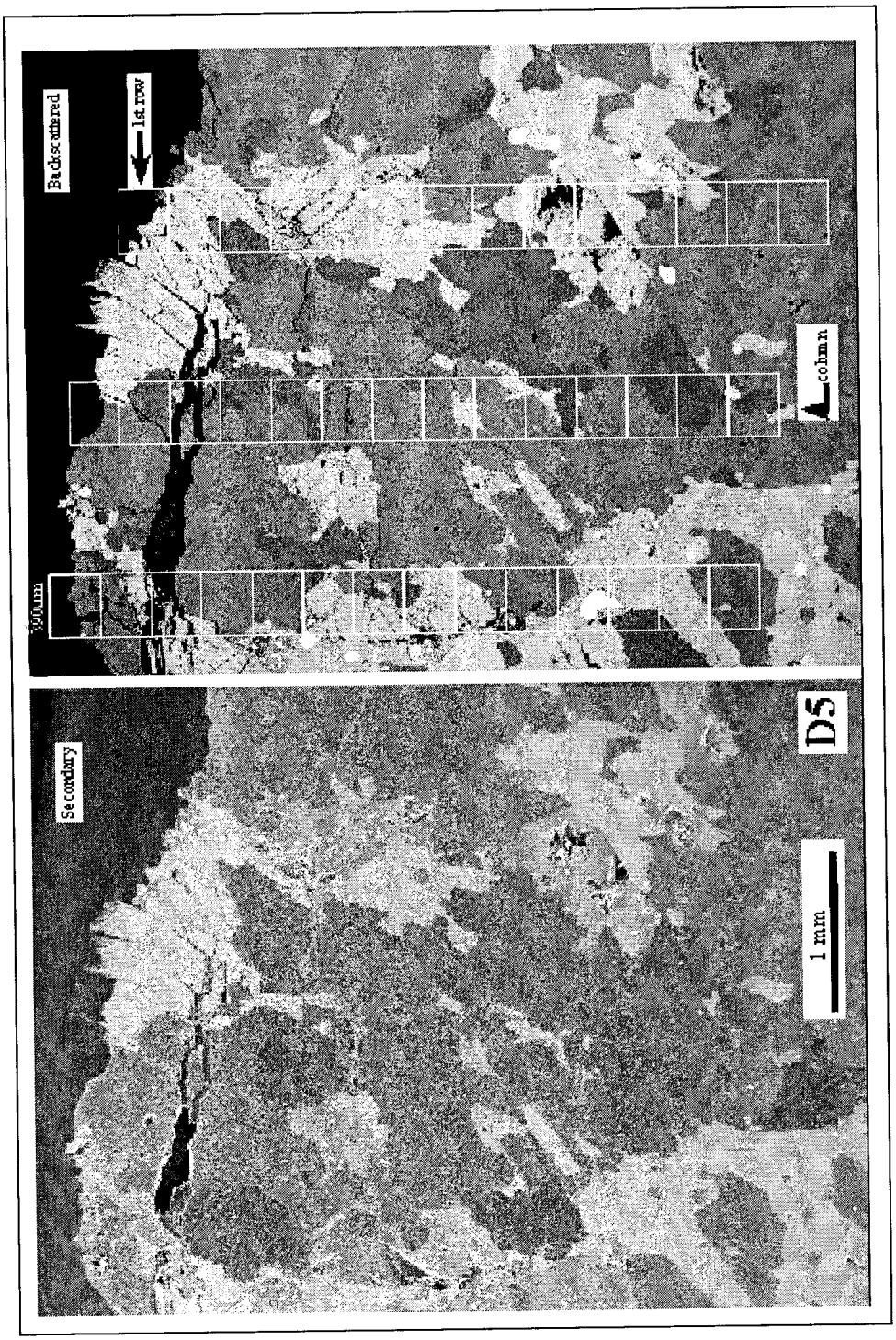

***Figure 2**. For a systematic quantification, profiles of contiguous zones perpendicular to the outer perturbed zone are imaged under different microscopes.*

1.3.2 Fractographic parameters

The following parameters: crack specific surface, crack orientation, crack aperture and crack volume percentage were used for documenting the fractographic nature of the disturbed zone, from the external to the internal (less disturbed) zone.

Crack specific surface (Sv). Area of the microcrack surfaces by volume unit of the rock; it is expressed in $\mu m^2/\mu m^3$ $[L^{-1}]$.
The crack specific surface was evaluated according to its textural position (inter, intra, etc.) in relation to two mineral clusters: a) felsic (quartz and feldspar) and b) mafic (hornblende and biotite). It was measured estimating the Sv of microcracks both intergranular and intragranular (affecting clusters of mafic and felsic minerals).

Crack orientation. With respect to the rock wall surface.

Crack aperture. Expressed in terms of mean crack aperture and crack aperture distribution.

Crack volume percentage. The percentage of area occupied by cracks is an estimator of the crack volume percentage.

1.3.3 Microscopy

1.3.3.1 Sample preparation

All the fractographic studies have been carried out on so called "vertical sections" normal to the walls of the drilled holes (in this case) and isotropic in direction in this wall surface. In these sections, Sv can be estimated without requiring any assumptions about the orientation or other characteristics of the surface under study.

Sketches of each one of the five provided specimens follow (Figures 3, 4, 5 and 6). The position of the red mark, surfaces for rock cutting and schistosity are shown. The names, position and characteristics of each studied rock section are also included.

The references for the characteristics of preparation for each rock slab follow:

*Thin section	**T**	*Rhodamine	**R**
*Slab	**S**	*Vacuum	**V**
*Isomet	**I**	*Vacuum Pressure	**VP**
*Green Resin (1 or 2 surfaces)	**1G/ 2G**		

The corresponding microscopical sections were prepared using a non standard procedure for avoiding artifacts (Montoto et al. 1981).

The procedure for the orientation of these vertical sections is described in detail in Baddeley et al. (1986). Following their recommendation we have selected a random direction for the first vertical section, taking as the 0° direction the vertical red line that was originally marked in each sample; other two directions were systematically spaced with respect to the first one, but as accorded in the contract, only one of these two directions were selected for the second vertical section. From each of these primary vertical sections, parallel and perpendicular slabs for microscopy were cut.

The notation, position and characteristics of each studied vertical rock section are also included in those sketches.

From the provided samples chips of about 30x25x18 mm have been obtained, cut again using a low deformation rock saw to obtain two symmetrical chips. One of this halves is impregnated with resin dyed with a 'red' fluorescence (Rhodamine B) using a two step procedure. The other halve, only impregnated with a fluorescent 'green' resin from its outer surface, is used to measure the penetration depth of the resin. Final prisms of about 30x25x9 were produced for the preparation of the artifacts-free polished sections.

To avoid artifacts, most of the studies were undertaken using polished rock slabs; a supplementary grinding of about 700 to 900 μm was performed on those slabs prior to the final polishing.

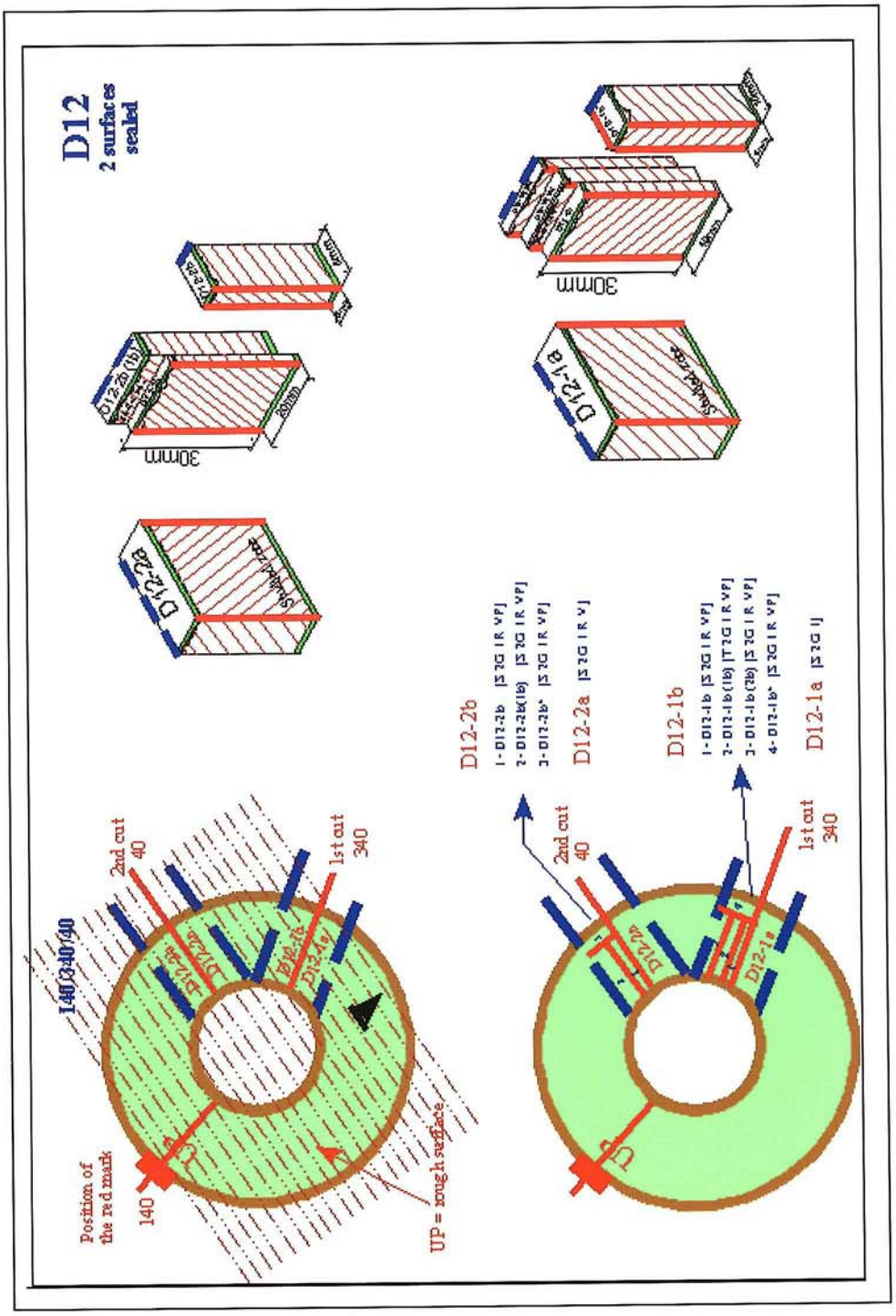

Figure 3. *Sketch for Sample D12 with the position of the red mark, surfaces for rock cutting and schistosity; the names, position and characteristics of each rock section are also shown.*

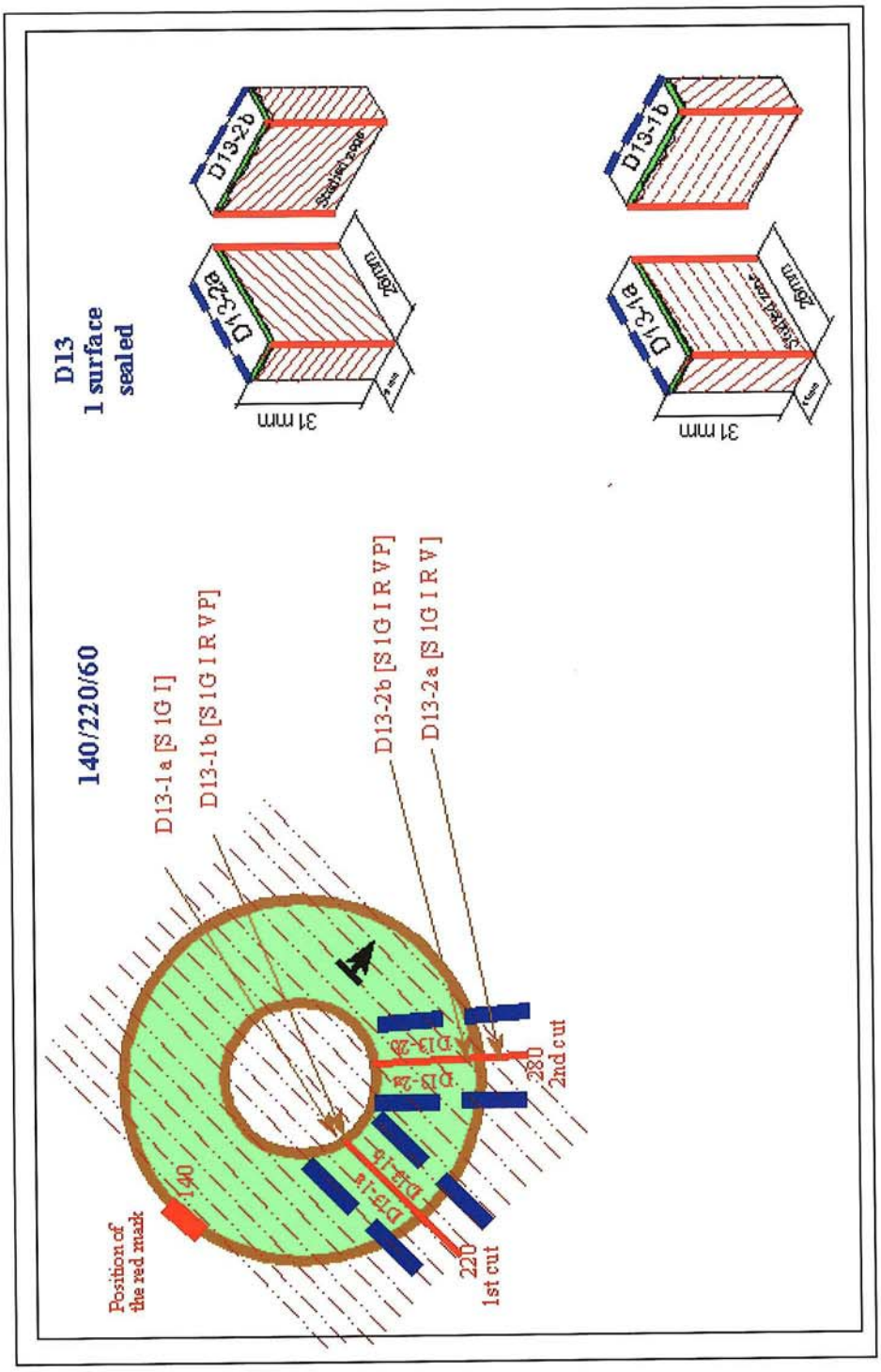

Figure 4. *Sketch for Sample D13 with the position of the red mark, surfaces for rock cutting and schistosity; the names, position and characteristics of each rock section are also shown.*

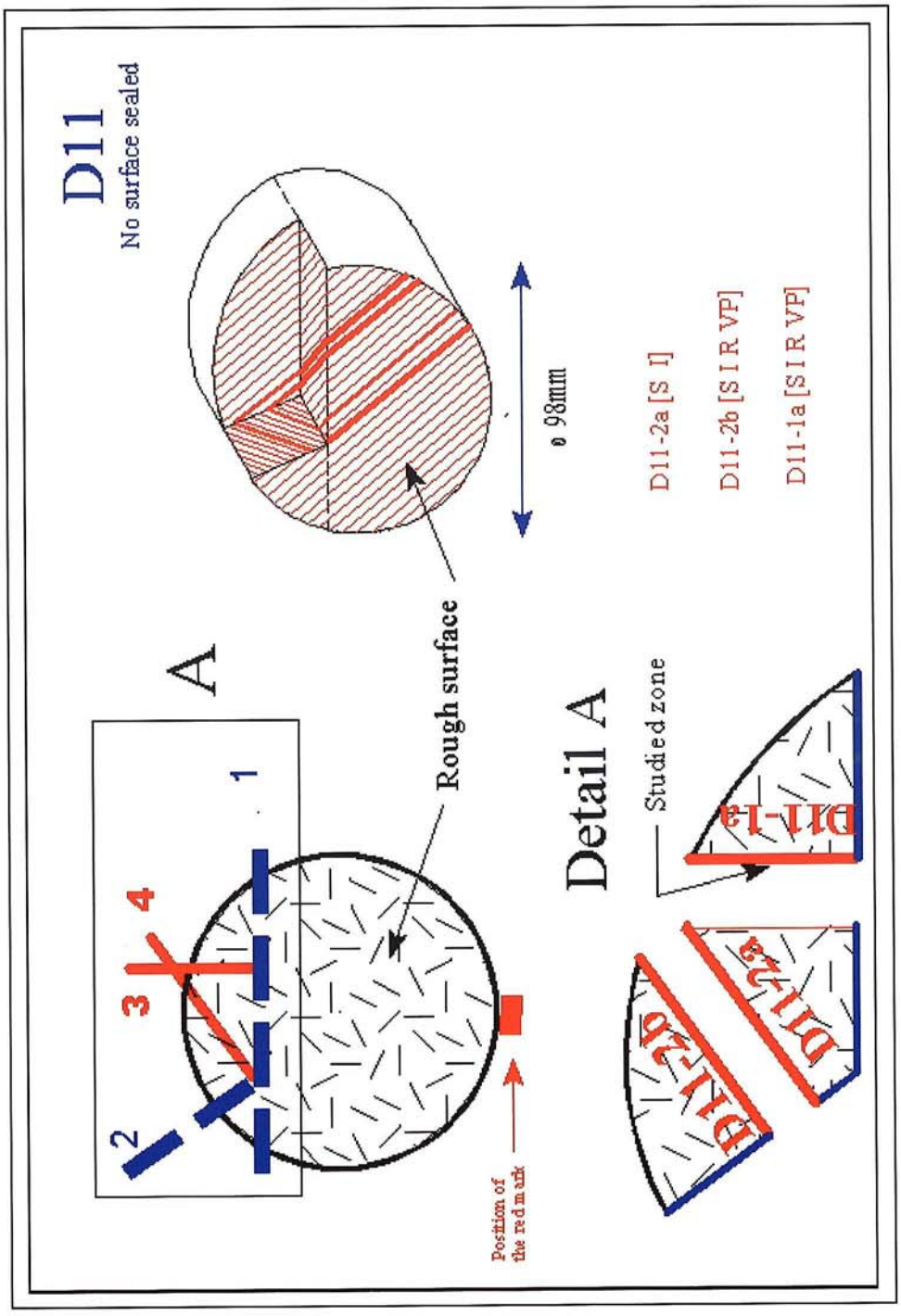

***Figure 5**. Sketch for Sample D11 with the position of the red mark, surfaces for rock cutting and schistosity; the names, position and characteristics of each rock section are also shown.*

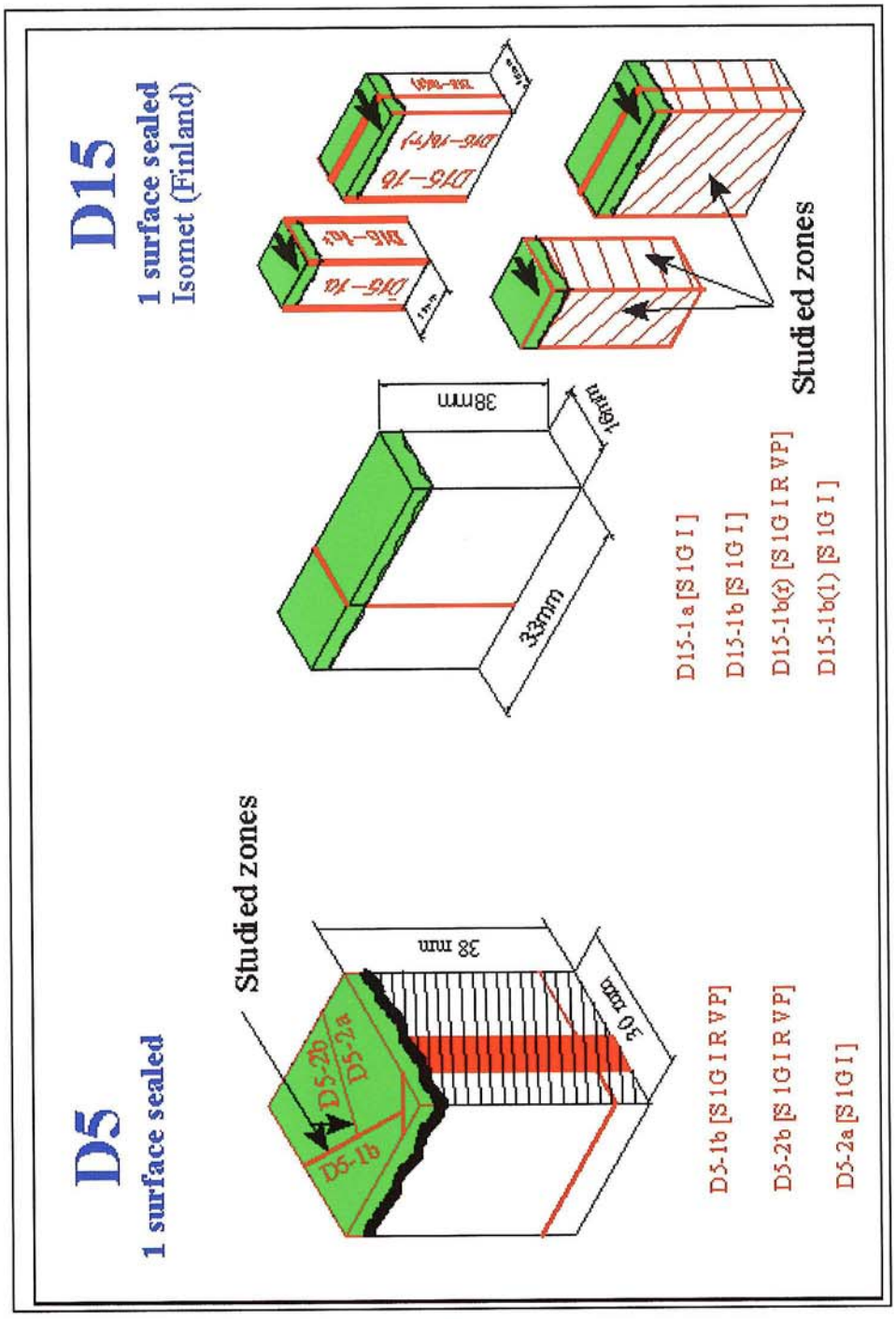

***Figure 6**. Sketch for Samples D5 and D15 with the position of the red mark, surfaces for rock cutting and schistosity; the names, position and characteristics of each rock section are also shown.*

1.3.3.2 Quantitative microscopy

Specific procedures for stereology and image analysis has been implemented for this study, specially for measuring the crack specific surface, probably the most important microfractographic parameter. The adopted procedures are the result of very numerous mineralogical and fractographical observations of the disturbed and non disturbed zones.

Procedure for evaluating fractographic parameters using digital image analysis

A new image analysis procedure has been developed, using the Leica Qwin software. This procedure is used for studying Confocal Laser Scanning Microscopy (CLSM) images where only the resins impregnated cracks can be observed (Figure 7).

With the image processing method, cracks are discriminated in function of their higher intensity; depending on the used magnification the values of area and thickness of the impregnated cracks appear different (we call this phenomenon the "magnification effect"). This induced error is illustrated in Figure 8, Figure 9 and Figure 10 were the same area of one sample has been observed with different objective lens and photomultiplier gain values.

High gain values produces higher crack areas due to the halo effect. Low magnification produces low resolution and high focal depth images. The first factor affects crack areas because the intensity of the fluorescence should be increase to discriminate the cracks, the second one affects because crack areas above and below the focal plane are also collected.

In order to avoid these errors all the processed images have been taken at high magnification (60 x objective lens) and with a normal photomultiplier gain level (not saturation). Only in this case the crack boundary can be clearly observed.

Number of rows and columns studied under CLSM is the following for each sample:

Sample	Rows	Columns
D5-1B	12	10
D11-1A	11	10
D13-1A	6	10
D13-2B	12	10
D12-1A	7	10
D12-2B(1B)	12	10
D15-1A*	6	10
D15-1B	12	10

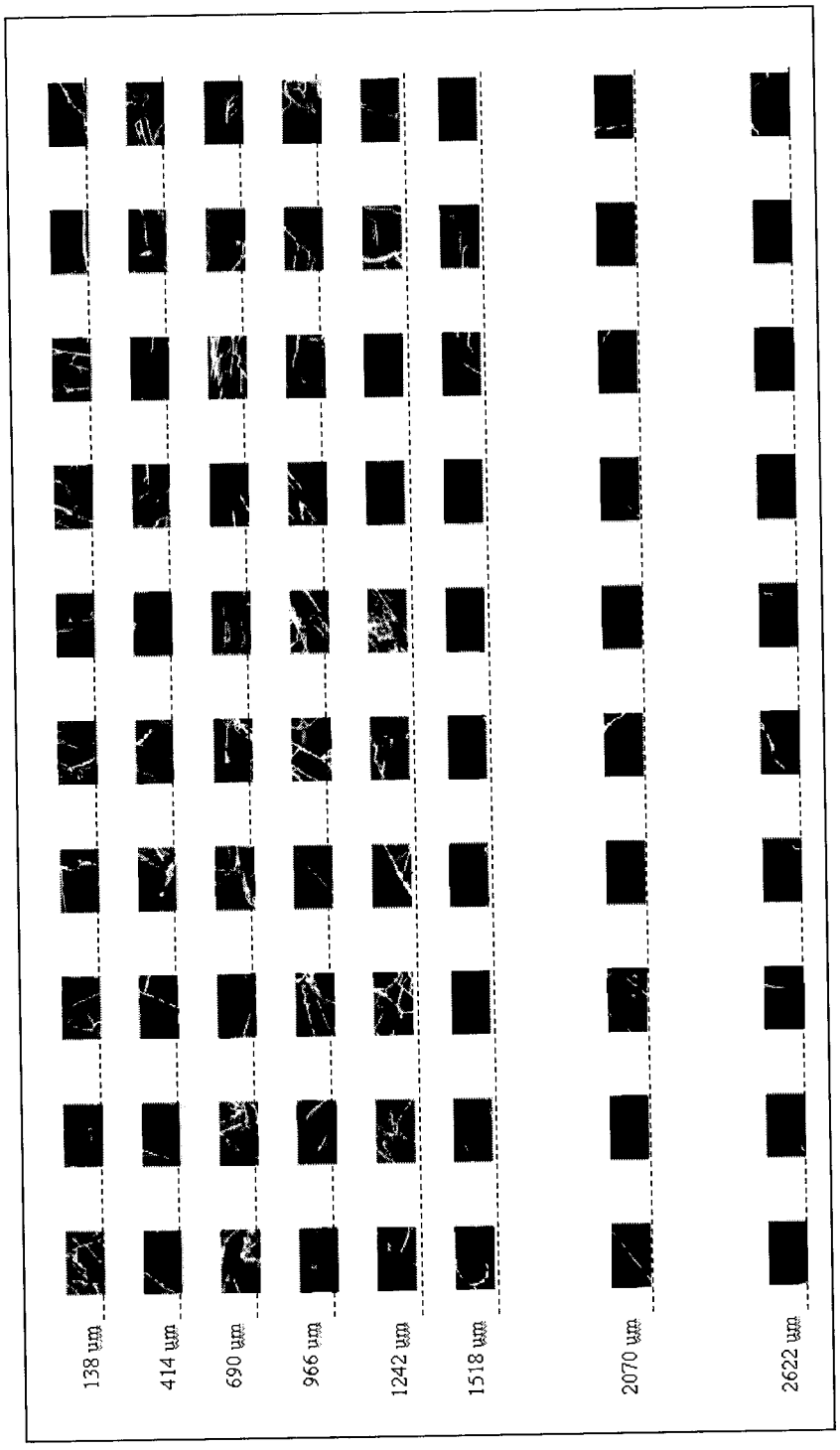

***Figure** 7. Sampling methodology under CLSM for estimating fractographic parameters using digital image analysis. A grid of eight rows of ten images (207x138 µm) by row was designed. The first six rows, 278µm apart, near the hole border, were obtained with a blue filter (488 nm) in order to collect the green fluorescence emitted by cracks impregnated with the epoxy based sealant. The other two rows, 552 µm apart, were obtained with a green filter (568 nm) in order to collect the red fluorescence emitted by cracks impregnated by the Rhodamine resin. Four more rows per sample at a distance of 3, 4, 5 and 6 mm respectively from the hole border were also measured.*

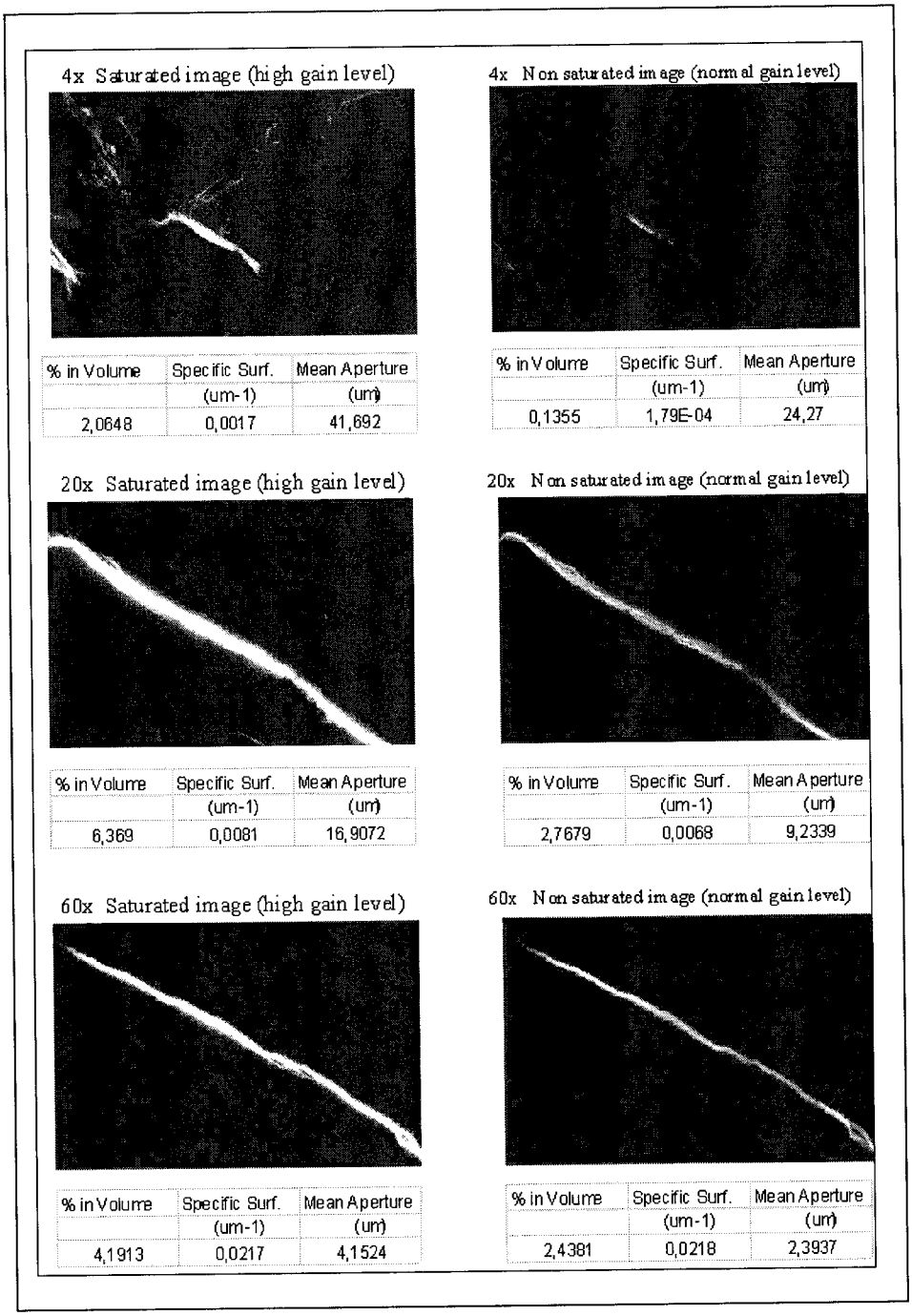

% in Volume	Specific Surf. (um-1)	Mean Aperture (um)
2,0648	0,0017	41,692

% in Volume	Specific Surf. (um-1)	Mean Aperture (um)
0,1355	1,79E-04	24,27

% in Volume	Specific Surf. (um-1)	Mean Aperture (um)
6,369	0,0081	16,9072

% in Volume	Specific Surf. (um-1)	Mean Aperture (um)
2,7679	0,0068	9,2339

% in Volume	Specific Surf. (um-1)	Mean Aperture (um)
4,1913	0,0217	4,1524

% in Volume	Specific Surf. (um-1)	Mean Aperture (um)
2,4381	0,0218	2,3937

Figure 8. *Images of the same area of sample D5-1B obtained under different objective lens and photomultiplier gain leve . The parameters: % crack in volume, crack specific surface and crack mean aperture has been calculated for each image in order to illustrate the influence-error source- of magnification and gain level in the final values.*

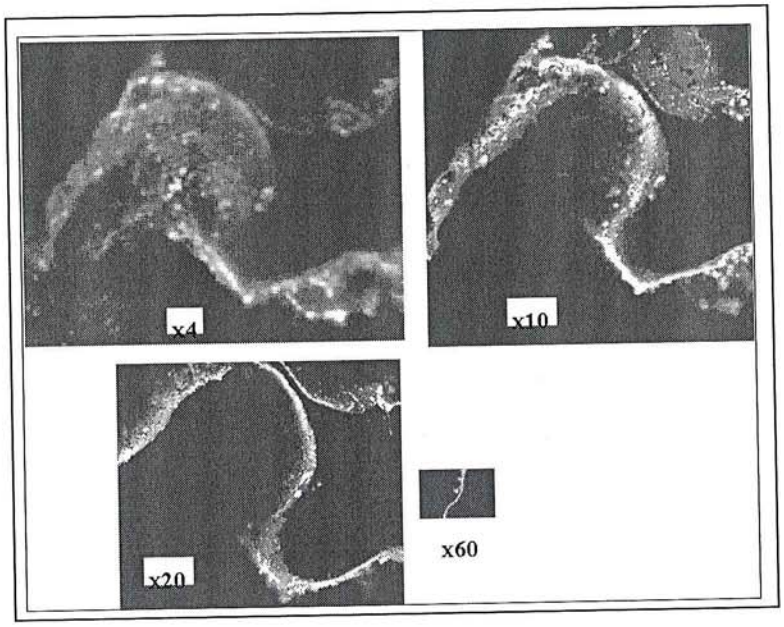

***Figure 9**. Resolution and "magnification effect" under fluorescence microscopy (CLSM). The same rock area image under different magnification(x4, 10, 20, 60)*

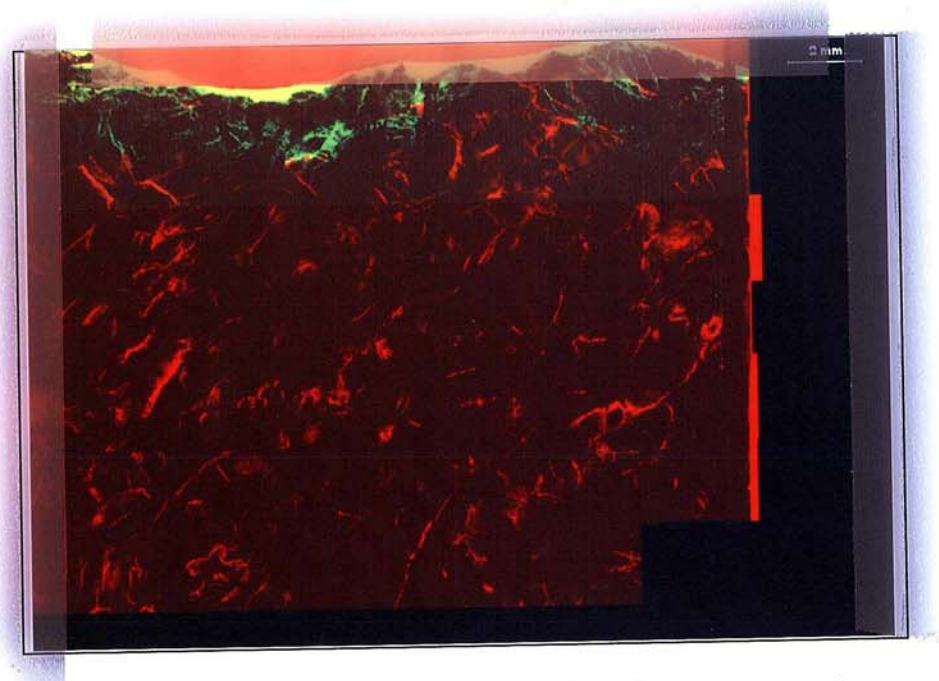

***Figure 10**. When the rock is observed under fluorescence microscopy at low magnification it seems to have a greater crack density than in reality, what we call the "magnification effect". The position of the crack in Fig 8 is here shown.*

Procedure for evaluating the crack specific surface using image analysis

In image analysis studies, this parameter is obtained measuring the length of the crack traces and applying the formula (Cruz-Orive , 1987). The mean crack specific surface is referred to all the images of the same row.

$$Sv = \frac{4}{\pi} \frac{\sum li}{Aref}$$

were:

L_i = Crack traces length,
A_{ref} = Area of the image.

Procedure for evaluating the crack specific surface using stereology

This parameter was evaluated in terms of textural and mineral position considering a mineral cluster as a grain. Profiles of images of 390 x 310 μm. were obtained under scanning electron microscopy, with a simultaneous use of secondary and back scattered detectors, according to the sketch in Figure 11. In these images both impregnated and no-impregnated microcracks are counted.
A foil with a stereological grid with points and cycloid lines is superimposed on the screens of the microscope; the number of intersections of the crack traces with a cycloid line are counted, as well as the number of the points that fall within the rock surface. From these data, Sv is estimated.

More details of the stereological method for estimation of Sv on vertical sections can be found in Baddeley et al. (1986).

Number of rows and columns studied under SEM are the following for each sample:

Sample	Rows	Columns
D5-2b	28	10
D11-1a	27	11
D12-2a	27	12
D13-1a	28	13
D12-1b(1b)	14	7
D12-2b(1b)	18	8
D15-1b(r)	29	6

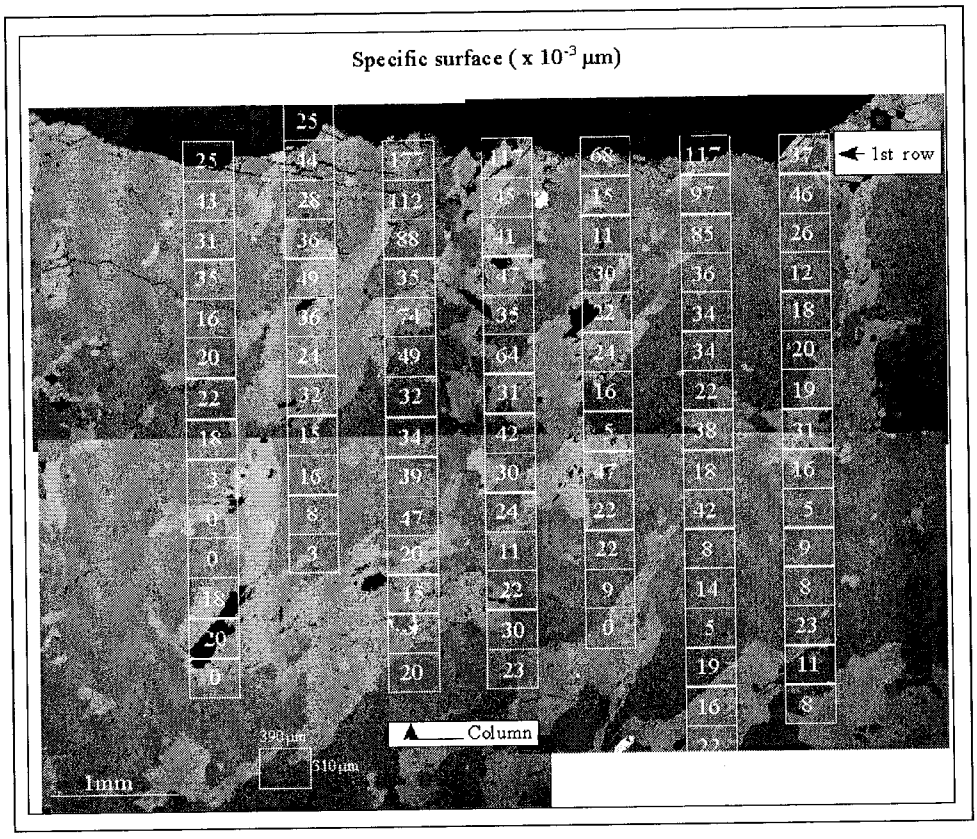

Figure 11. *Procedure for estimation the Crack Specific Surface using stereology under SEM (secondary electrons + back scattered). Profiles of contiguous zones (390 x 310µm) perpendicular to the outer disturbed zone are imaged and quantified. The included figures correspond to the total Sv in each image for specimen D12-1b(1b).*

Procedure for evaluating the crack aperture using image analysis combined with confocal laser scanning microscopy

The middle lines of the cracks are determined and the distance from each point of this line to the crack boundary is measured; the crack aperture is two times this distance. From this value the mean crack aperture and the crack aperture distribution in five classes were calculated for each image.

Procedure for evaluating the crack aperture using stereology

The results of a pilot study show that at very high magnifications, a large number of images has to be counted due to the high percentage of very fine microcracks; at a magnification of 1200, more than 90 % of the microcracks fall into only the two smaller established aperture classes (approximately thinner than 3 μm). Consequently, it is necessary to use a magnification of 2600 to spread the microcrack aperture distribution in more than 5 classes. To obtain unbiased and confident estimates of the microcrack aperture at so high magnification, a very large number of images (to the order of many hundreds, just for this parameter) should be counted. Consequently, no evaluation of crack aperture under stereology has been done.

Procedure for evaluating the crack orientation using image analysis

A polygonal approximation is applied to the middle line of the crack area and this polygonal is used to calculate an orientation histogram of the image cracks. Values will be presented as rosette graphs where each radio represents the cracks length for a direction range (intervals 20°). Directions are between 0° and 180°. The 0° direction is parallel to the wall of the hole border (Figure 12).

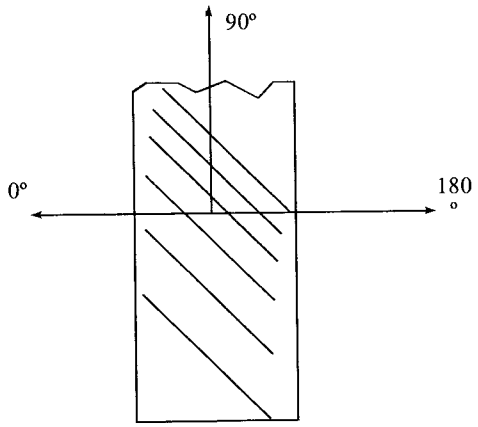

Figure 12. *Values of directions in relation with the sample position.*

Procedure for evaluating the crack volume percentage using image analysis

This parameter was evaluated from the confocal images using an image analysis procedure to calculate the cracks area. The percentage of area occupied by cracks is an estimation of the crack volume percentage; the results are presented in terms of the mean percentage of crack volume per image.

Procedure for estimating the penetration depth of the epoxy based sealant under reflected light fluorescence microscopy

Polished vertical sections impregnated only with the "green" epoxy based sealant have been imaged under reflected light fluorescence microscopy at a magnification that allows that cracks of aperture about 2,5 microns can be observed.
The vertical section for each rock slab is divided vertically in columns 2 mm width, starting 3 mm apart from the border (to avoid possible artifacts). The depth of penetration is measured as follows:

- The E-W cross hair of the microscope eyepiece is located in the higher point of the profile of the rock wall hole (Figure 13): this is the initial position on this column.
- The field of view is moved down in the column until the last microcrack is observed.
- The E-W cross hair of the eyepiece is located at the lower end of this microcrack profile (Figure 13): final position.
- The distance moved between the final and the initial position is recorded as the penetration depth in that column.
- The procedure is repeated in all the remaining columns and data of each vertical section are represented in a graph.

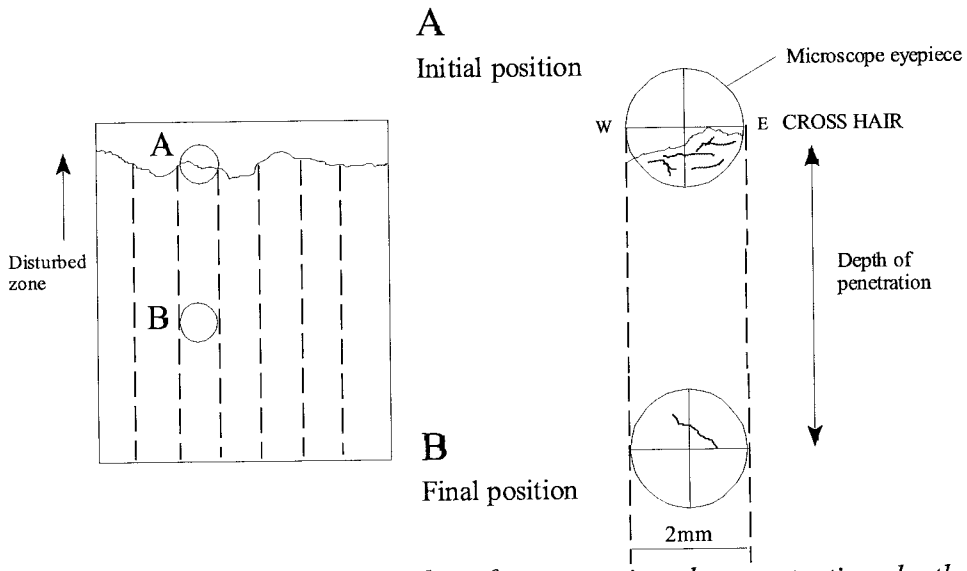

Figure 13. *Scheme showing the procedure for measuring the penetration depth of the epoxy based sealant.*

2 RESULTS

2.1 Presentation

Although more images than accorded have been quantified, the results here presented should be considered as an example of what can be achieved with the study of more thin sections and more fields. In fact, with the obtained data, no conclusive answer about the extension of the disturbed zone can be given nor its division in subzones.

In general the most disturbed zone is surprisingly restricted to some few mm; less generalised fissured zones can be observed up to a depth of about 3 mm. Only a microcracked zone at a greater depth, 7 mm, has been observed in a particular zone of sample D12-1a (Figure 14). The new developed microfractographic network seems to be mainly parallel to the outer surface.

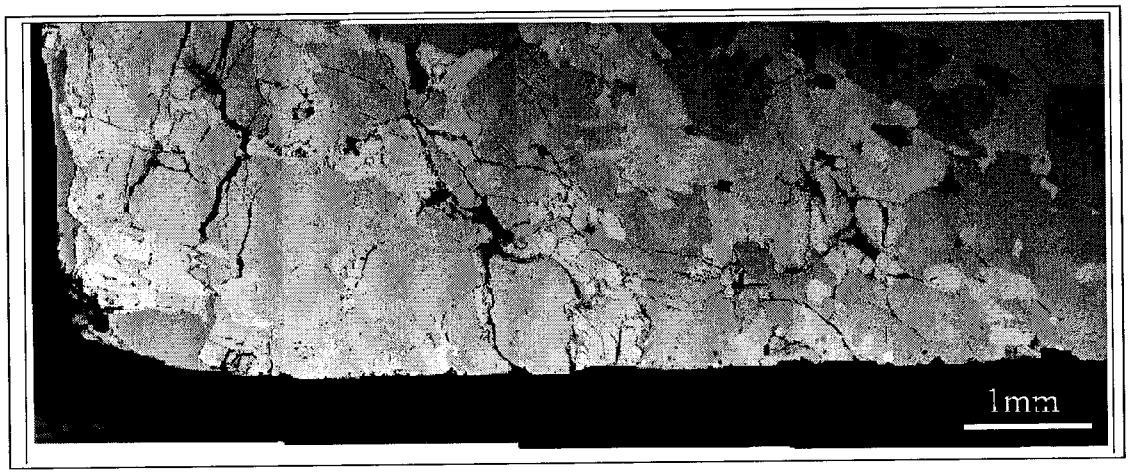

Figure 14. *Only in a sample, D12-1a, and only in a given area of it, a microcracked zone has been observed at a greater depth than normal, 7 mm. The disturbed zone is at the left side.*

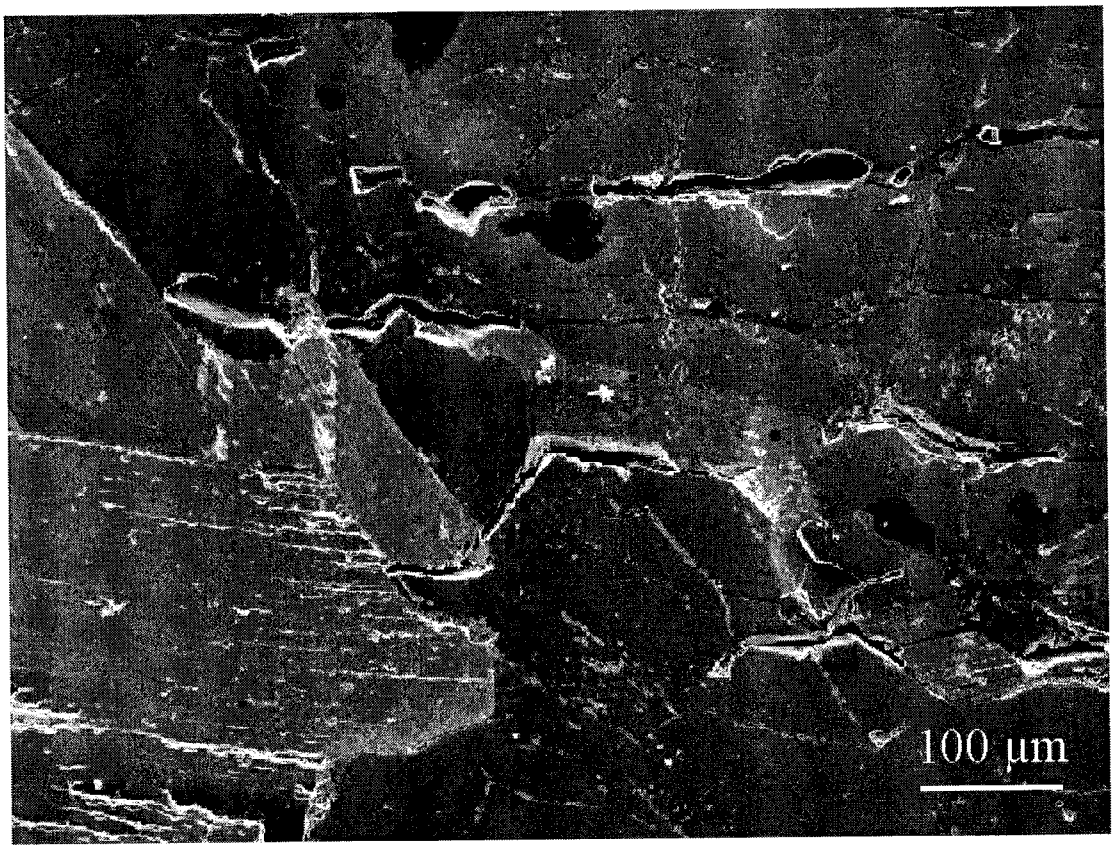
100 µm

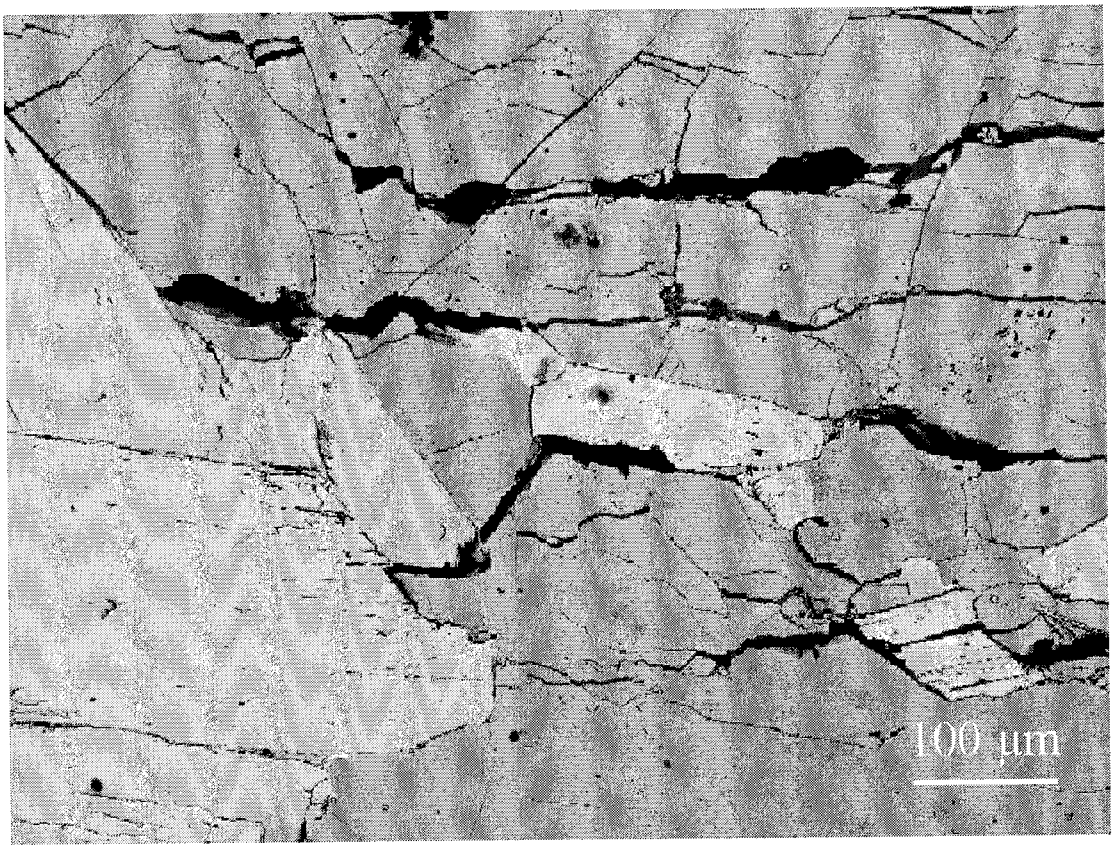
100 µm

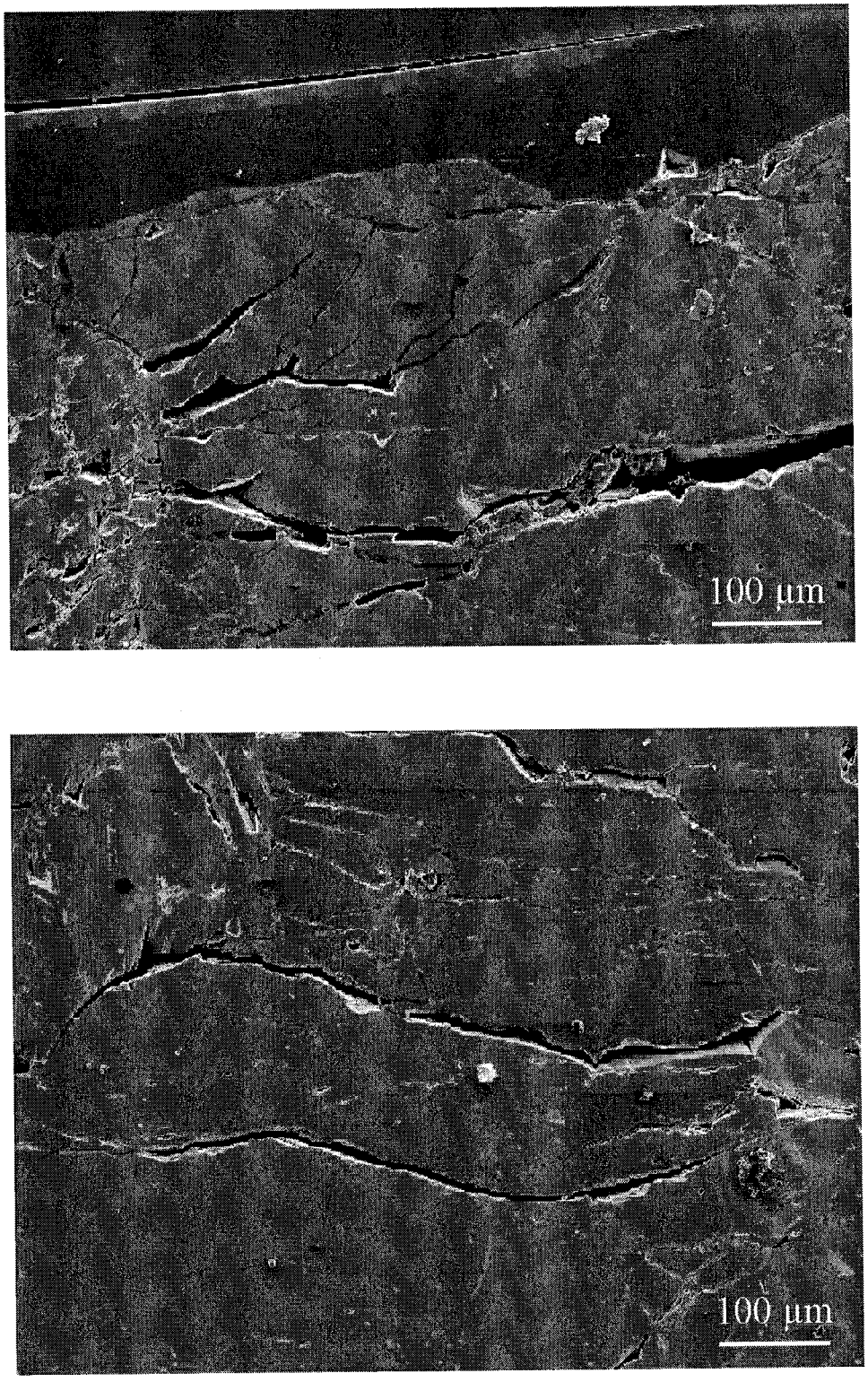

Figure 15. *The wider cracks are located in the outer zone and are subparallel to the rock wall. During grinding and polishing the green resin has been partially removed from them.*

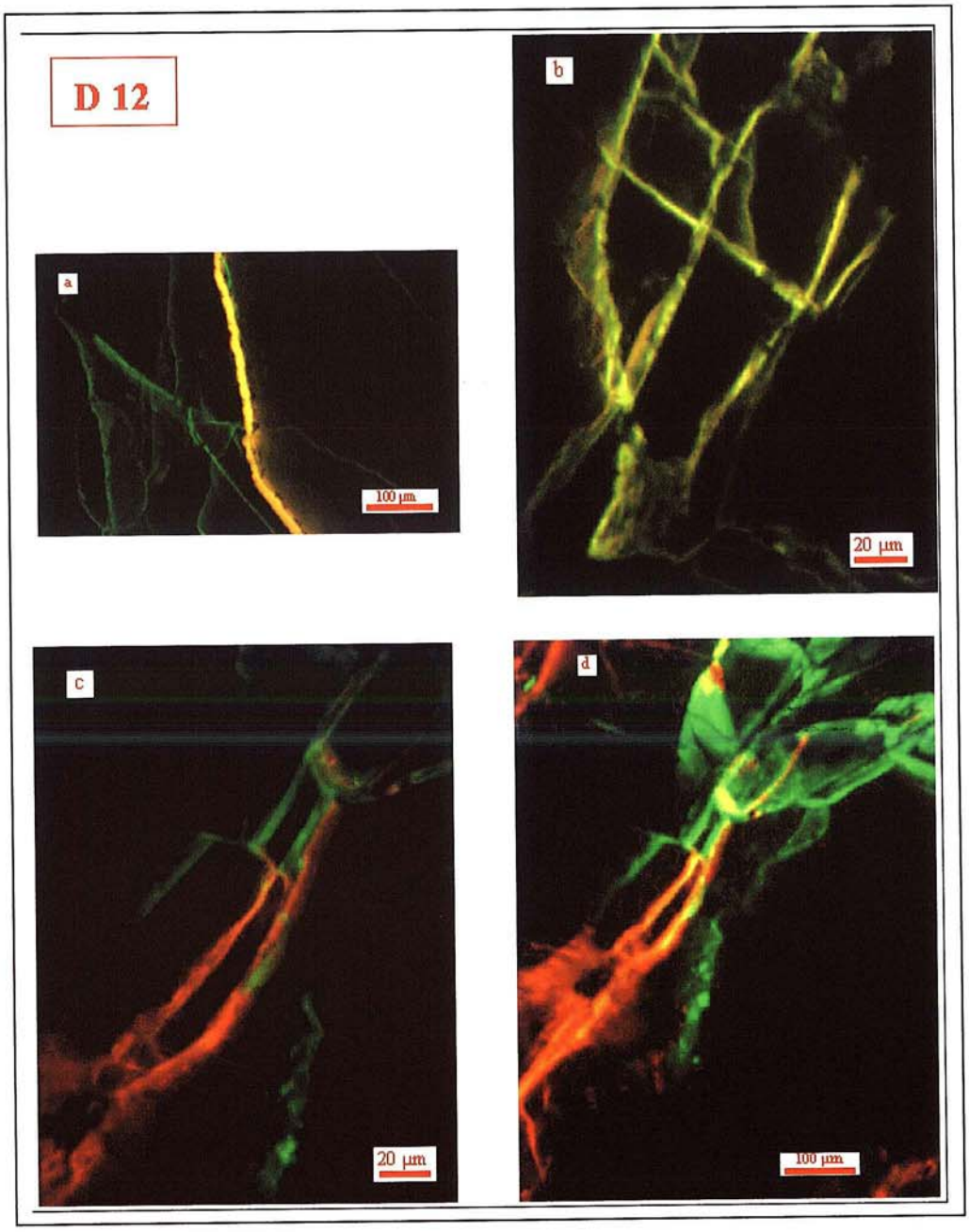

***Figure 16**. Differences in fluorescent emission has been found between the green ("Finish") and the red ("Spanish") resins with the excitation light and the barrier filters used in confocal laser scanning microscopy.Cracks showing yellow emission color have been refilled with both resins. The upper part of the crack in (c) and (d), 1 mm from the outer surface, can be observed refilled with the epoxy resin and the lower one with the Rhodamine resin.*

These cracks refilled with both resins show a similar emission under scanning electron microscopy but different curing; sometimes the fissures impregnated with the red Rhodamine are "decorated" with thin cracks parallel to their inner border.

For each of the five studied specimens, a general photomosaic under scanning electron microscopy has been obtained. The general aspect of the rock microfractography, mineralogy and texture can be observed, as well as the orientation and depth of the most important cracks in the disturbed zone.

The obtained results for the different fractographic parameters and specimens are presented in the following chapters.

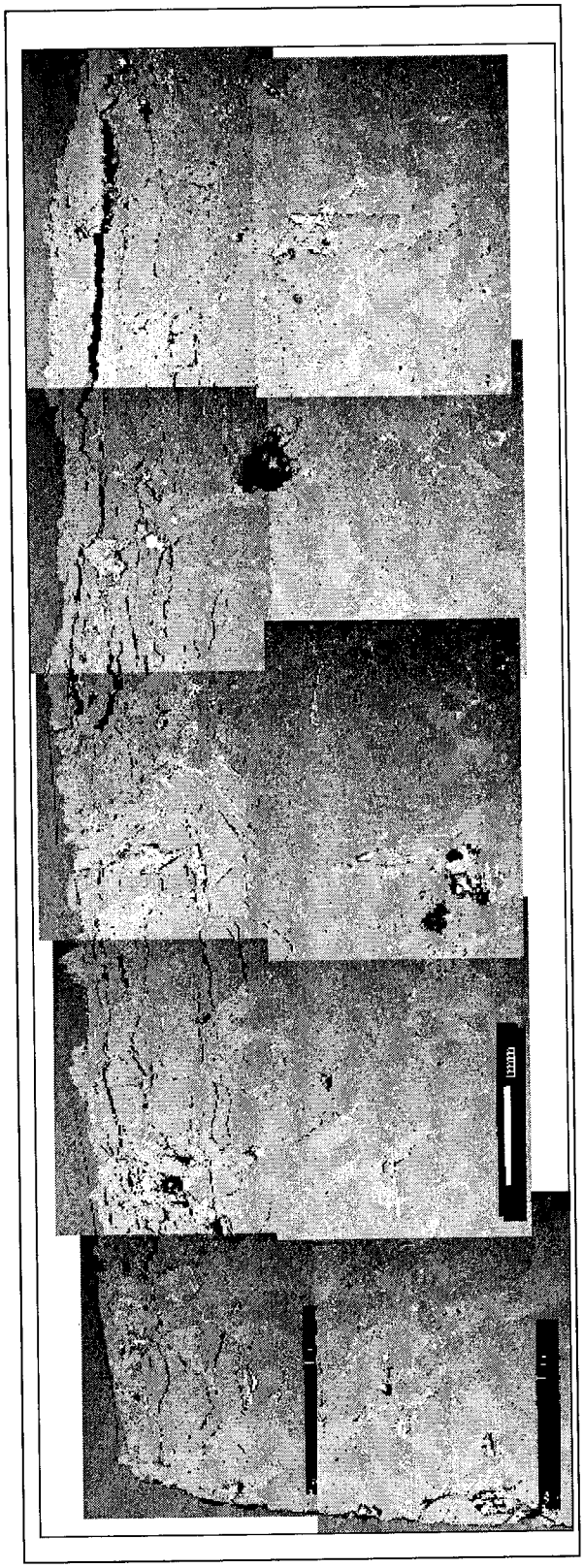

Figure 17*. Photomosaic of outer disturbed zone of sample D12-2a.*

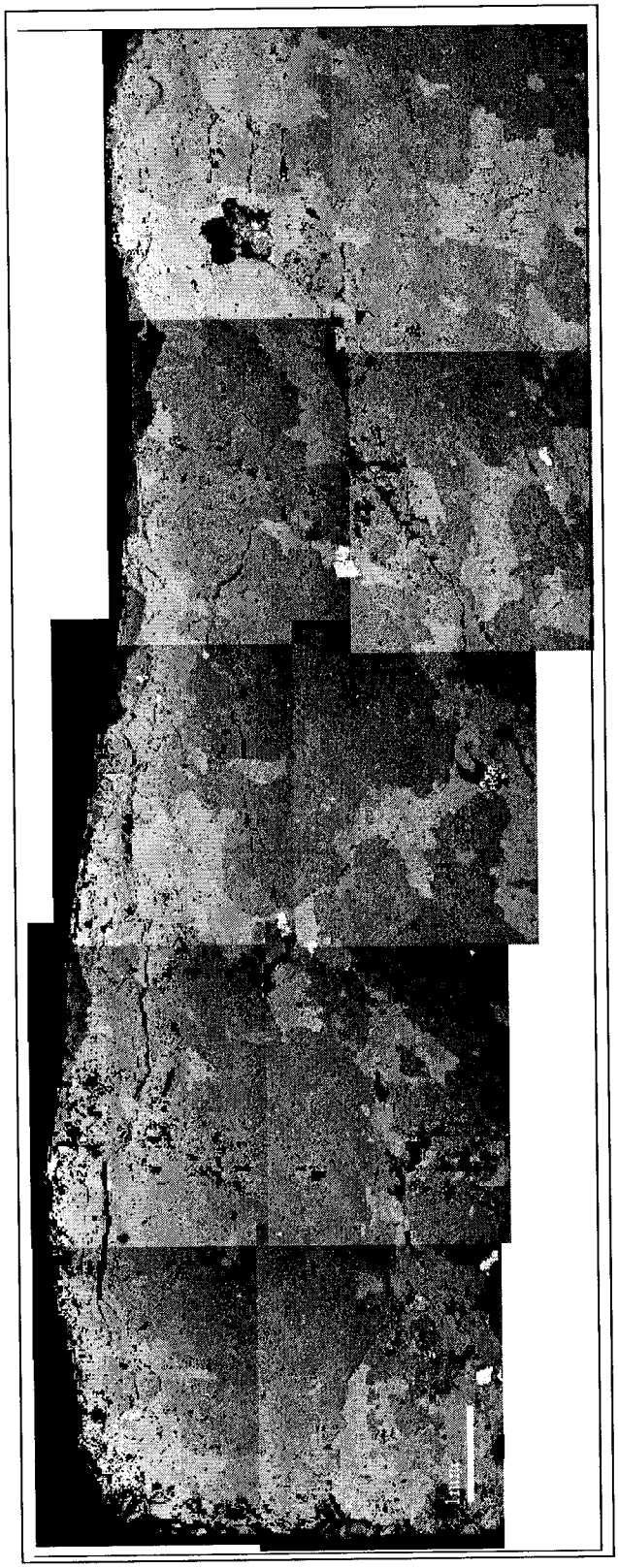

Figure 18. *Photomosaic of outer disturbed zone of sample D13-1a.*

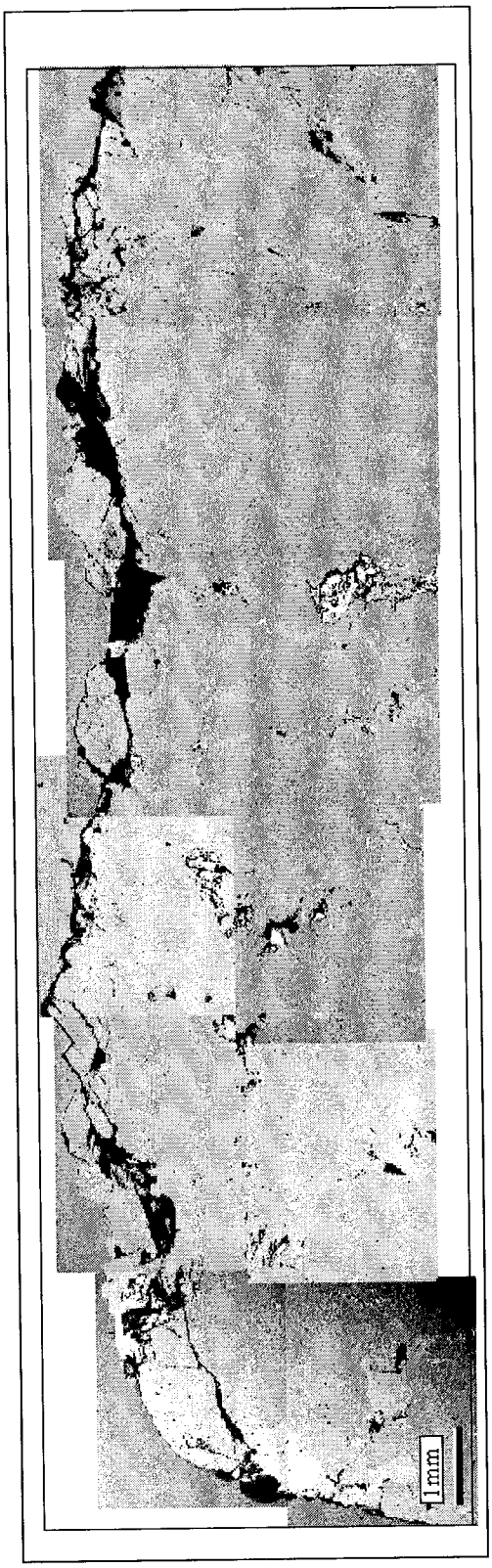

***Figure 19**. Photomosaic of outer disturbed zone of sample D11-1a.*

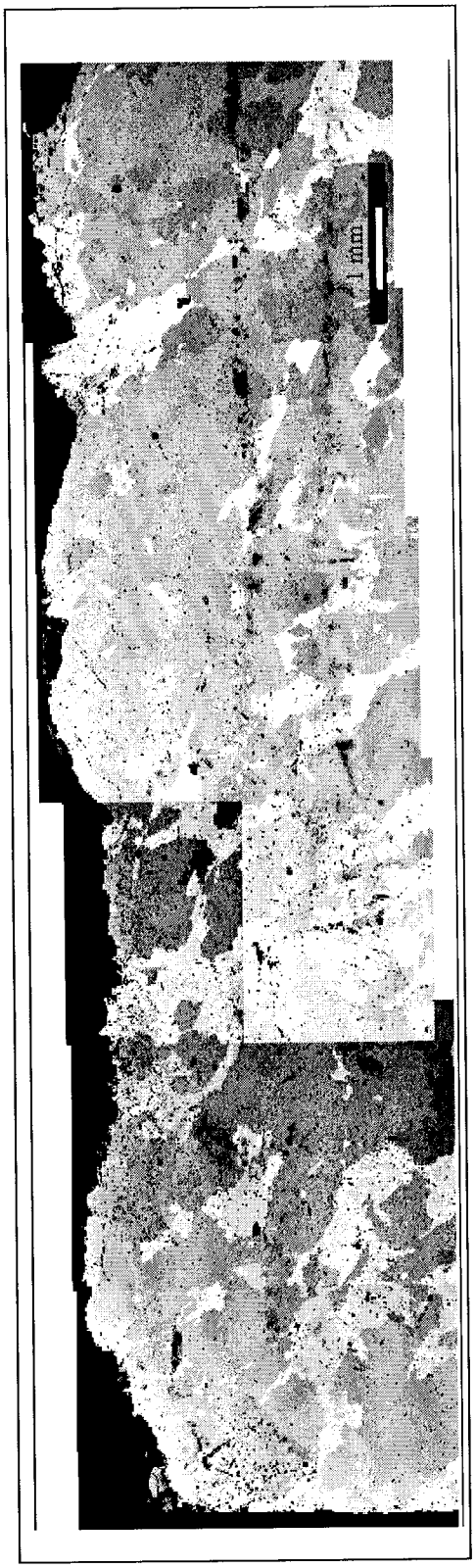

***Figure 20**. Photomosaic of outer disturbed zone of sample D15-1b(r).*

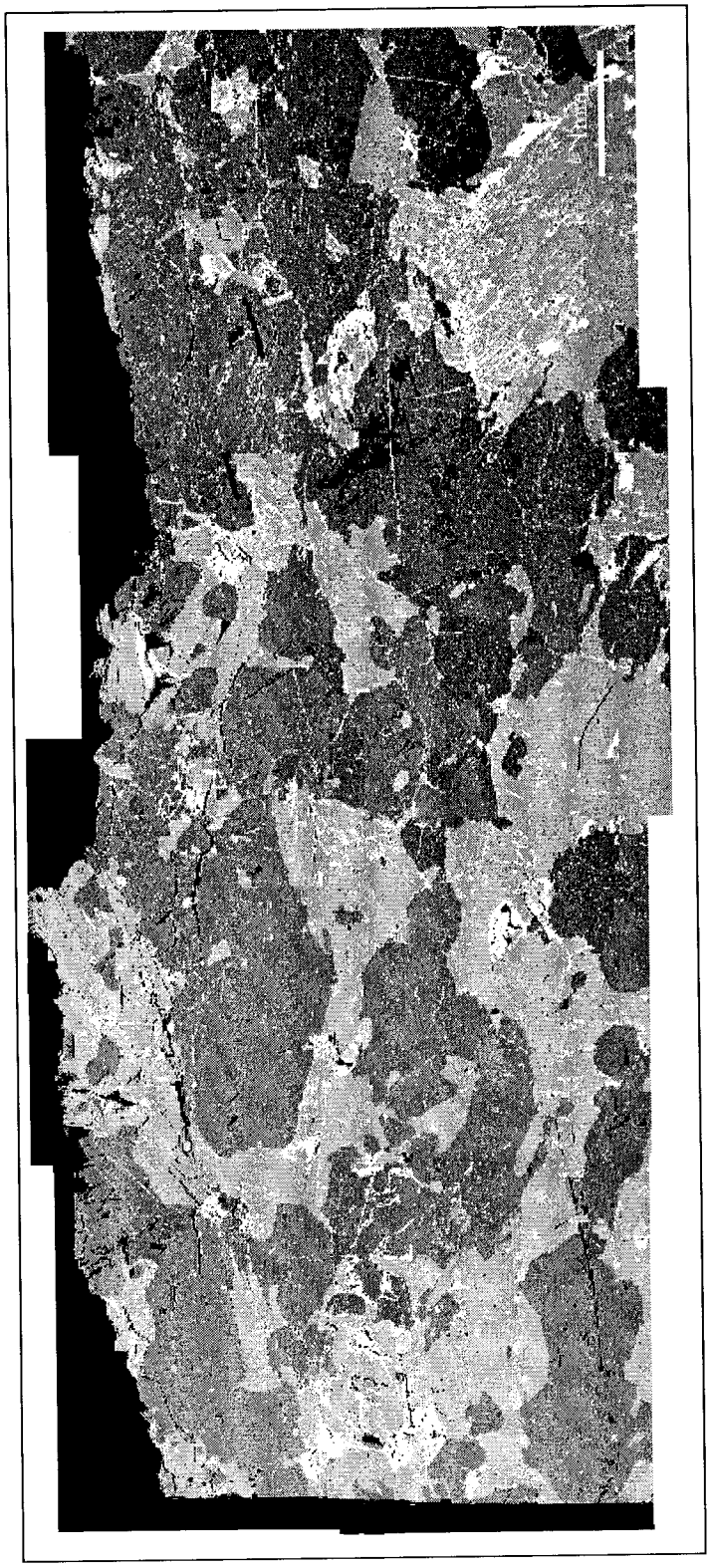

***Figure 21**. Photomosaic of outer disturbed zone of sample D5-2b. Artifacts under the form of black lines can be observed on this image; they correspond to scratches on the Au-Pd thin layer of the rock section.*

2.1.1 Penetration depth of the epoxy based sealant

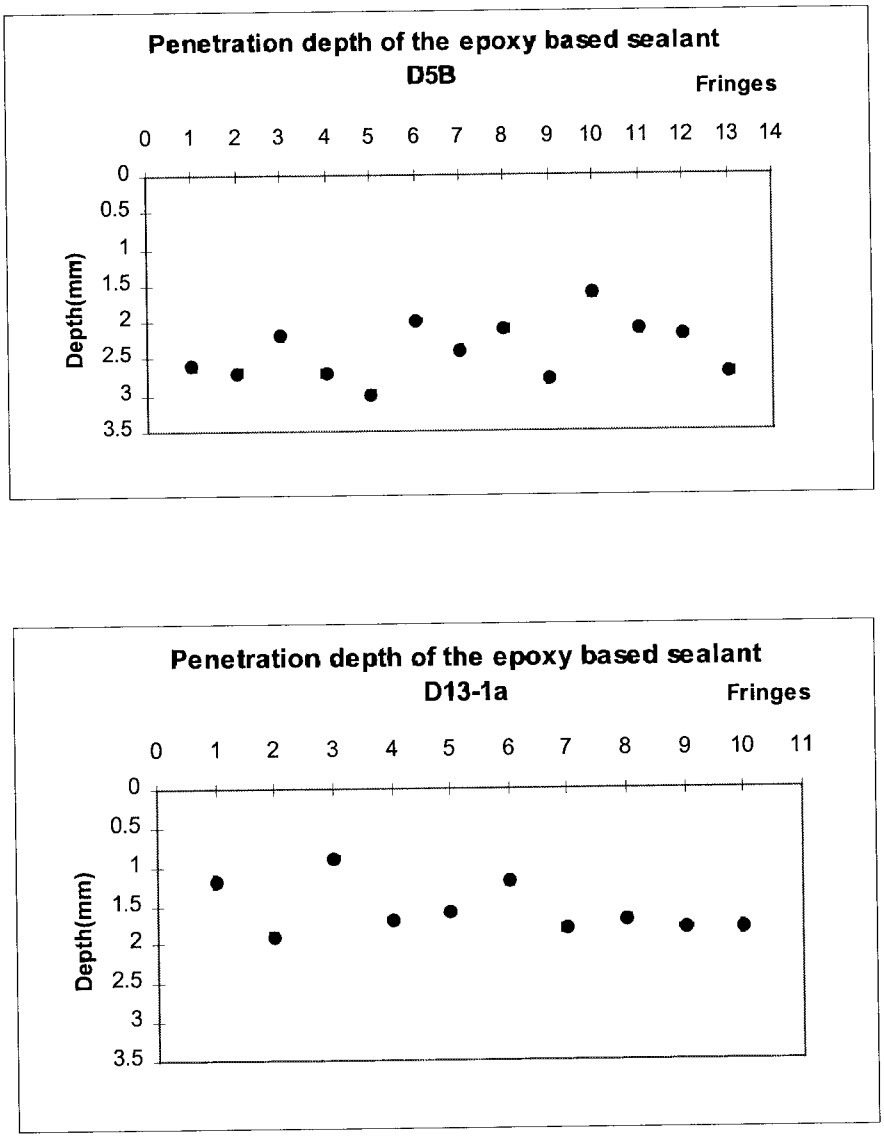

***Figure 22**. Penetration depth of the epoxy based sealant studied under reflected light fluorescence microscopy of samples D5B (top), D13-1a (bottom).*

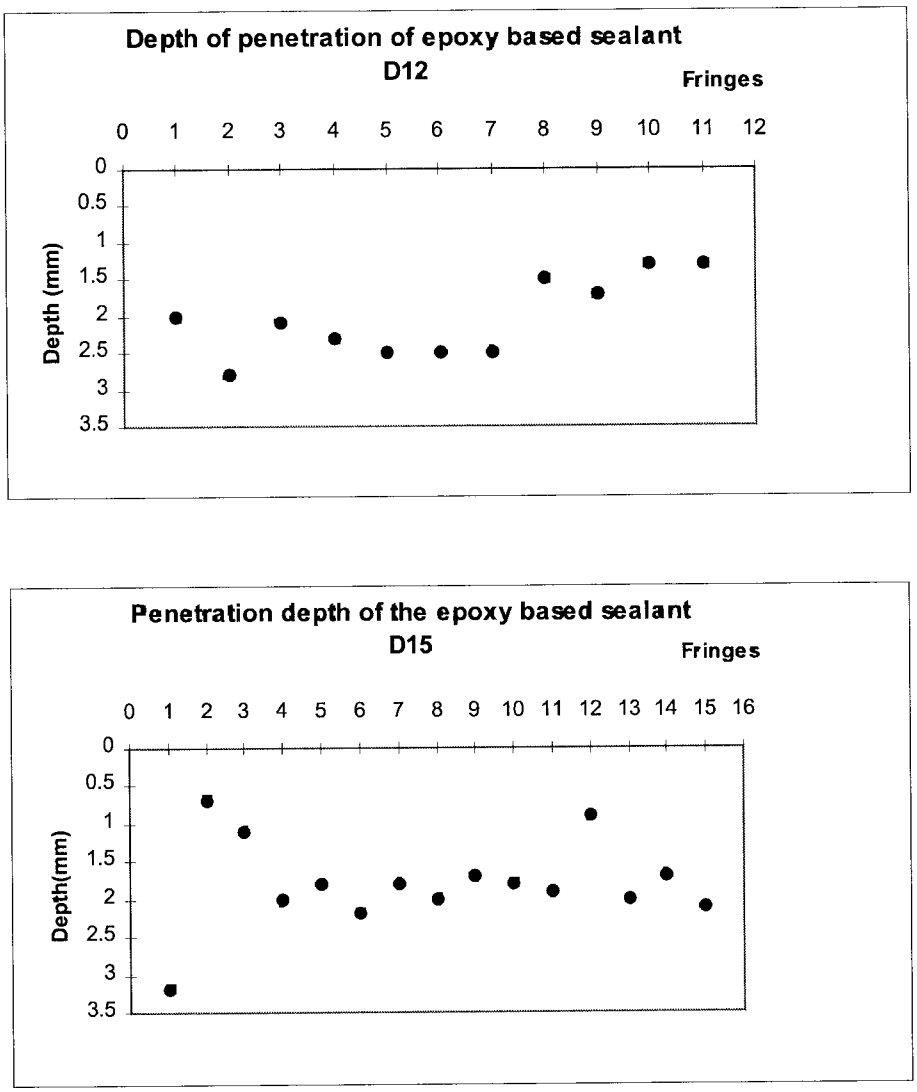

Figure 23. *Penetration depth of the epoxy based sealant studied under reflected light fluorescence microscopy of samples D12(top) and D15(bottom).*

All the samples show a similar behaviour in relation to the depth of penetration of the resin which is mainly in the range of 2-3 mm. Only samples D15 and, mainly, D13 show a relatively smaller depth of penetration, less than 2 mm.

2.1.2 Crack Orientation using Image Analysis

The orientation of the microfractographic network is described in terms of the crack aperture. The wider cracks (>5.5 μm) are mainly parallel to the outer surface and they only represents less than the 10 % of the total crack population.

The most abundant cracks, those narrower than 5.5 μm, are not regularly oriented in relation to the outer border.

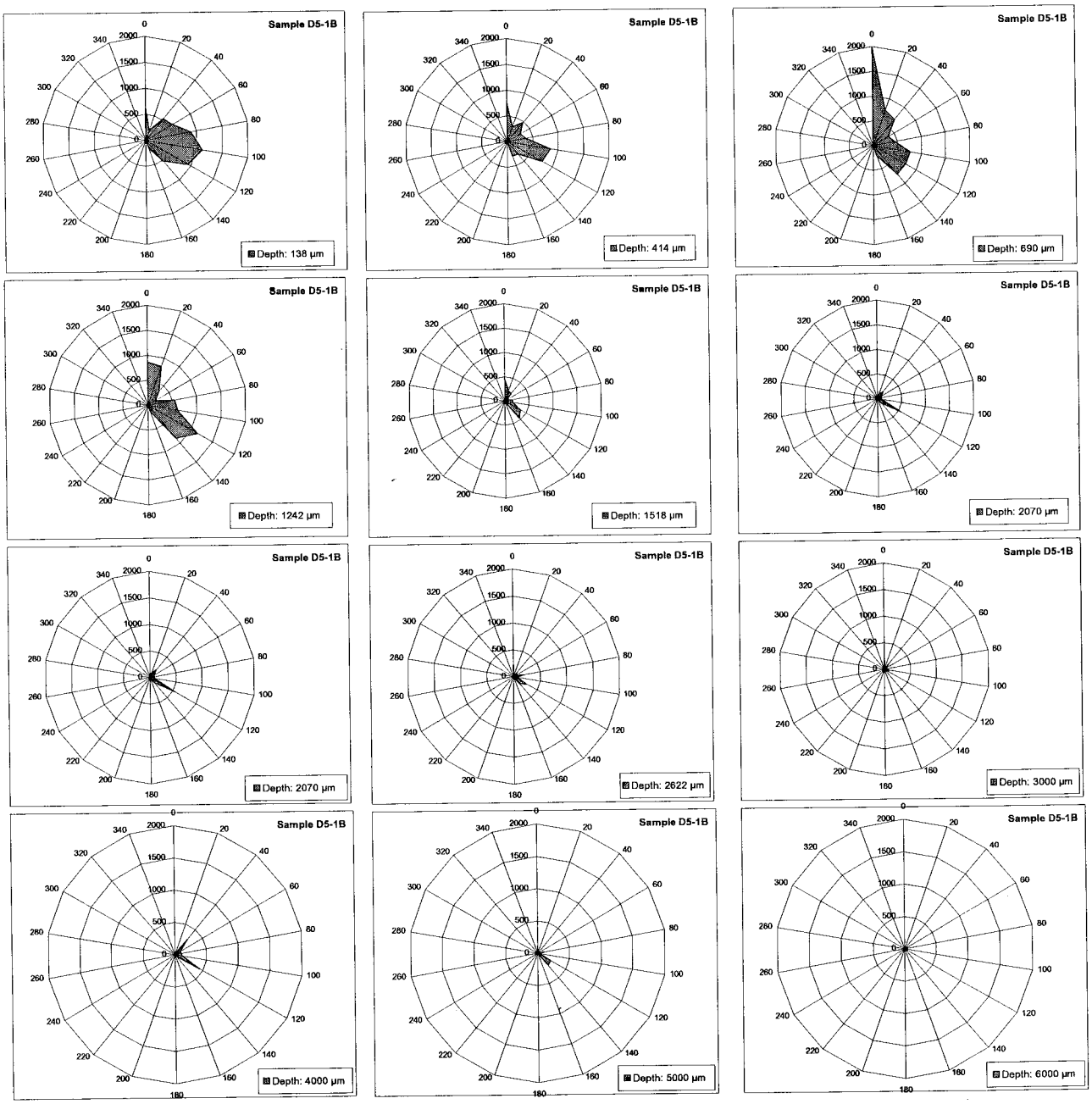

Figure 24. *Crack orientation using Image Analysis. D5-1B. Each graph represents the crack orientation in degrees vs the sum of crack traces in μm, obtained for all the images at the indicated depth.*

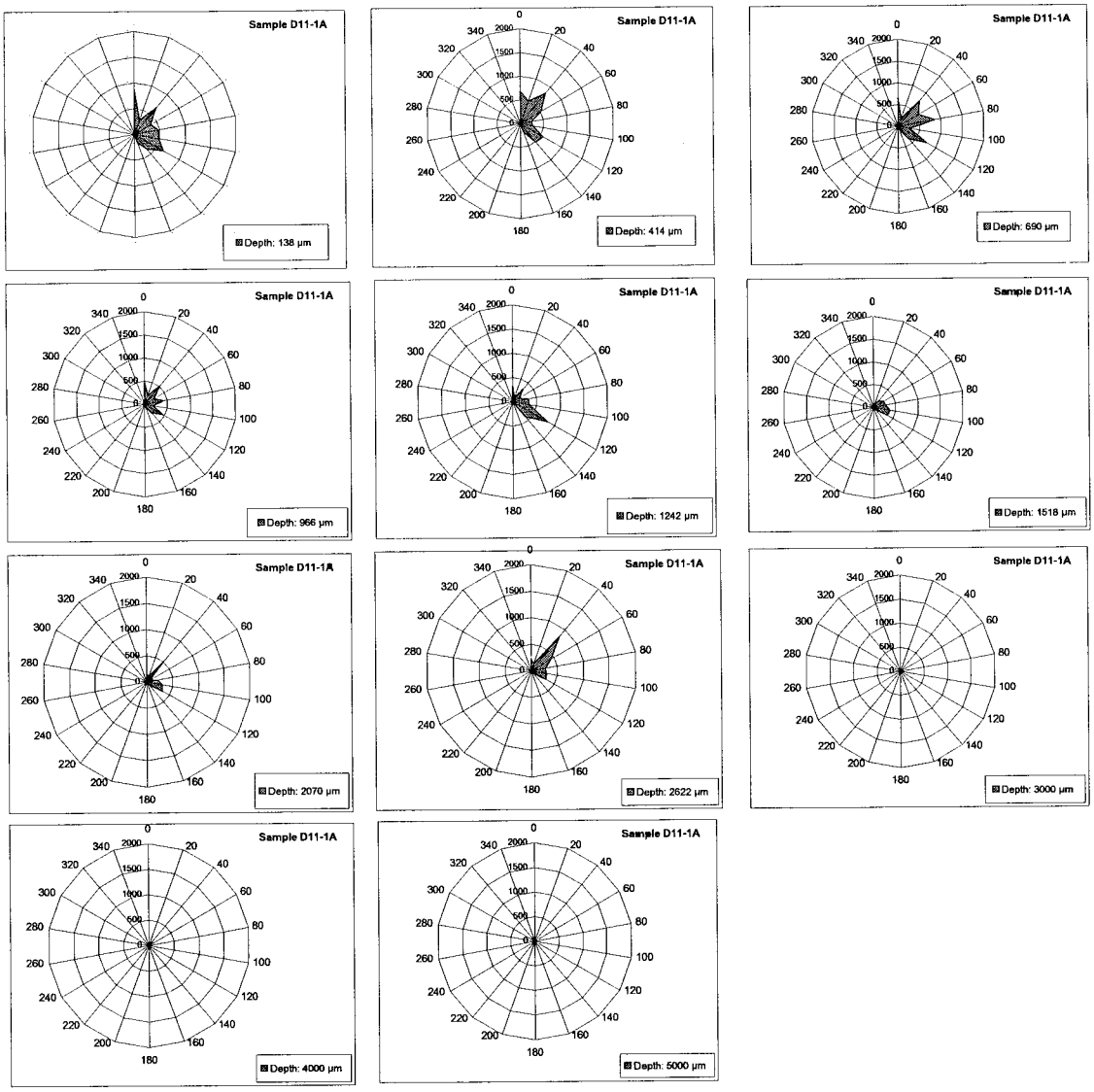

***Figure 25**. Crack orientation using Image Analysis D11-1A. Each graph represents the crack orientation in degrees vs the sum of crack traces in µm, obtained for all the images at the indicated depth.*

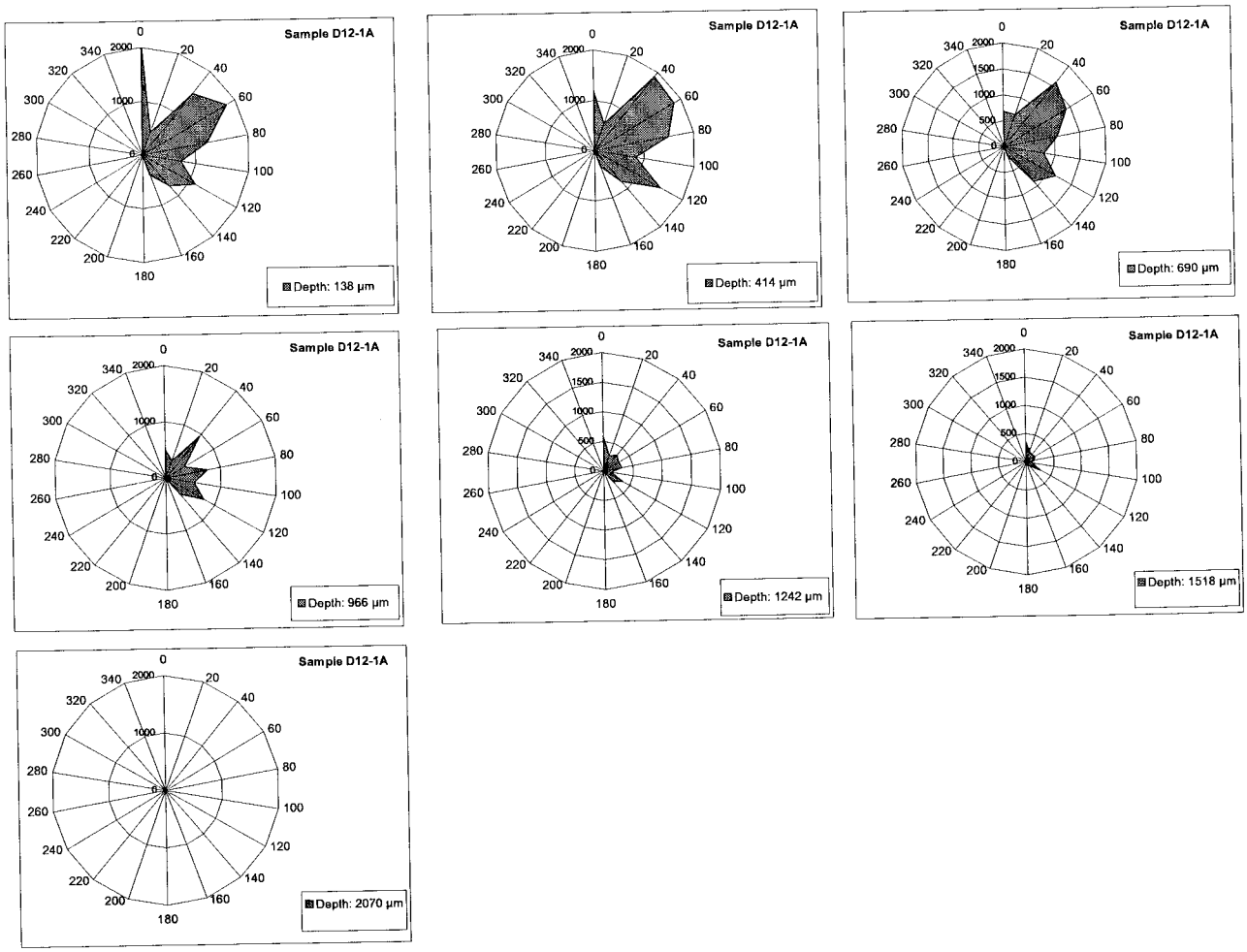

Figure 26. *Crack orientation using Image Analysis D12-1A. Each graph represents the crack orientation in degrees vs the sum of crack traces in µm, obtained for all the images at the indicated depth.*

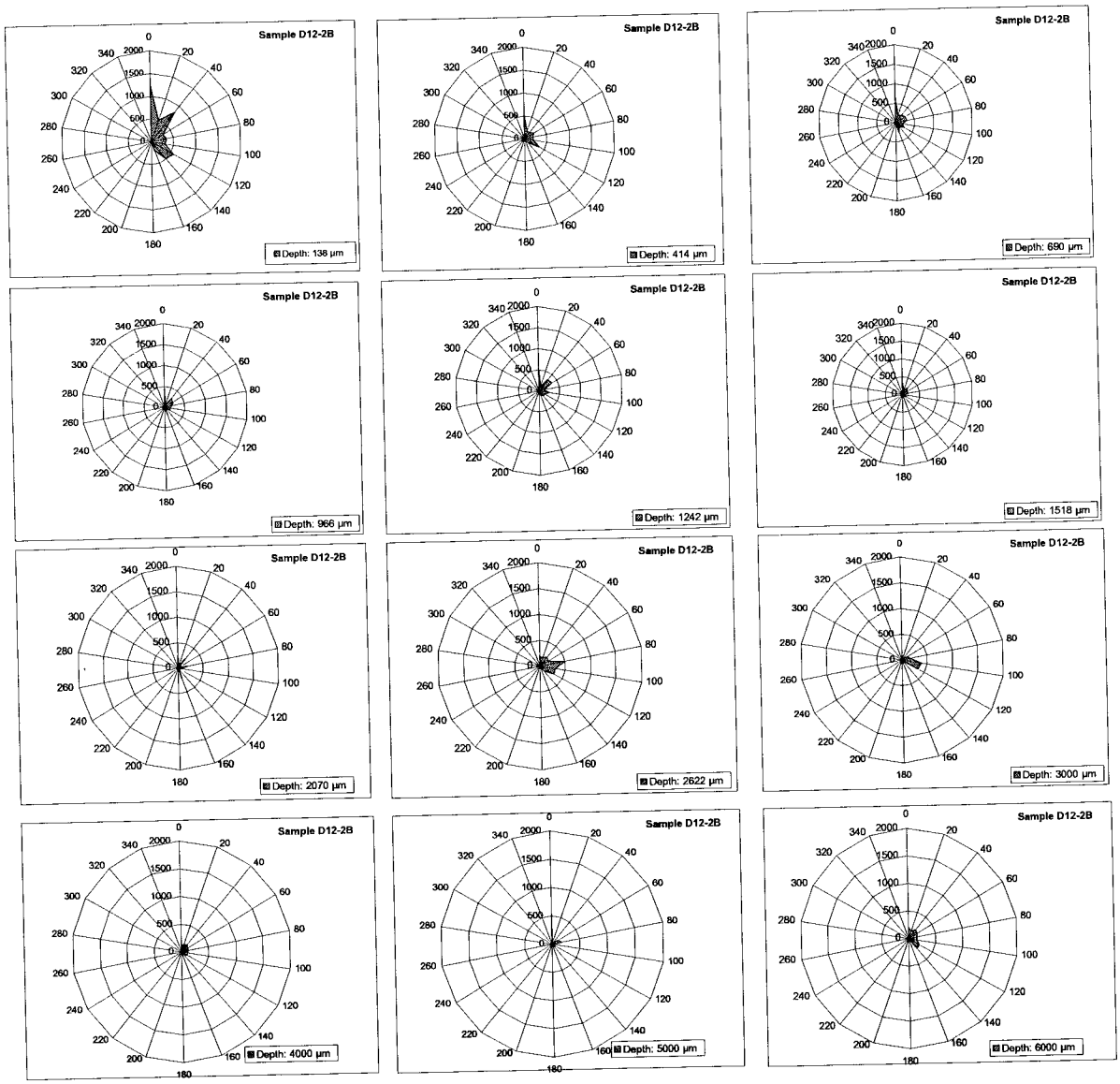

Figure 27*. Crack orientation using image analysis. D12-2B. Each graph represents the crack orientation in degrees vs the sum of crack traces in µm, obtained for all the images at the indicated depth.*

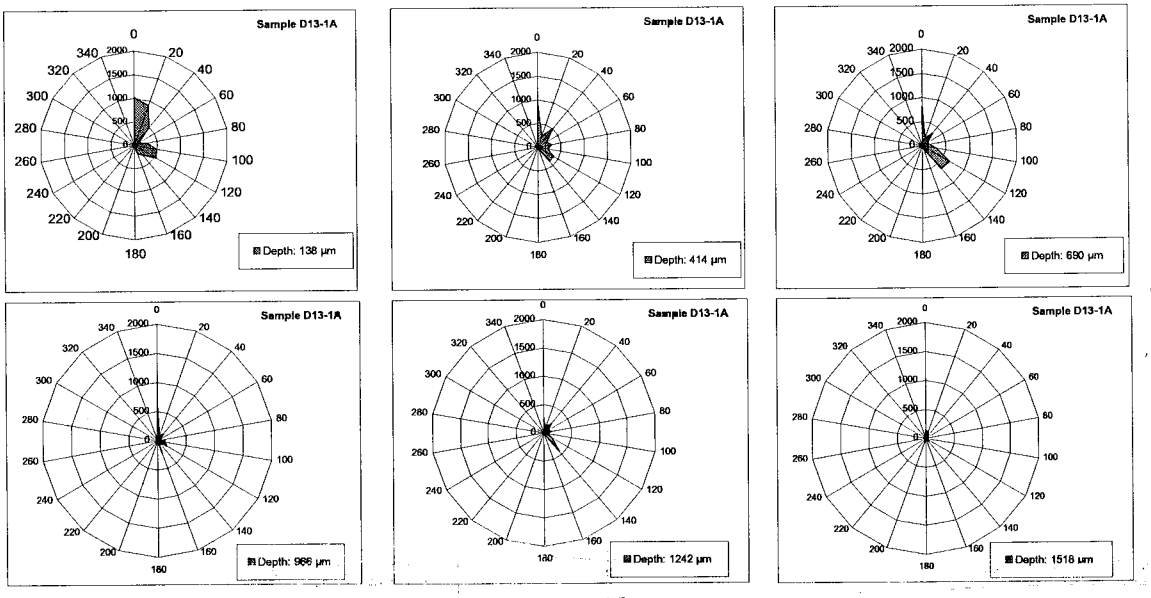

***Figure 28**. Crack orientation using Image Analysis. D13-1A. Each graph represents the crack orientation in degrees vs the sum of crack traces in µm, obtained for all the images at the indicated depth.*

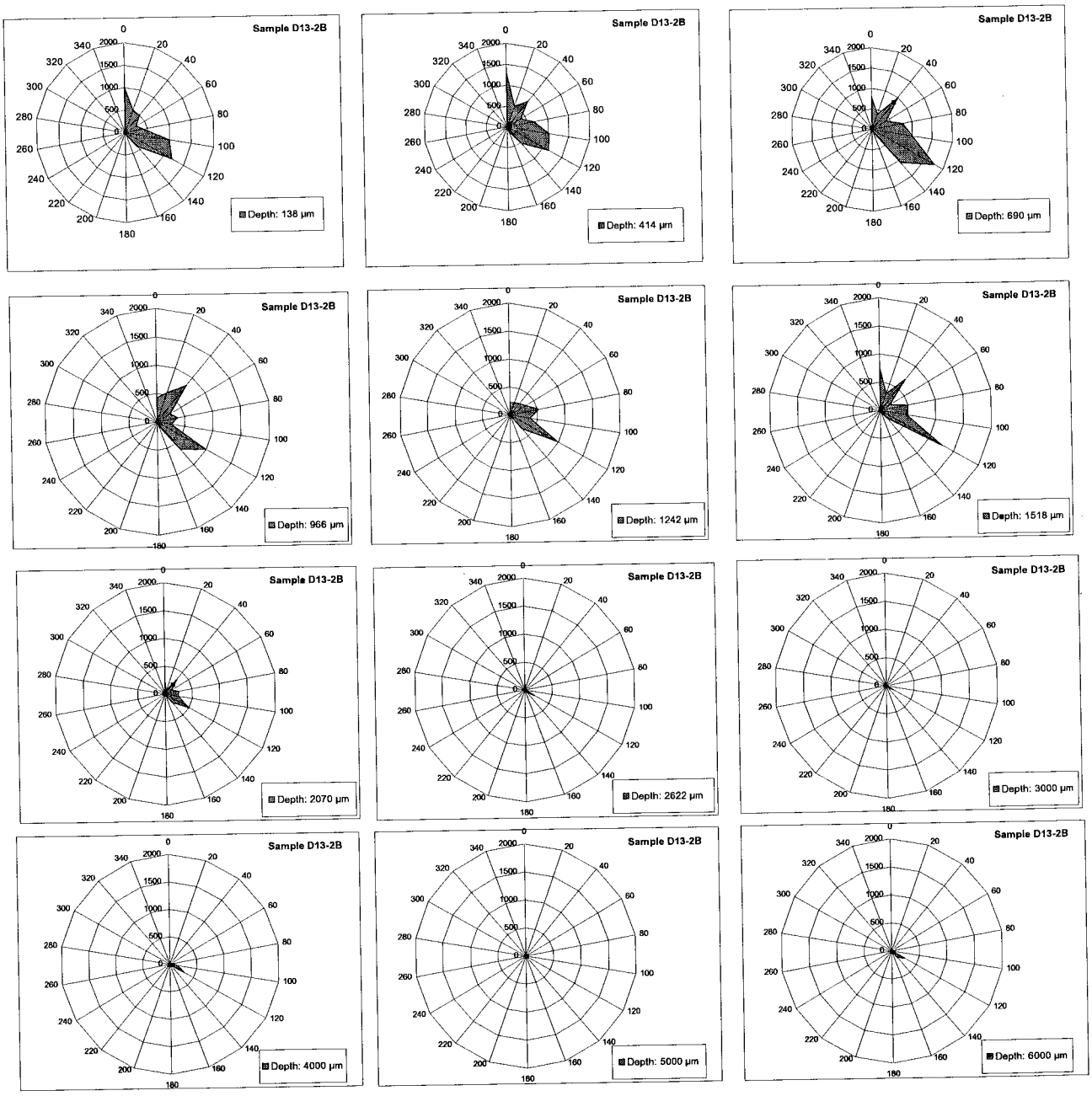

Figure 29. *Crack orientation using Image Analysis. D13-2B. Each graph represents the crack orientation in degrees vs the sum of crack traces in µm, obtained for all the images at the indicated depth.*

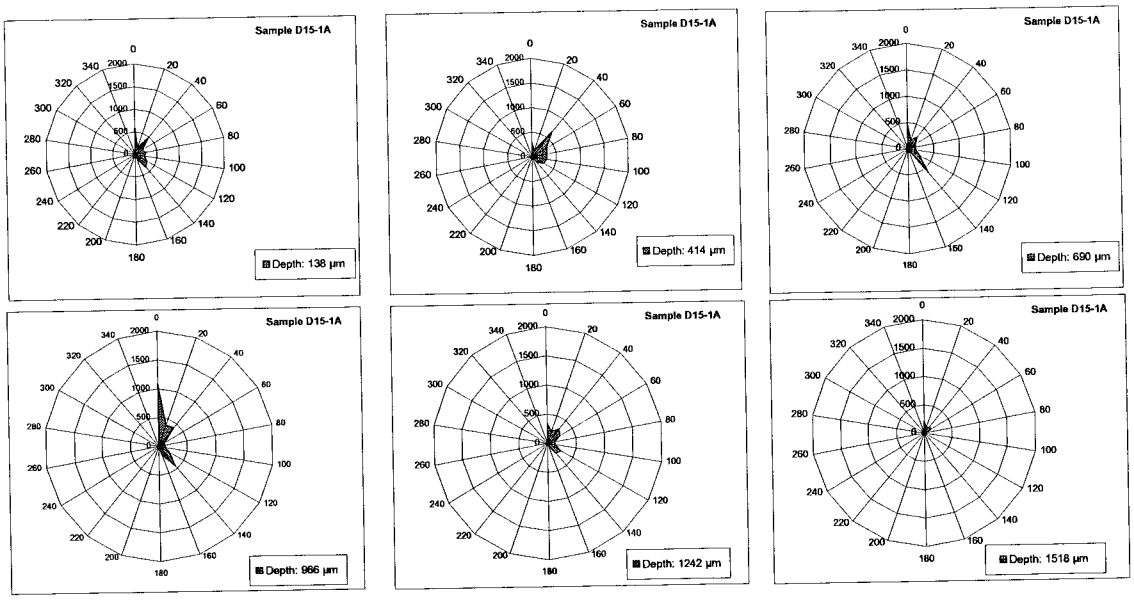

***Figure 30**. Crack orientation using Image Analysis. D15-1A. Each graph represents the crack orientation in degrees vs the sum of crack traces in µm, obtained for all the images at the indicated depth.*

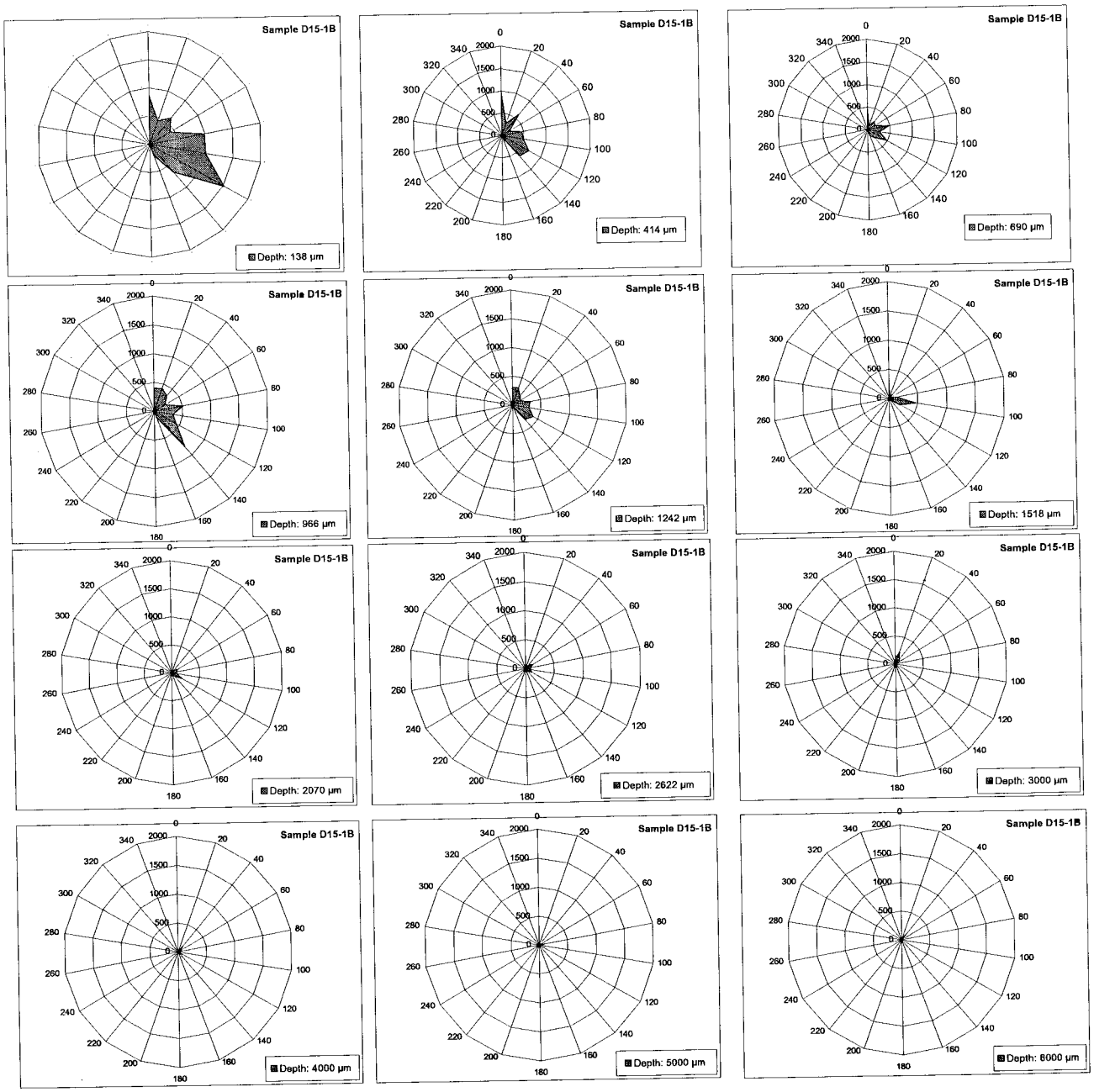

***Figure 31**. Crack orientation using Image Analysis. D15-1B. Each graph represents the crack orientation in degrees vs the sum of crack traces in µm, obtained for all the images at the indicated depth.*

2.1.3. Crack specific surface

2.1.3.1 Crack specific surface using stereology

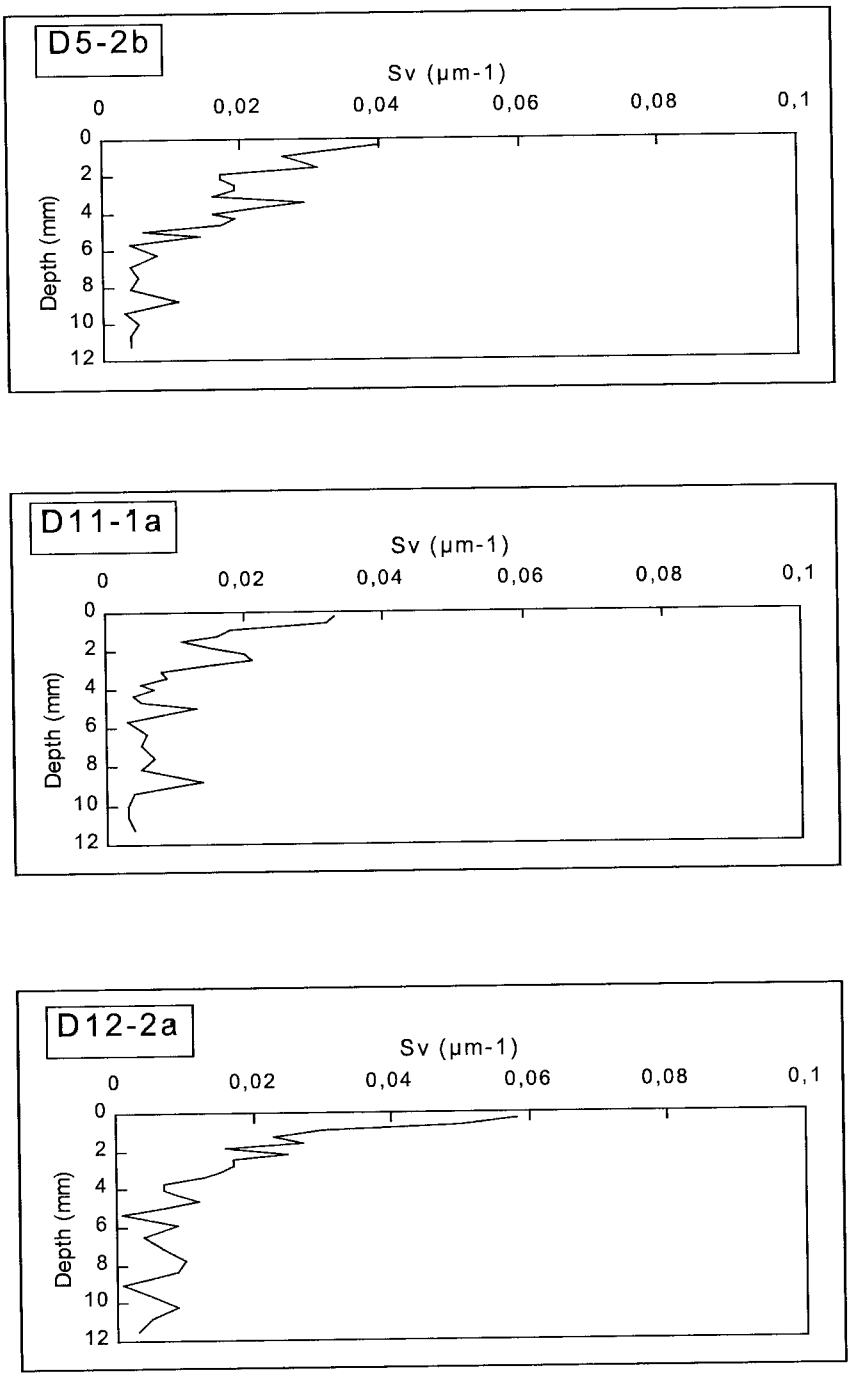

Figure 32. *Total Crack Specific Surface (Sv) using Stereology. D5-2b (top), D11-1a (middle) and D12-2a (bottom).*

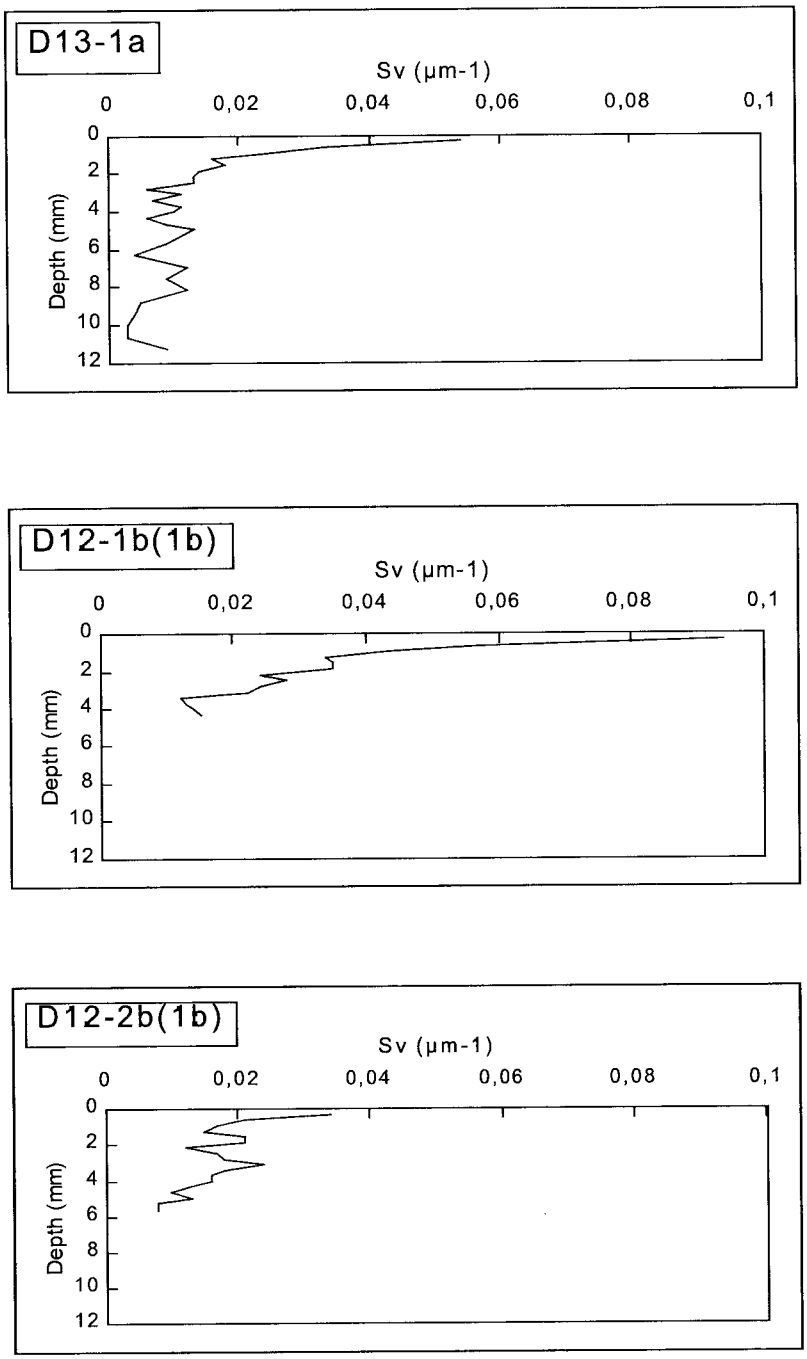

***Figure 33**. Total Crack Specific Surface (Sv) using Stereology. D13-1a (top), D12-1b (1b) (middle) and D12-2b (1b) (bottom).*

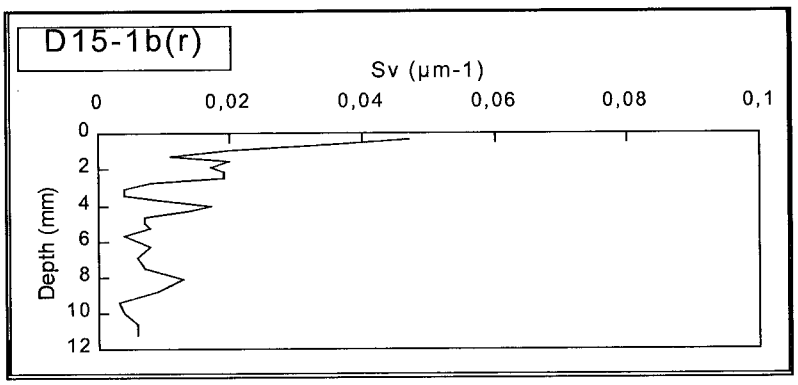

Figure 34. *Total Crack Specific Surface (Sv) using Stereology D15-1b (r).*

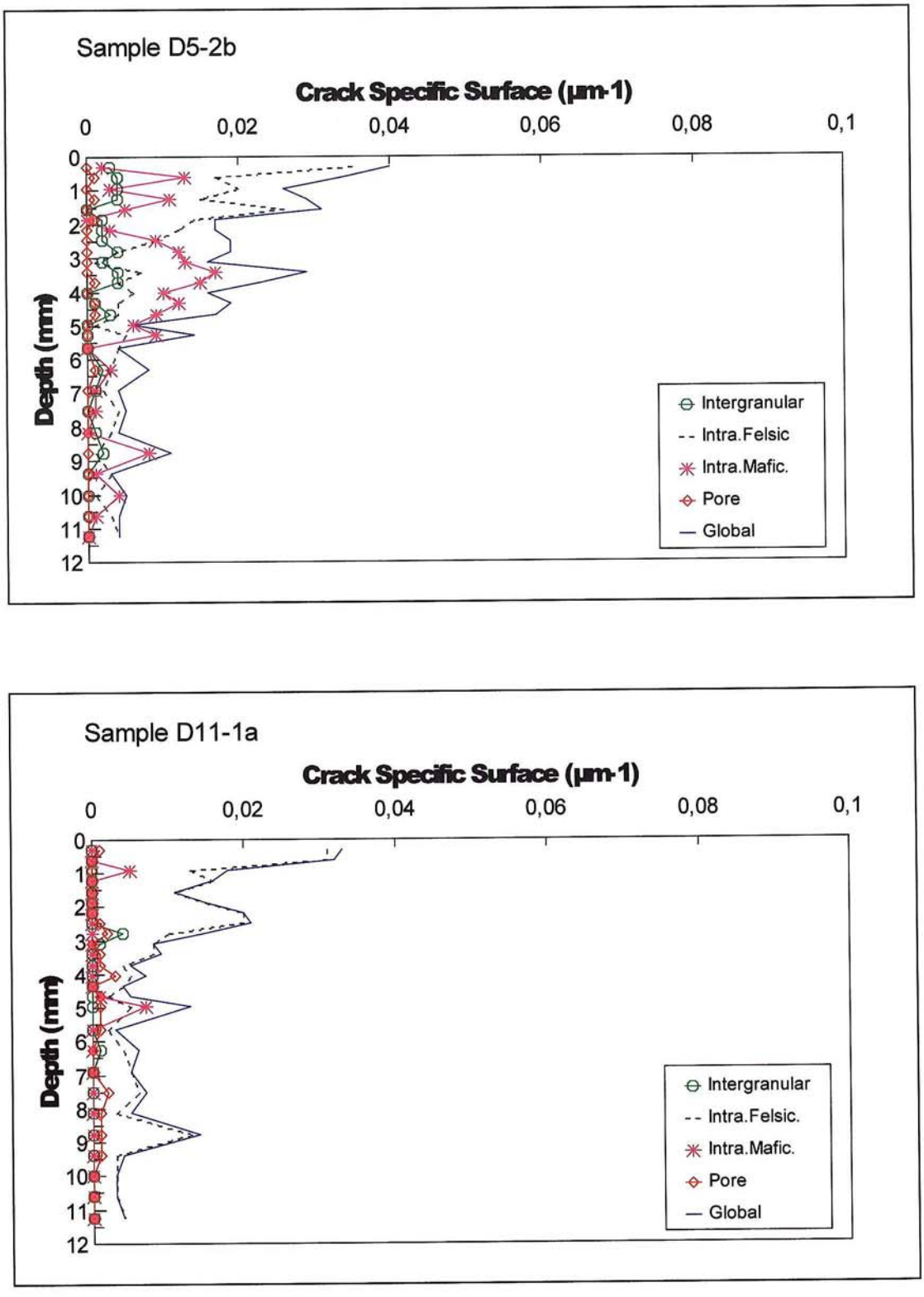

***Figure 35**. Crack Specific Surface using stereology of samples D5-2b (top) and D11-1a (bottom) according to its textural position in relation to two mineral clusters: felsic and mafic.*

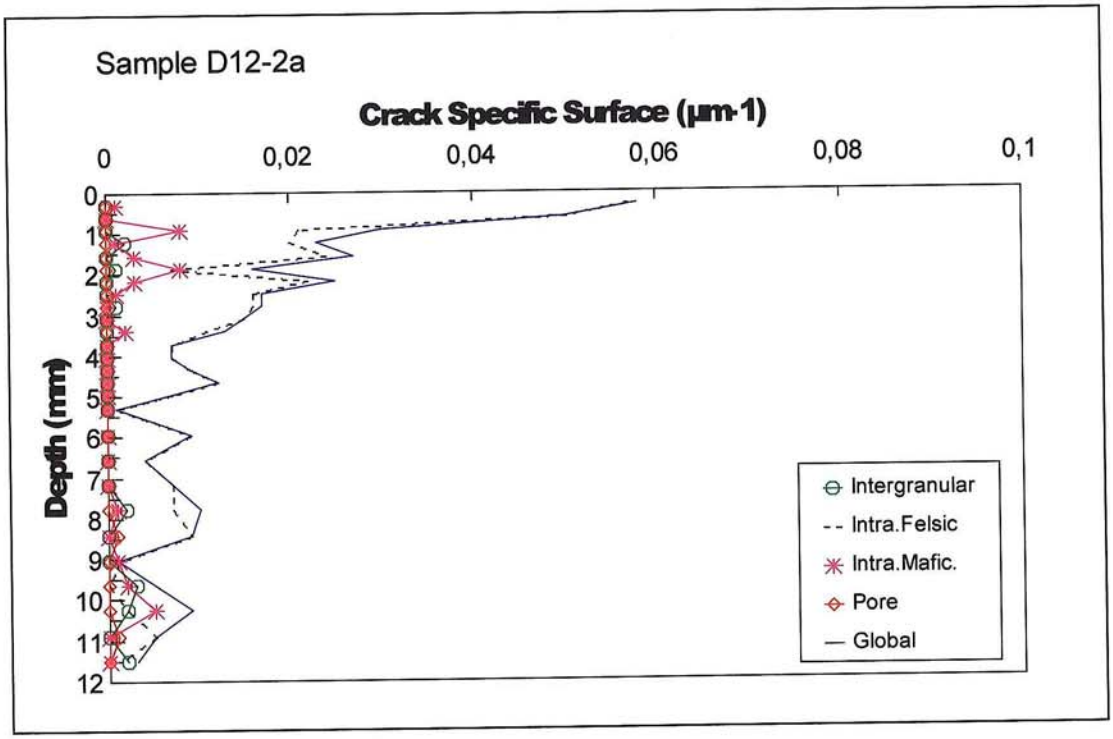

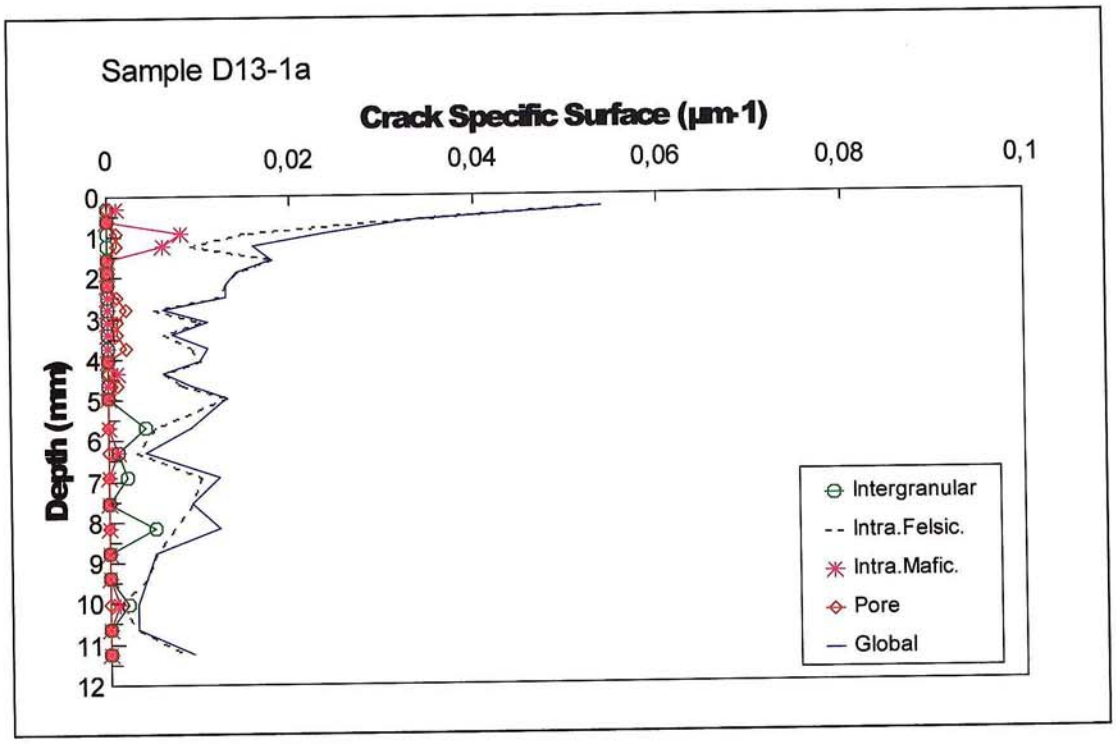

***Figure 36**. Crack Specific Surface using stereology of samples D12-2a (top) and D13-1a (bottom) according to its textural position in relation to two mineral clusters: felsic and mafic.*

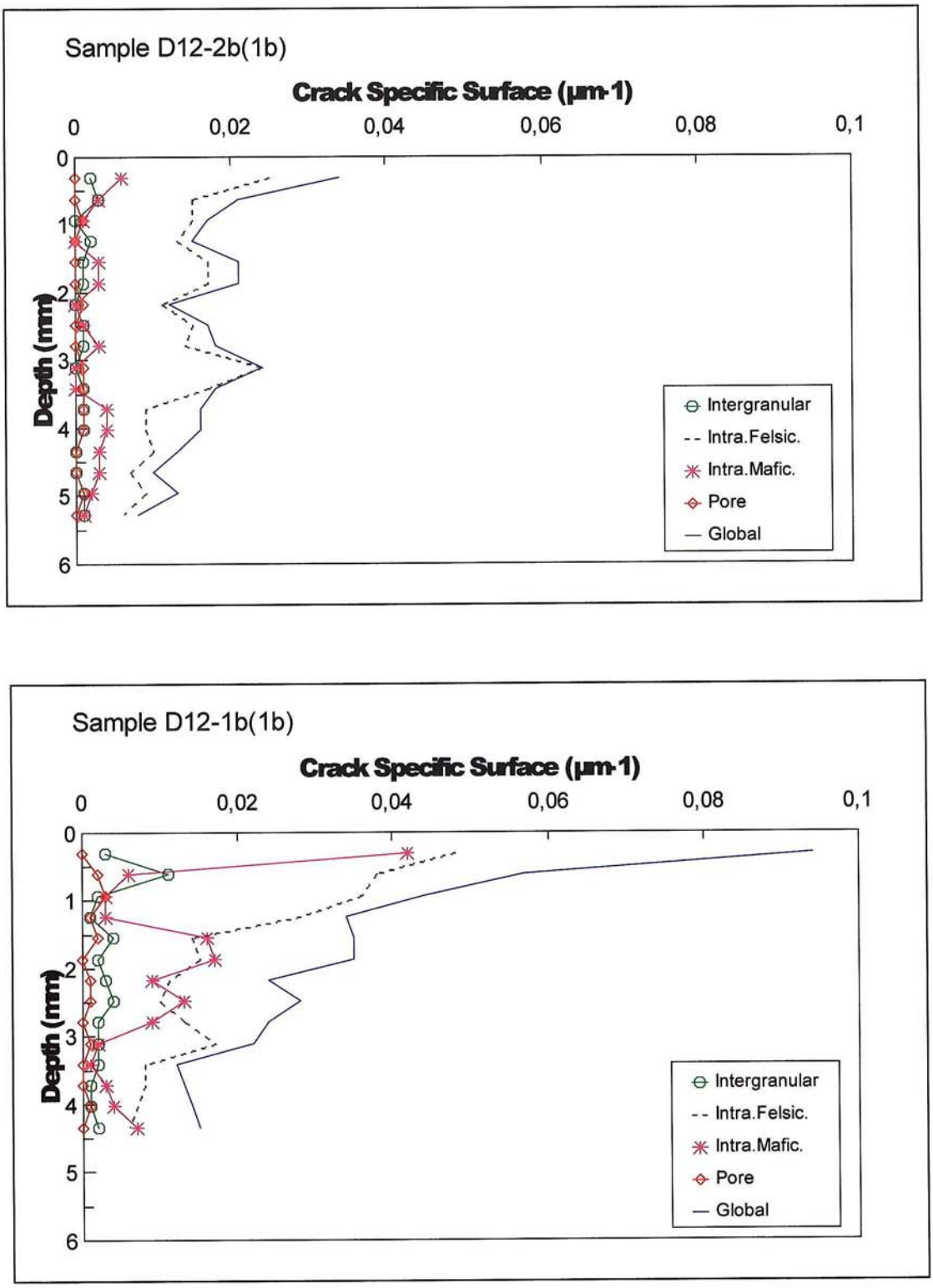

***Figure 37**. Crack Specific Surface using stereology of samples D12-2b(1b) (top) and D12-1b(1b) (bottom) according to its textural position in relation to two mineral clusters: felsic and mafic.*

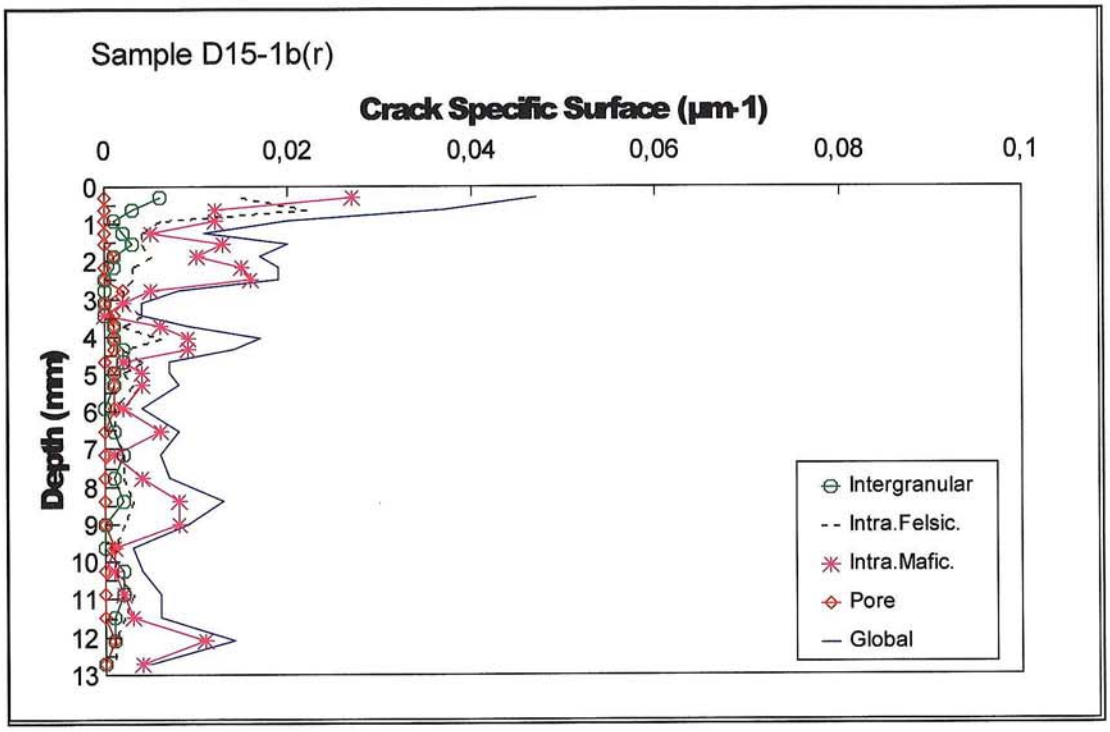

Figure 38. *Crack Specific Surface using stereology of sample D15-1b(r) according to its textural position in relation to two mineral clusters: felsic and mafic. For a better identification of the rock-forming minerals, X-ray analysis was used in this sample.*

2.1.3.2 Crack Specific Surface using Image Analysis

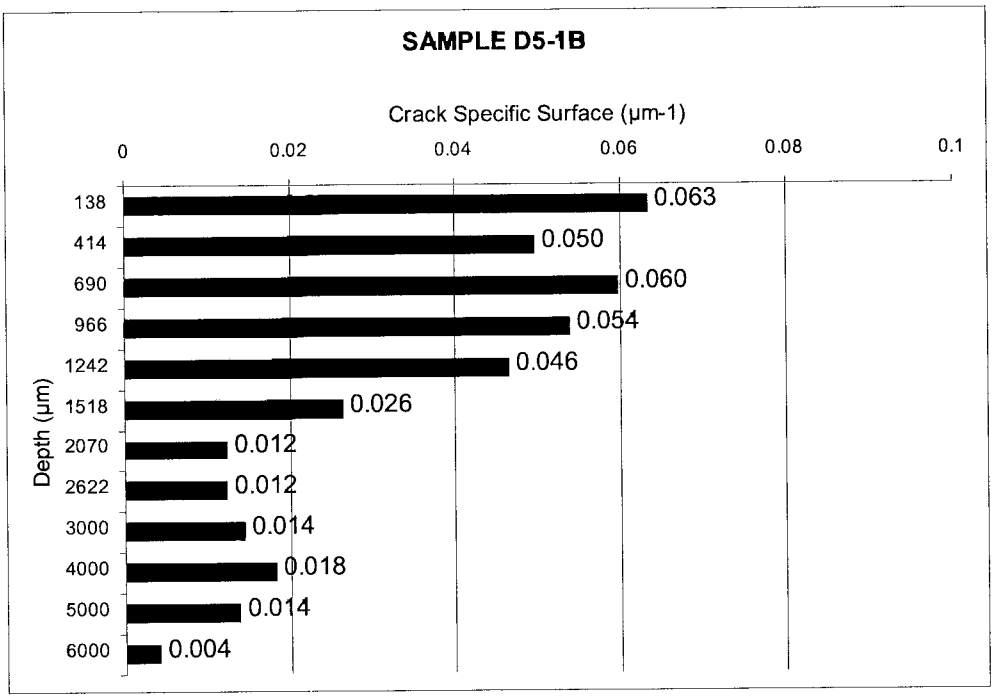

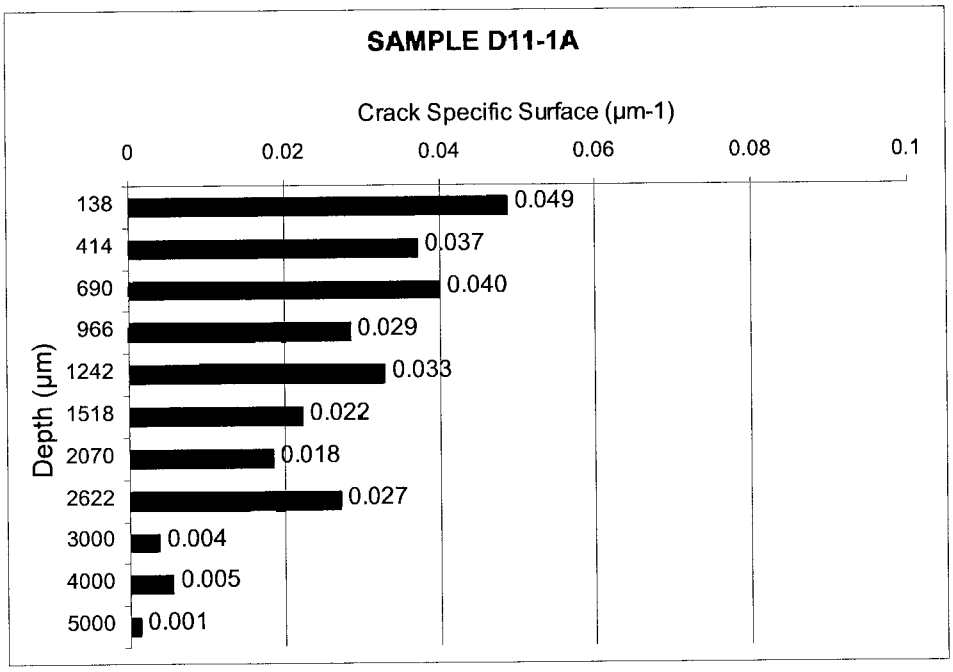

Figure 39. *Crack Specific Surface using Image Analysis. D5-1b (top) and D11-1a (bottom). Each bar represents the mean crack specific surface obtained for all the images at the same depth.*

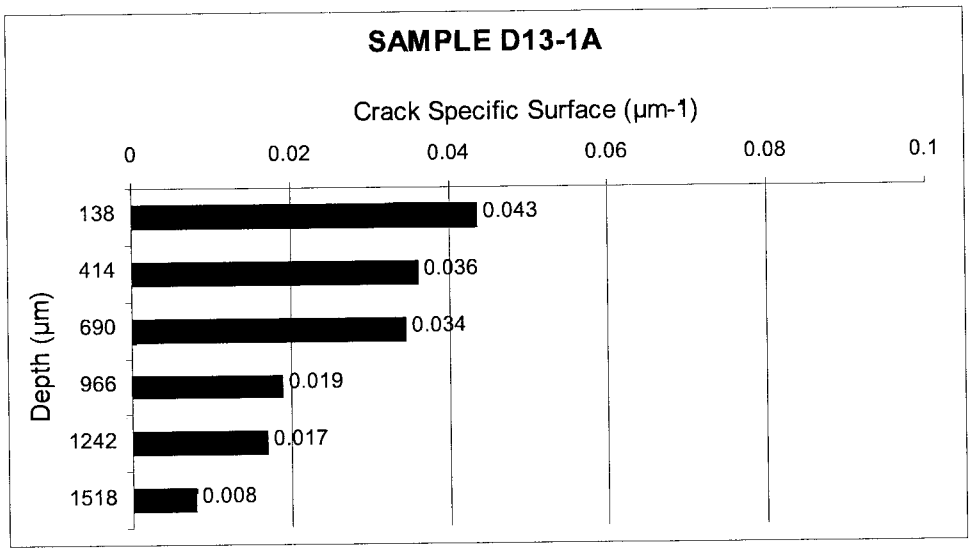

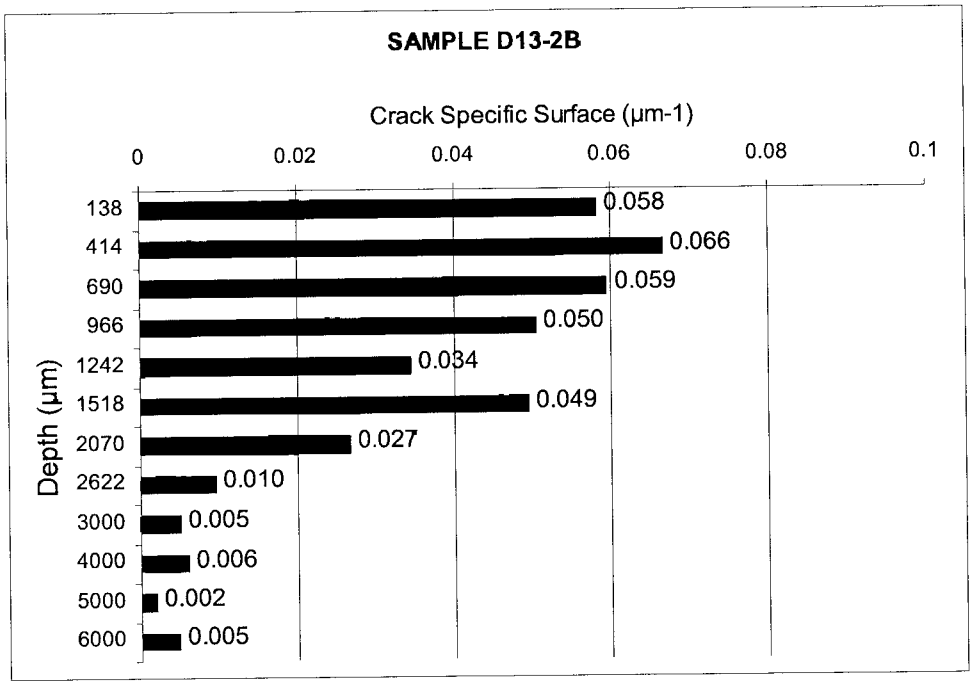

***Figure 40**. Crack Specific Surface using Image Analysis. D13-1A (top) and D13-2B (bottom). Each bar represents the mean crack specific surface obtained for all the images at the same depth.*

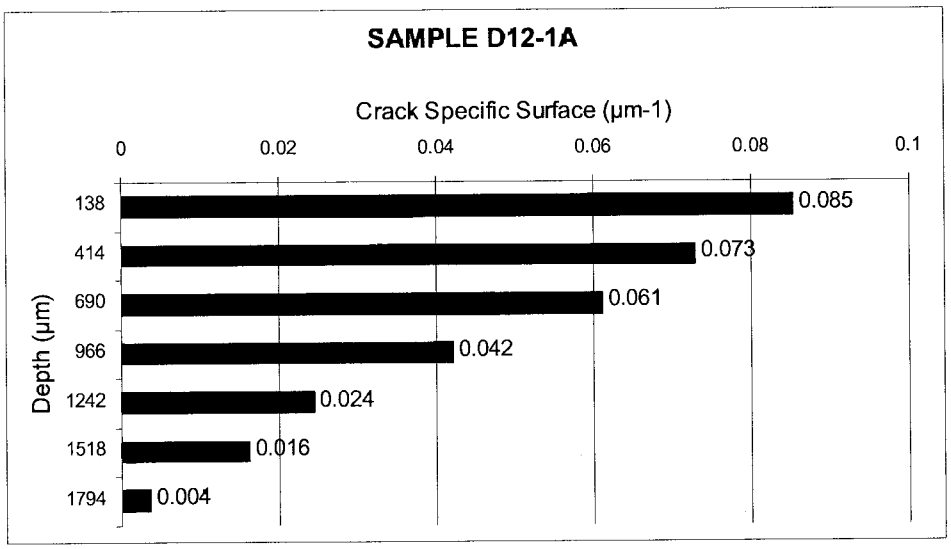

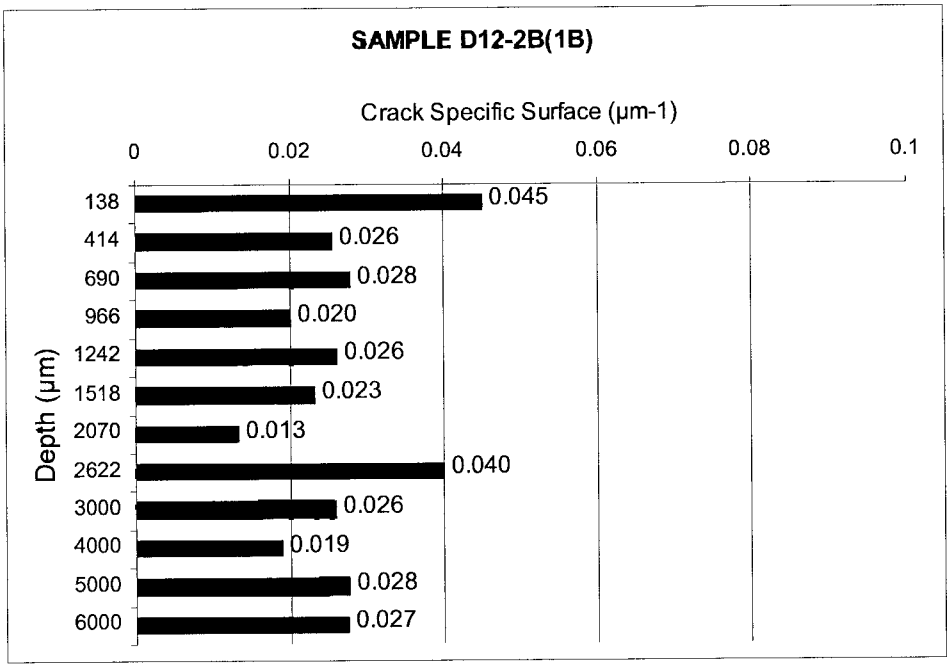

***Figure 41**. Crack Specific Surface using Image Analysis. D12-1A (top) and D12-2B(1B) (bottom). Each bar represents the mean crack specific surface obtained for all the images at the same depth.*

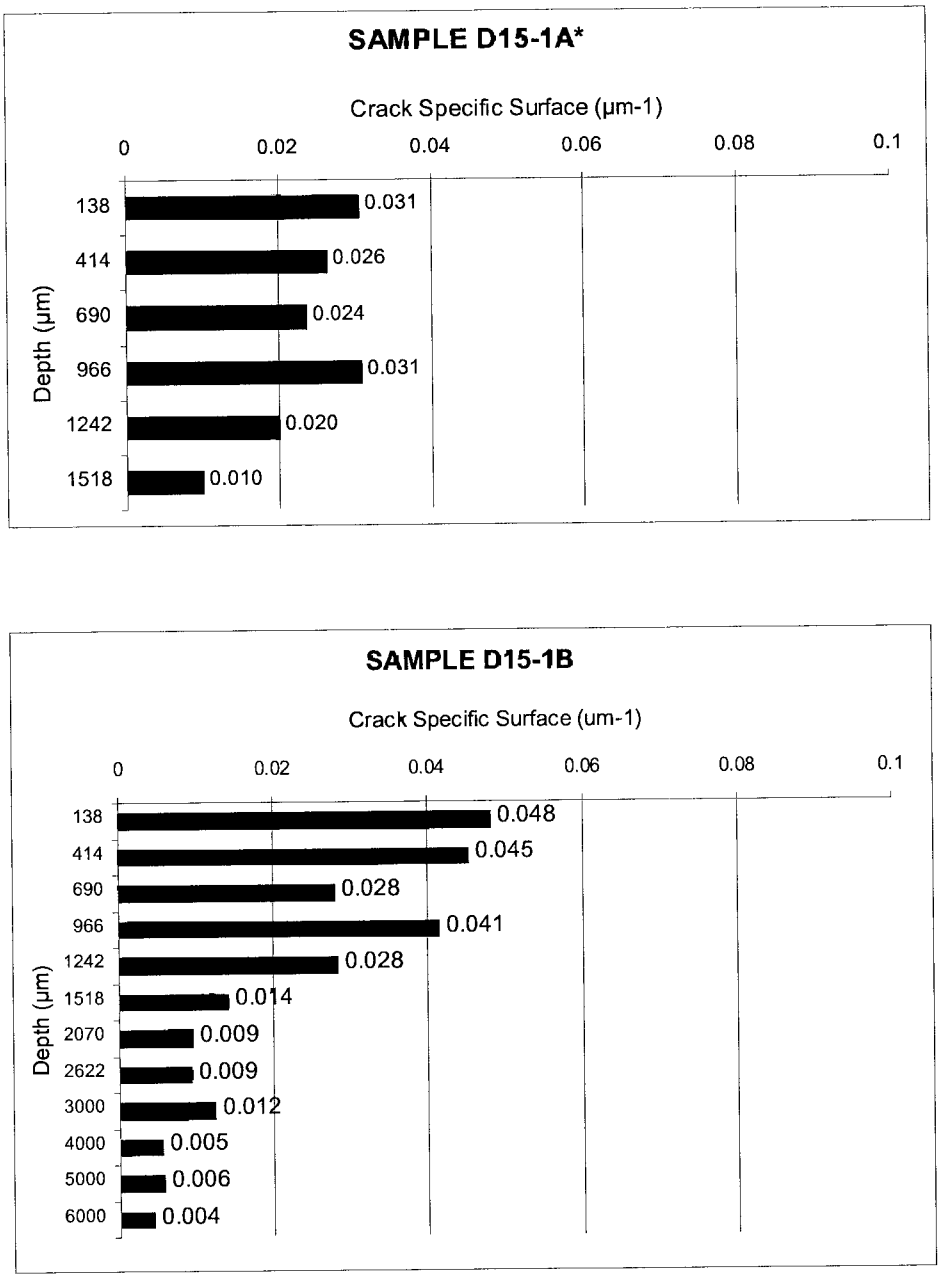

Figure 42. *Crack specific surface using Image Analysis. D15-1A* (top) and D15-1B (bottom). Each bar represents the mean crack specific surface obtained for all the images at the same depth.*

The Sv values in the disturbed zone of all the samples are relatively low. It ranges between 0.03 m^{-1} (in samples D-11and D15) and 0.09 m^{-1} (in one of the sections from sample D-12). In all cases, Sv values falls very fast after the first 3-4 mm and keeps at relatively low values (between 0.005 and 0.01 m^{-1}) from the 4 to 12 mm of depth for all the samples.

Most of Sv in all the samples is of intragranular type. At this point, it would be worth to notice that, when counting for stereological estimation of Sv, any intersection between a cycloid line and a microcrack trace is considered as inter or intragranular just depending on the characteristics at that point; that is, a crack that in part runs between nests of mafic and felsic minerals is only considered as intergranular if the intersection with a cycloid line is produced in this length; otherwise is considered as intragranular when the intersections occurs when the crack runs inside a nest of minerals.

The breakdown of the Sv values in relation to the mineralogy carried out by stereology has raised some problems that could be solved in a higher time-consuming study.

The best procedure is to count intersections of the grid system with the crack traces in an image under CLSM (the best technique to image cracks) and to check their relation with the mineralogy in the same field imaged under transmitted light polarising microscopy (the best technique to identify the mineralogy).This detailed procedure implies the use of a microscope able to alternate from CLSM to polarising microscopy and viceversa in every field of view; obviously, the procedure is extremely time-consuming.

Other possibility is to use scanning electron microscopy as we did in this study: the backscattered electron (BSE) images are best suited to discriminate minerals, or better, groups of minerals (in fact we had decided to distinguish only felsic and mafic minerals).But for cracks as narrow as 1 micron in aperture, this BSE emission may represent a problem because it is not the best technique to obtain a good topographic contrast; for this reason we have studied images with a mix of 50 % of the secondary electron (SE) images and the other 50 % of BSE. At the same time the use of BSE requires a thinner conductive layer, but such a thin layer represents a problem for imaging very thin cracks.

Nevertheless we have found other kind of problems: in some cases it is difficult to discriminate between biotite and plagioclase, as can be seen in figure 43 where only the exfoliation of the biotite make possible to distinguish from the plagioclase. Although this image has been obtained under secondary and backscattered electrons, the problem can also appear in 100 % backscattered images, figure 44.

As a consequence, energy dispersive X-ray analysis was sometimes used (fig. 44) to identify the rock-forming minerals; nevertheless, as it is a highly time-consuming task, only it was used for sample (D15-1b(r)) here provided.

Therefore, the numerical values for the crack specific surface (Sv) for mafic minerals (biotite and amphibole) using stereology, here reported, could be underestimated; consequently, the felsic minerals (quartz and plagioclase) could be overestimated. In any case the Sv for amphibole is, in general, very low.

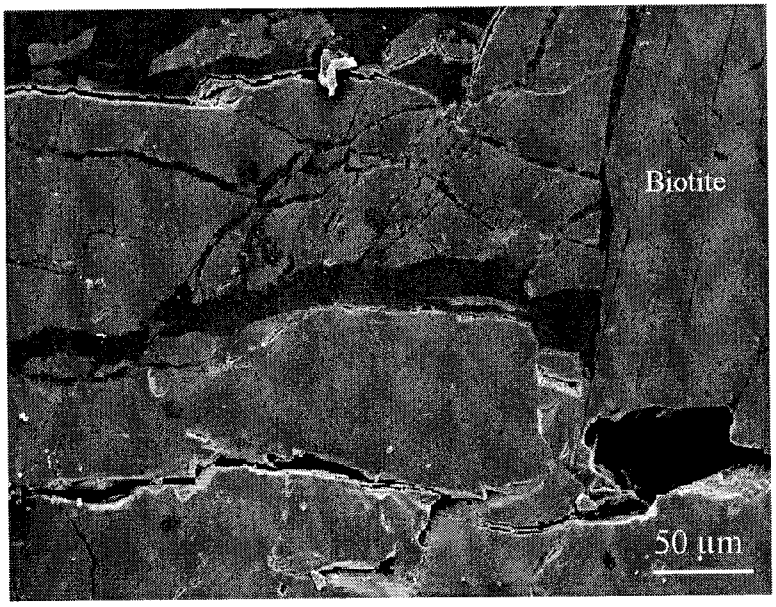

***Figure 43**. SEM image of a sample showing the similar emission of felsic minerals and biotite.*

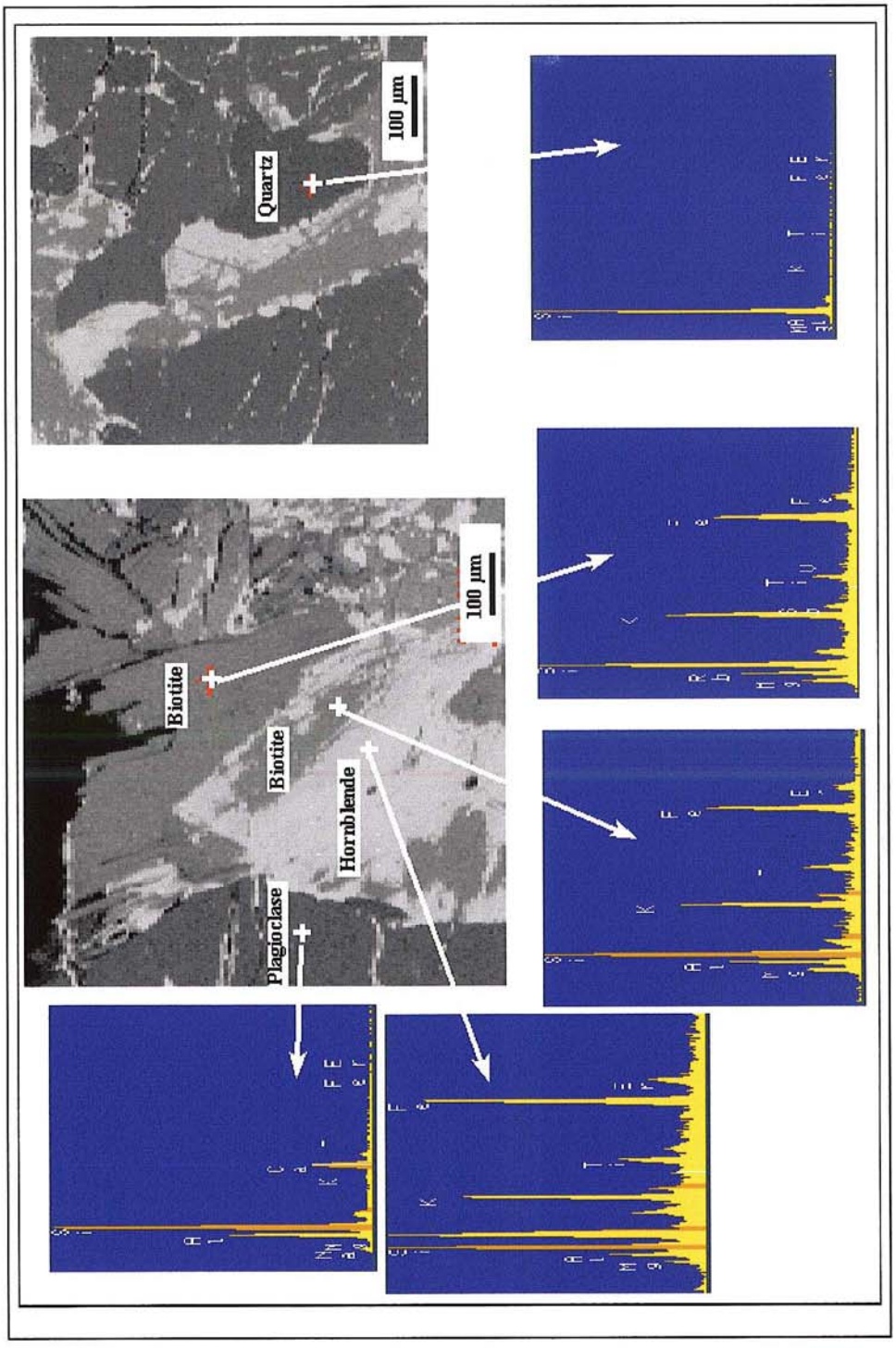

Figure 44. *BSEM images and X-ray energy dispersive analysis for a complete discrimination between the different rock-forming minerals present.*

2.1.4 Crack aperture

2.1.4.1 Crack aperture using Image Analysis

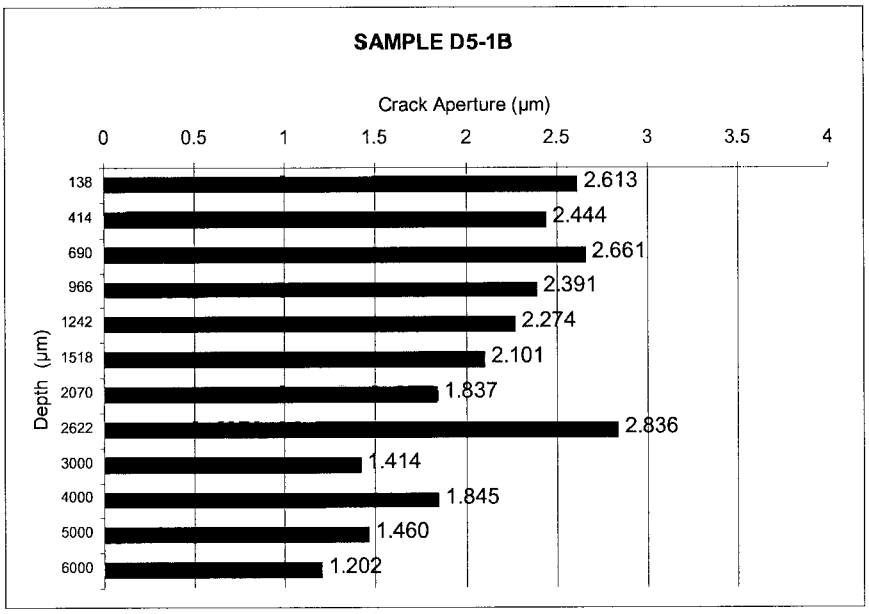

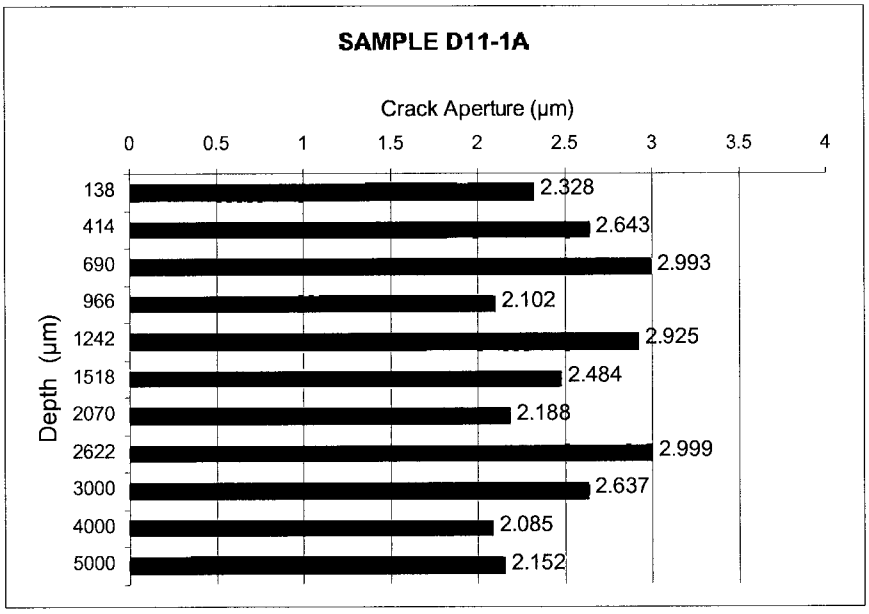

***Figure 45**. Crack aperture using Image Analysis. D5-1B (top) and D11-1A (bottom). Each bar represents the mean crack aperture obtained for all the images at the same depth.*

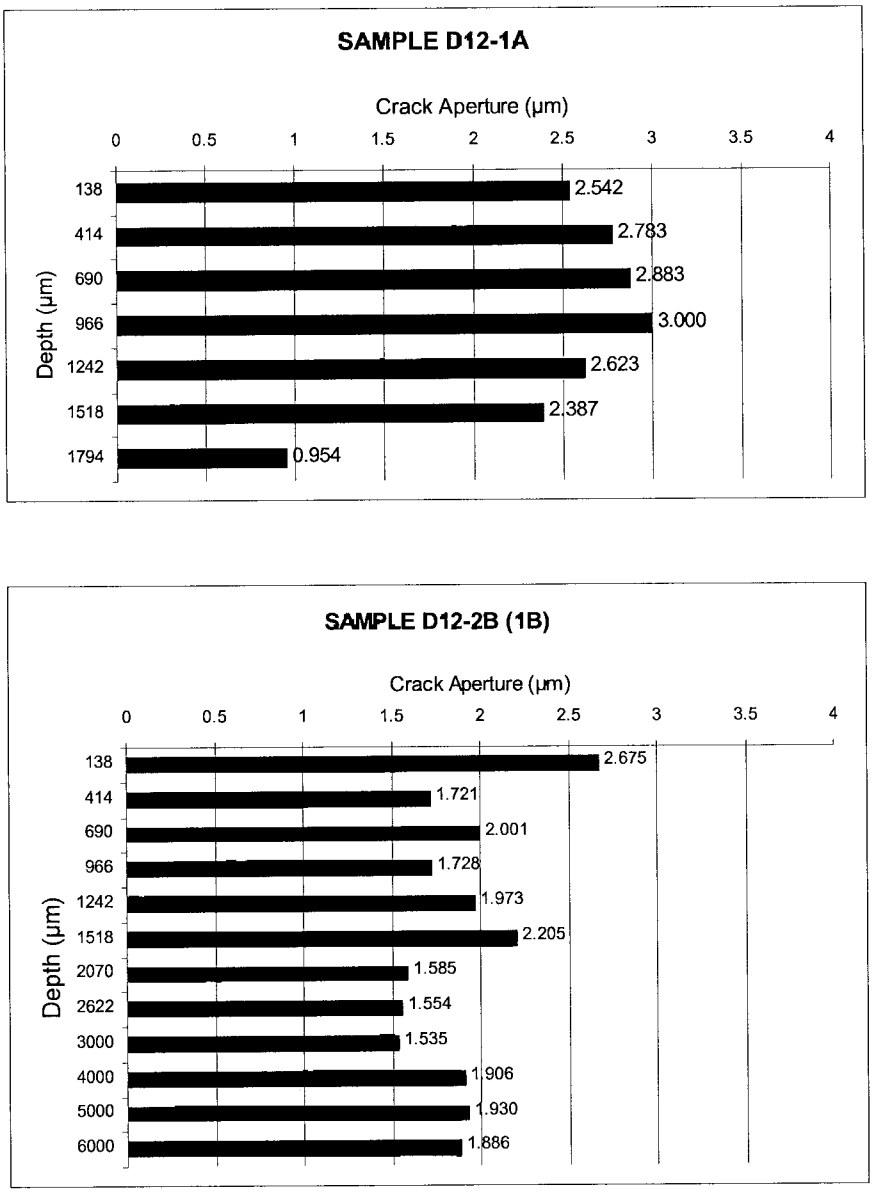

Figure 46. *Crack aperture using Image Analysis. D12-1A (top) and D12-2B(1B) (bottom). Each bar represents the mean crack aperture obtained for all the images at the same depth.*

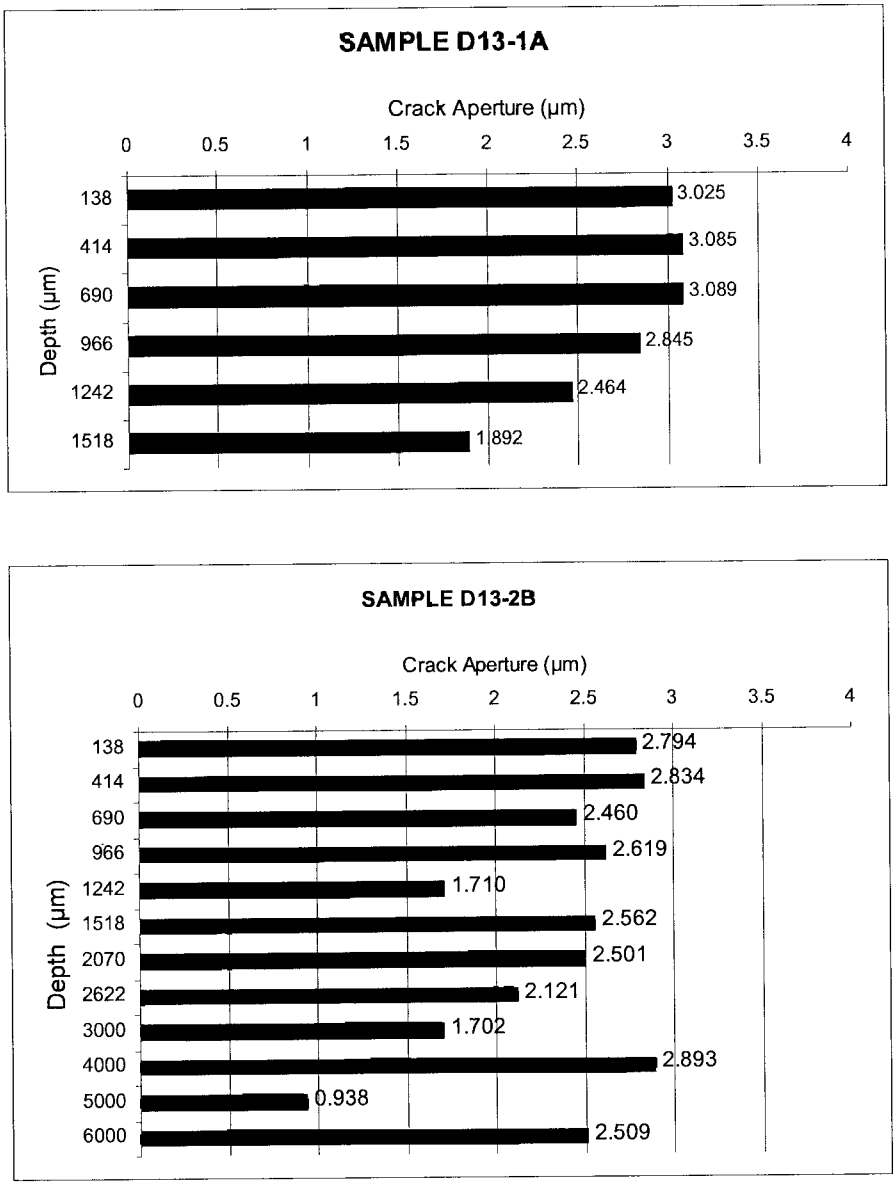

Figure 47. *Crack aperture using Image Analysis. D13-1A (top) and D13-2B (bottom). Each bar represents the mean crack aperture obtained for all the images at the same depth.*

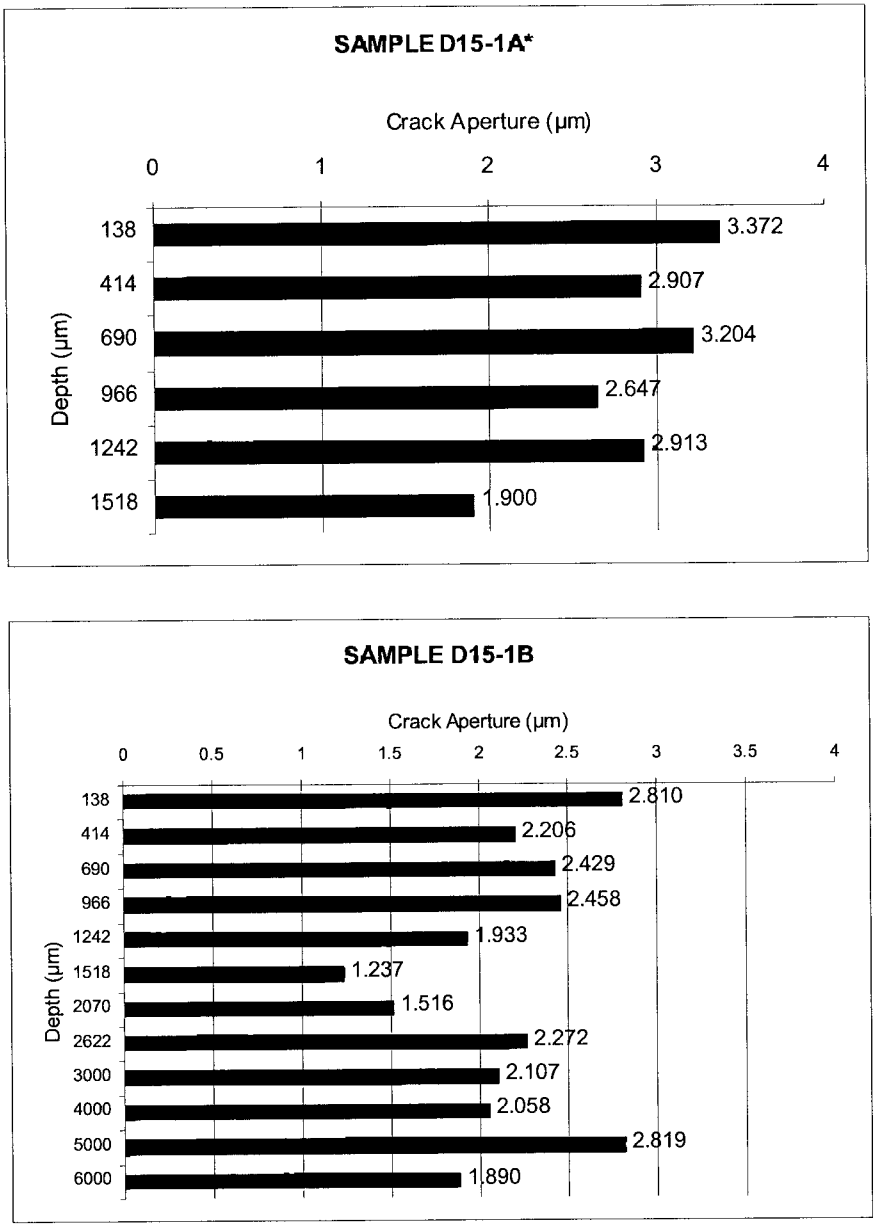

Figure 48. *Crack aperture using Image Analysis. D15-1A* (top) and D15-1B (bottom). Each bar represents the mean crack aperture obtained for all the images at the same depth.*

2.1.4.2 *Crack Aperture distribution (%) using Image Analysis*

The narrower cracks (up to a maximum of 5.4 μm in thickness) forms more than 90 % of the total crack population. It can not be observed a high variation of the mean crack aperture with depth.

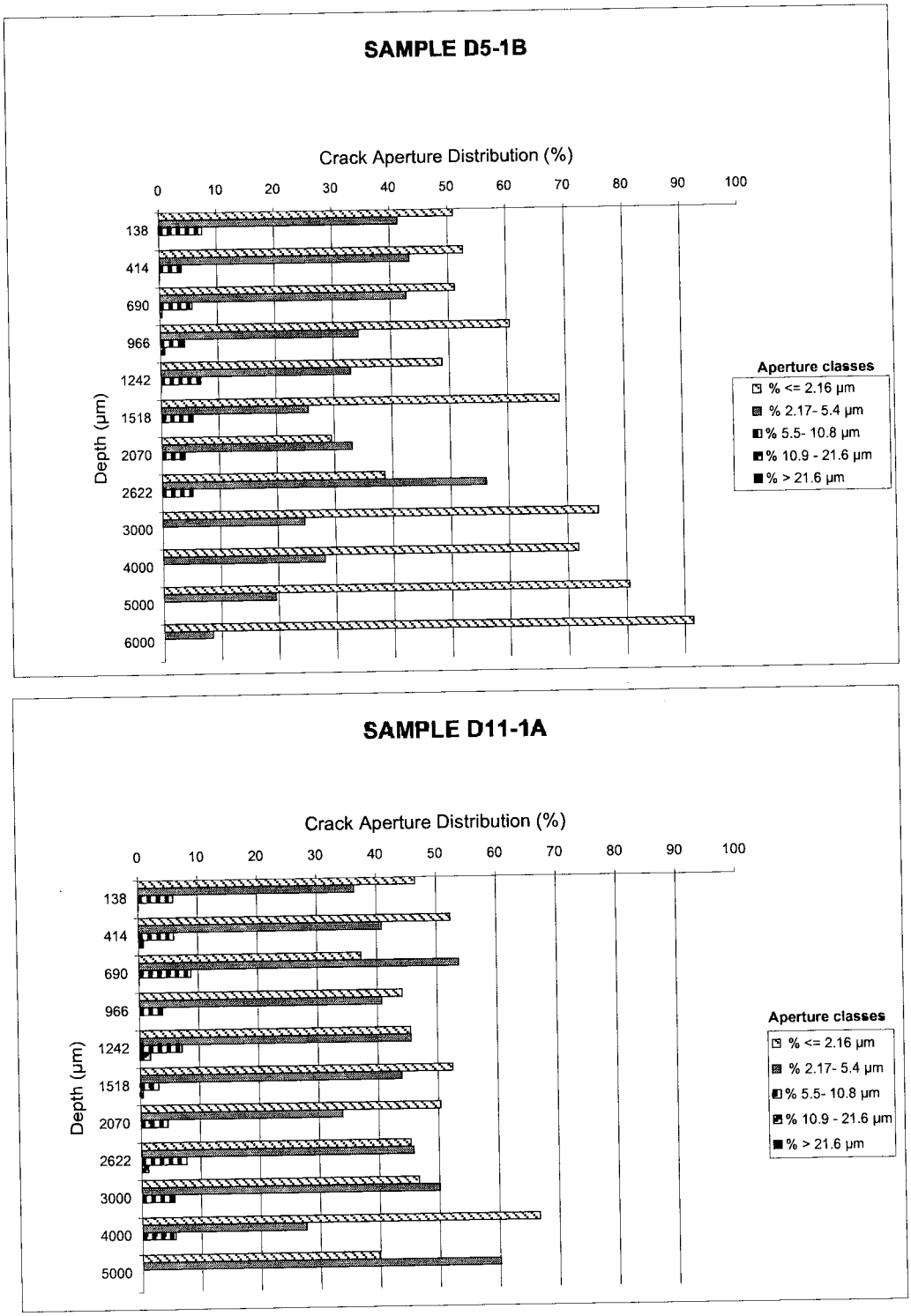

***Figure 49**. Crack aperture distribution using Image Analysis. D5-1B(top) and D11-1a (bottom). Each bar represents the percentage of crack aperture inside each of the five defined classes, obtained for all the images at the same depth.*

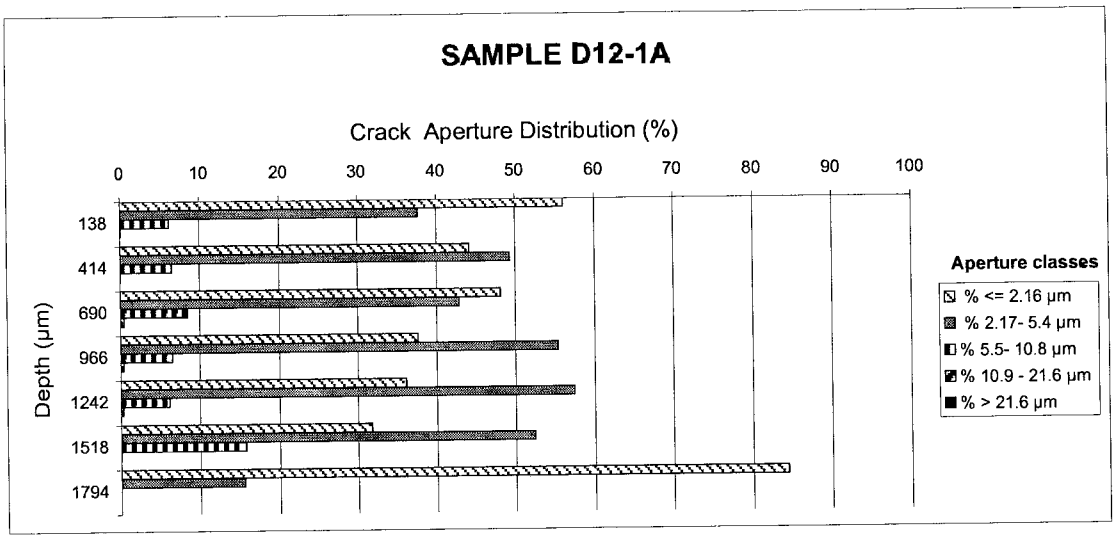

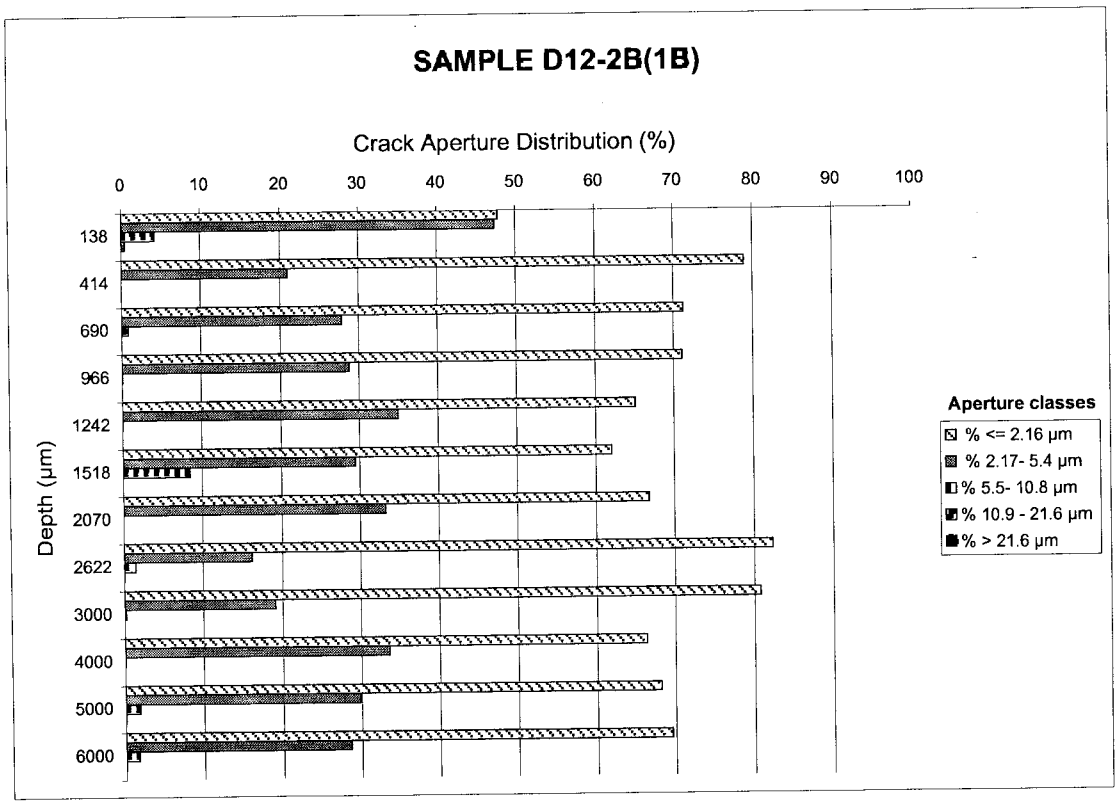

***Figure 50**. Crack aperture distribution using Image Analysis. D12-1A (top) and D12-1B(1B) (bottom). Each bar represents the percentage of crack aperture inside each of the five defined classes, obtained for all the images at the same depth.*

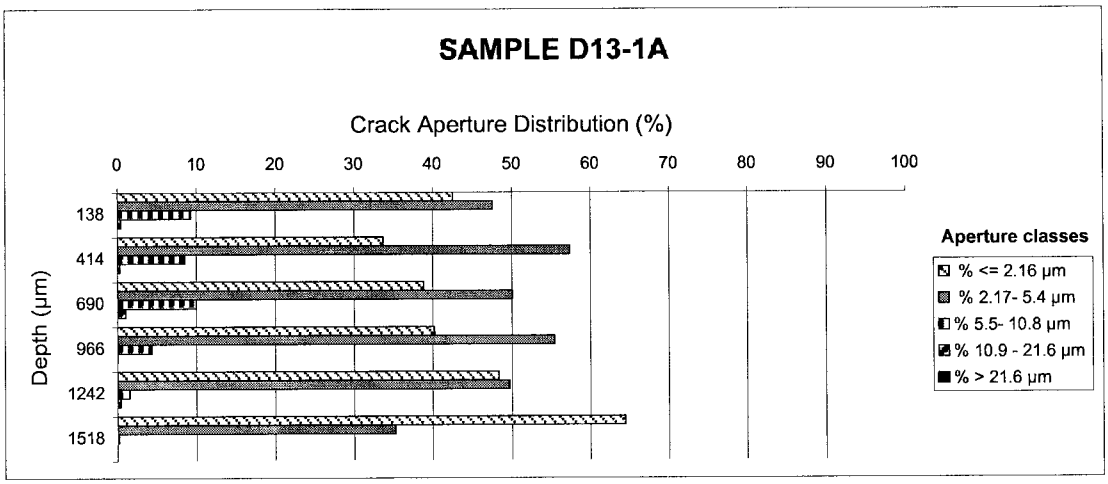

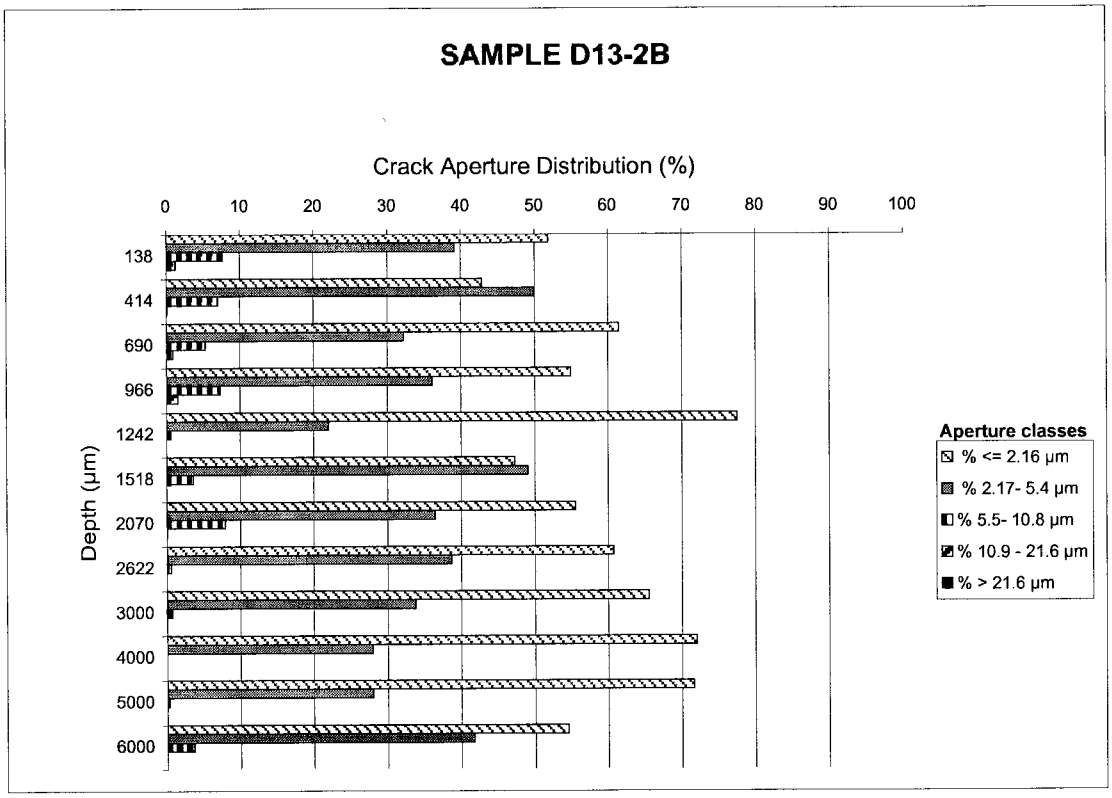

***Figure 51**. Crack aperture distribution using Image Analysis. D13-1A (top) and D13-2B (bottom). Each bar represents the percentage of crack aperture inside each of the five defined classes, obtained for all the images at the same depth.*

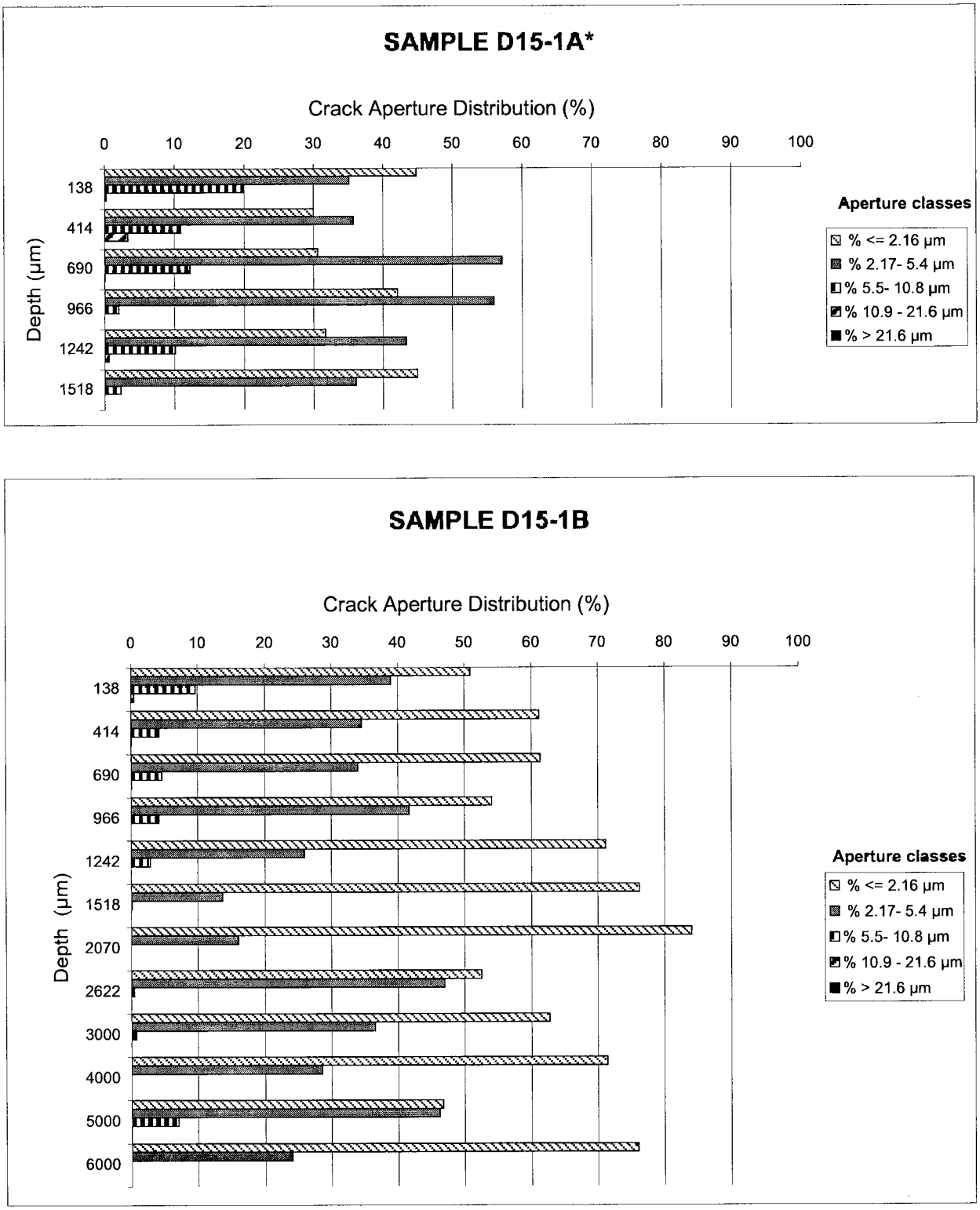

***Figure 52**. Crack aperture distribution using Image Analysis. D15-1A (top) and D15-1B (bottom). Each bar represents the percentage of crack aperture inside each of the five defined classes, obtained for all the images at the same depth.*

2.1.5 Crack Volume percentage using Image Analysis

This is a non-standard parameter, but in same aspects is related to porosity; the results can not be considered highly confident due to the small sampling. Nevertheless it shows, again, that the disturbed zone is, in general, restricted to the outer 1,5-2 mm.

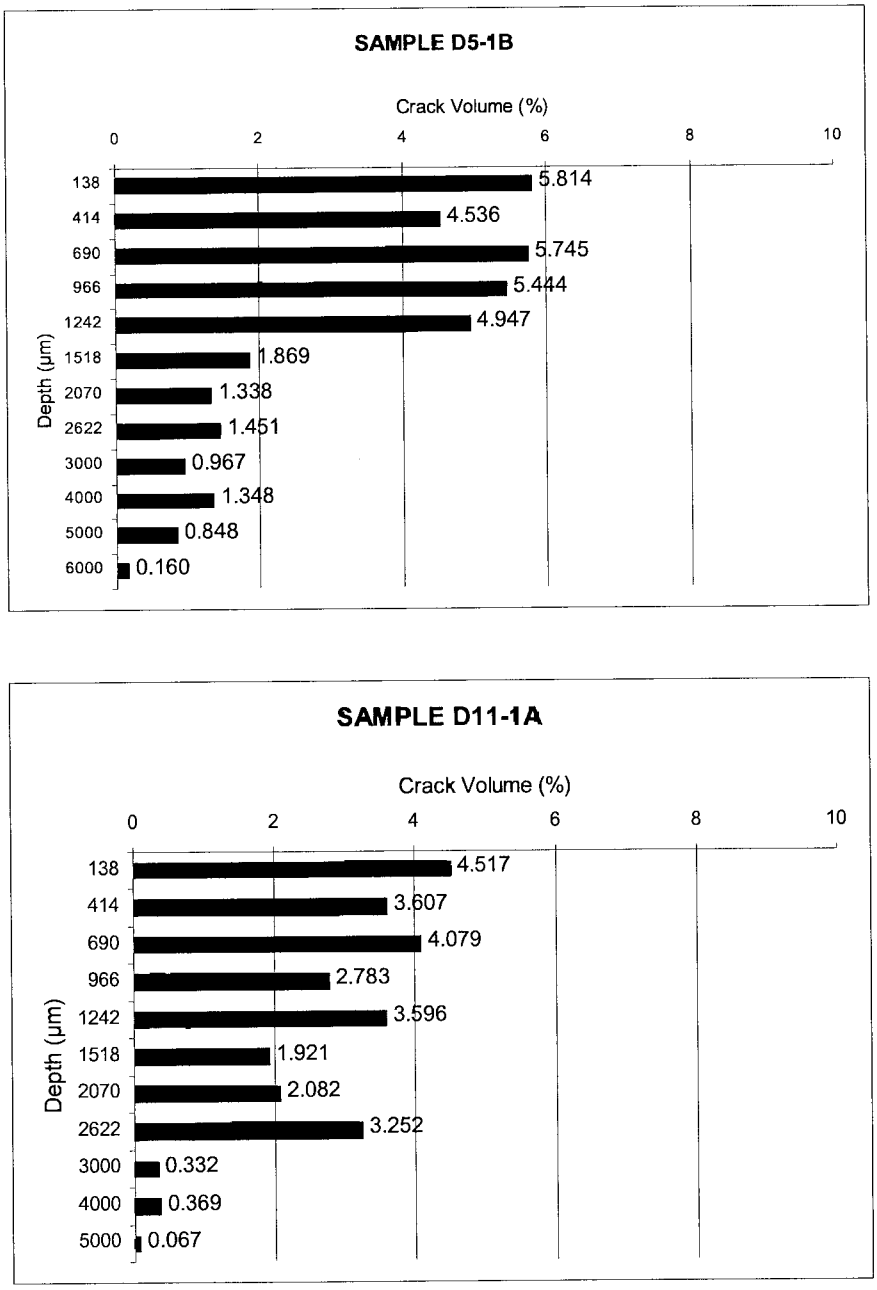

Figure 53. *Percentage of crack volume per image using Image Analysis. D5-1B (top) and D11-1A (bottom). Each bar represents the mean percentage obtained for all the images at the same depth.*

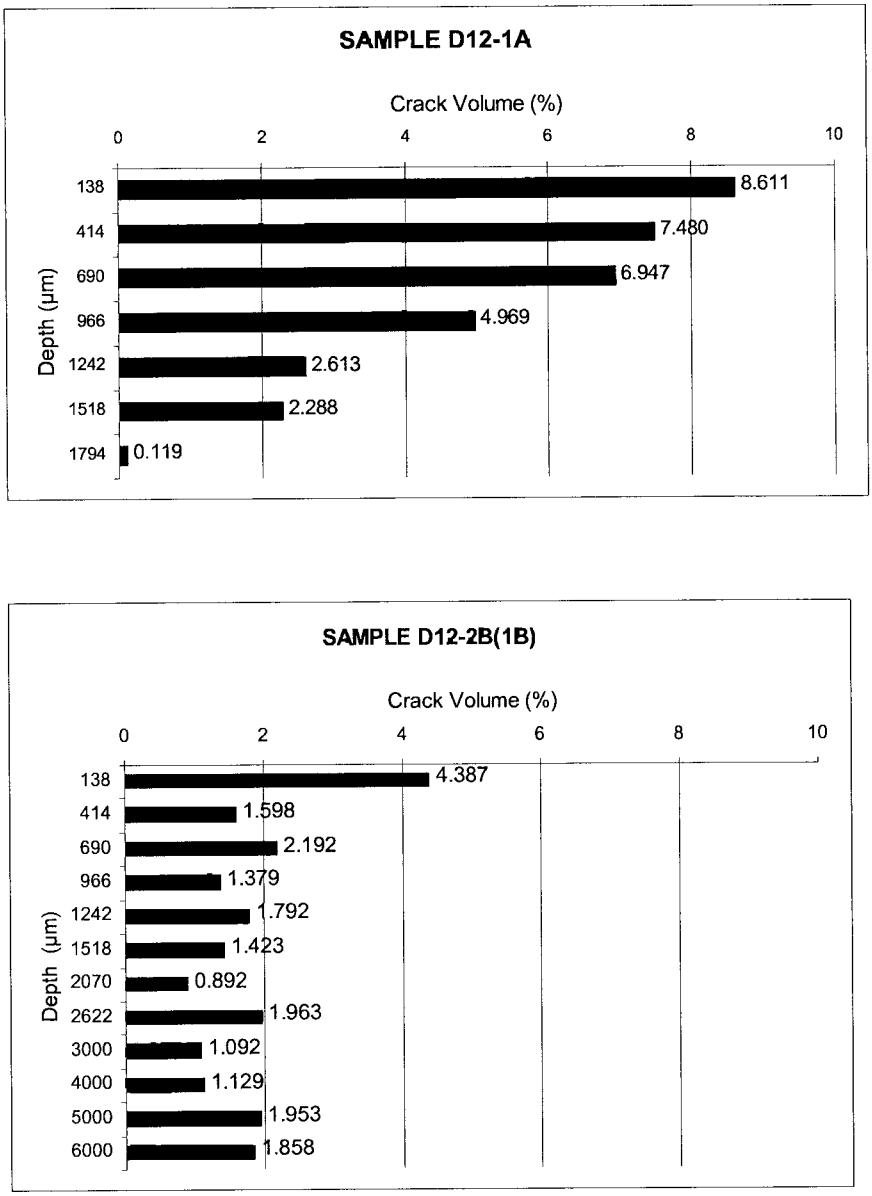

Figure 54. *Percentage of crack volume per image using Image Analysis. D12-1A (top) and D12-2B(1B) (bottom). Each bar represents the mean percentage obtained for all the images at the same depth.*

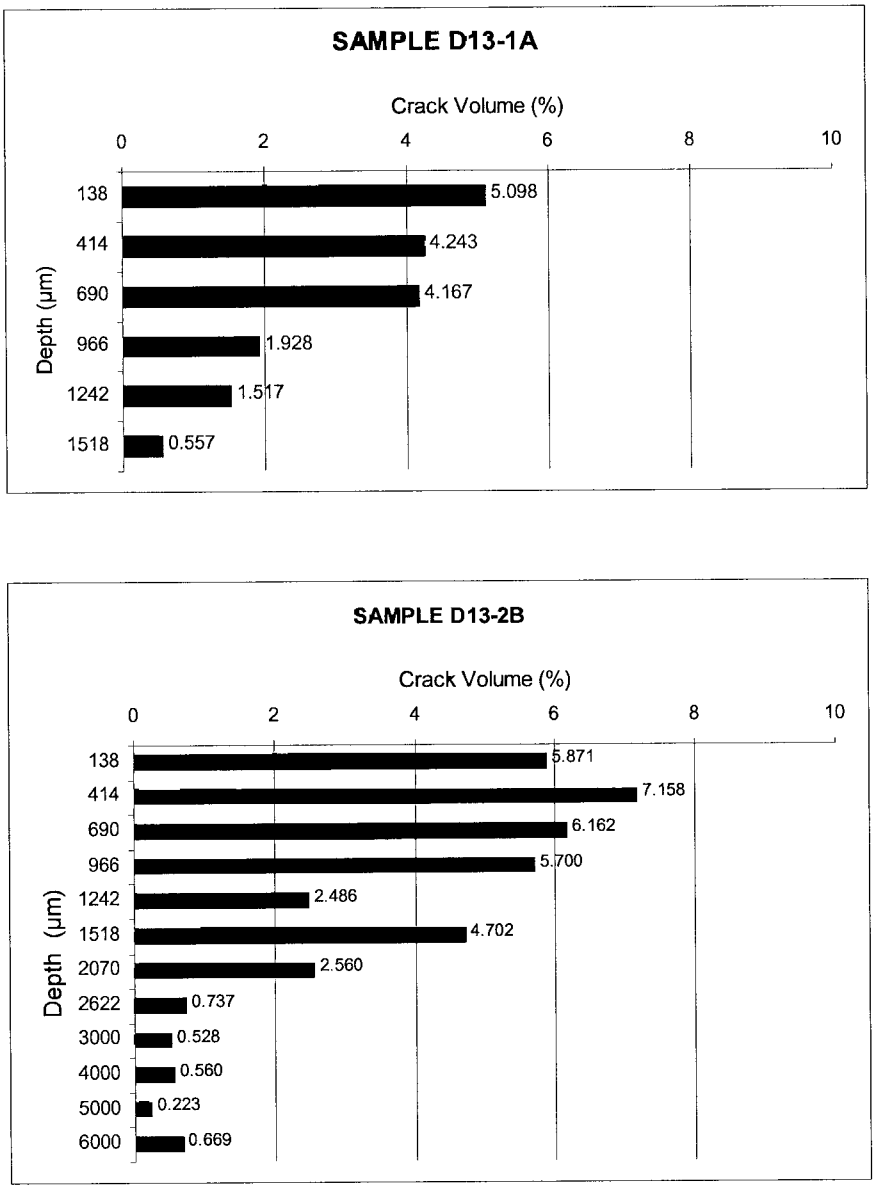

***Figure 55**. Percentage of crack volume per image using Image Analysis. D13-1A (top) and D13-2B (bottom). Each bar represents the mean percentage obtained for all the images at the same depth.*

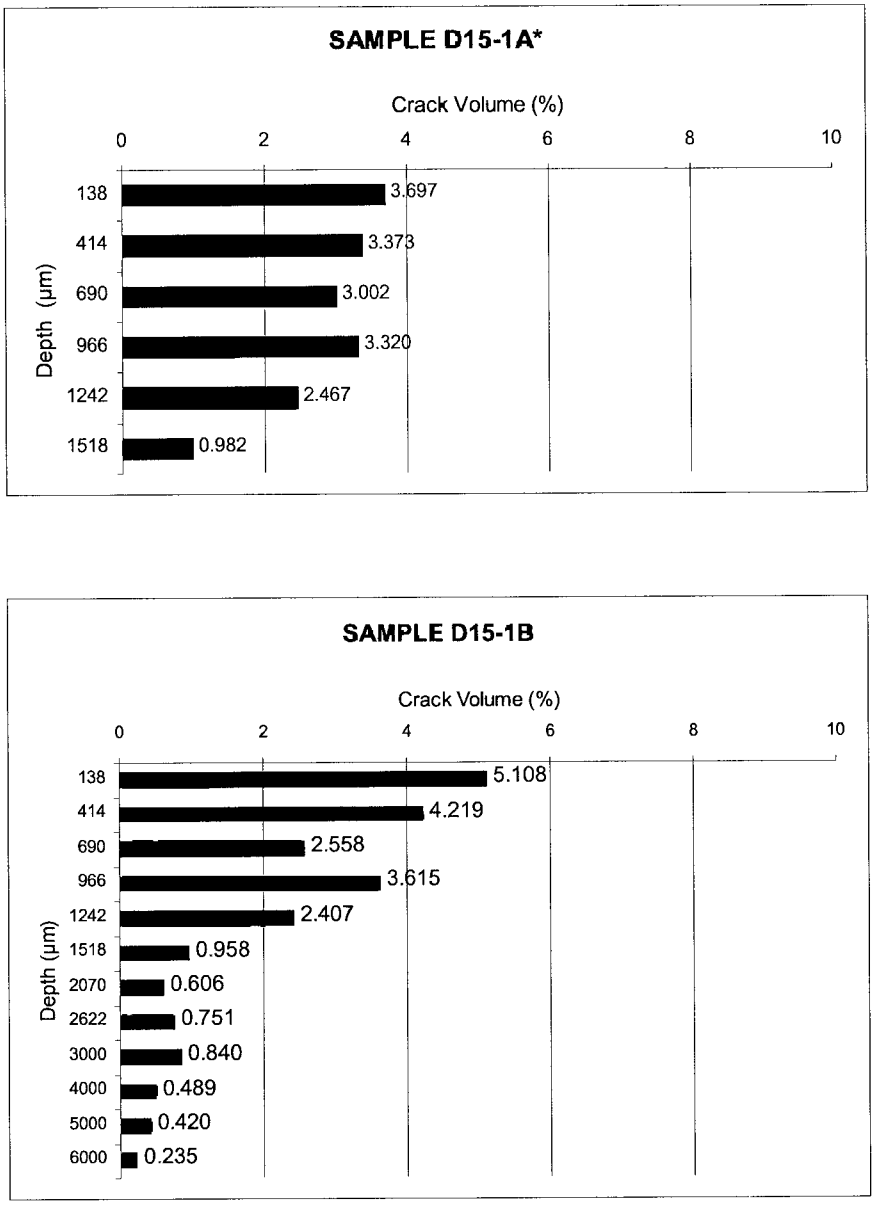

***Figure 56**. Percentage of crack volume per image using Image Analysis. D15-1A* (top) and D15-1B (bottom). Each bar represents the mean percentage obtained for all the images at the same depth.*

REFERENCES

Baddeley, A.J., Gundersen, H.J.G. & Cruz-Orive, L.M. (1986). Estimation of surface area from vertical sections. J. Microsc. 142, 259-276.

Martinez-Nistal, A. "Discriminación, cuantificación y cartografiado de componentes petrográficos mediante proceso digital de multi-imágenes microscópicas". Tesis Doctoral. Universidad de Oviedo (España), Dpto de Geología (1993).

Menéndez, B. "Cuantificación de componentes petrográficos mediante técnicas de microscopía y estereología". Tesis Doctoral. Universidad de Oviedo (España), Dpto de Geología (1992).

Montoto M., Montoto L., Roshoff K. and Leijon B. "Microfractographic study of heated and non-heated Stripa granite". Subsurface Space: Rockstore '80. 3, pp. 1357-1368. Pergamon Press. (1980).

Cruz Orive, L (1987). Avances recientes en estereología y su aplicación en Biología celular. Universidad de Berna , Instituto de Anatomía : Internal Report, nº215/LC 29.

APPENDIX 1

Crack specific surface by stereology. Tables 1-7.

***Table 1**: Crack Specific Surface data using Stereology applied to SEM images. Specimen D5-2b.*

Row	Depth(µm)	Depth(mm)	Intergr	Intra-Felsic.	Intra-Mafic.	Pore	Global
1	**310**	0,31	0,003	0,035	0,002	0,000	**0,040**
2	**620**	0,62	0,004	0,017	0,013	0,001	**0,034**
3	**930**	0,93	0,004	0,020	0,003	0,000	**0,026**
4	**1240**	1,24	0,004	0,015	0,011	0,001	**0,029**
5	**1550**	1,55	0,000	0,026	0,005	0,000	**0,031**
6	**1860**	1,86	0,002	0,014	0,000	0,001	**0,017**
7	**2170**	2,17	0,002	0,012	0,003	0,000	**0,017**
8	**2480**	2,48	0,002	0,009	0,009	0,000	**0,019**
9	**2790**	2,79	0,004	0,004	0,012	0,000	**0,019**
10	**3100**	3,1	0,002	0,001	0,013	0,000	**0,016**
11	**3410**	3,41	0,004	0,007	0,017	0,000	**0,029**
12	**3720**	3,72	0,004	0,004	0,015	0,001	**0,023**
13	**4030**	4,03	0,000	0,006	0,010	0,000	**0,016**
14	**4340**	4,34	0,001	0,004	0,012	0,001	**0,019**
15	**4650**	4,65	0,003	0,004	0,009	0,001	**0,017**
16	**4960**	4,96	0,000	0,001	0,006	0,000	**0,006**
17	**5270**	5,27	0,000	0,005	0,009	0,000	**0,014**
18	**5660**	5,66	0,000	0,004	0,000	0,000	**0,004**
19	**6280**	6,28	0,002	0,003	0,003	0,001	**0,008**
20	**6900**	6,9	0,001	0,002	0,001	0,000	**0,004**
21	**7520**	7,52	0,000	0,004	0,001	0,000	**0,005**
22	**8140**	8,14	0,001	0,003	0,000	0,000	**0,004**
23	**8760**	8,76	0,002	0,001	0,008	0,000	**0,011**
24	**9380**	9,38	0,000	0,003	0,001	0,000	**0,003**
25	**10000**	10	0,000	0,001	0,004	0,000	**0,005**
26	**10620**	10,62	0,000	0,003	0,001	0,000	**0,004**
27	**11240**	11,24	0,000	0,004	0,000	0,000	**0,004**

***Table 2**: Crack Specific Surface data using Stereology applied to SEM images. Specimen D11-1a.*

Row	Depth(µm)	Depth(mm)	Intergr	Intra-Felsic.	Intra-Mafic.	Pore	Global
1	**310**	0,31	0,000	0,031	0,000	0,001	**0,033**
2	**620**	0,62	0,000	0,031	0,000	0,000	**0,032**
3	**930**	0,93	0,000	0,013	0,005	0,000	**0,018**
4	**1240**	1,24	0,000	0,016	0,000	0,000	**0,016**
5	**1550**	1,55	0,000	0,011	0,000	0,000	**0,011**
6	**1860**	1,86	0,000	0,015	0,000	0,000	**0,015**
7	**2170**	2,17	0,000	0,020	0,000	0,000	**0,020**
8	**2480**	2,48	0,000	0,020	0,000	0,001	**0,021**
9	**2790**	2,79	0,004	0,010	0,000	0,002	**0,015**
10	**3100**	3,1	0,001	0,008	0,000	0,000	**0,008**
11	**3410**	3,41	0,000	0,008	0,000	0,001	**0,009**
12	**3720**	3,72	0,000	0,004	0,000	0,001	**0,005**
13	**4030**	4,03	0,000	0,005	0,000	0,003	**0,007**
14	**4340**	4,34	0,000	0,004	0,000	0,000	**0,004**
15	**4650**	4,65	0,000	0,002	0,001	0,001	**0,005**
16	**4960**	4,96	0,000	0,005	0,007	0,001	**0,013**
17	**5647**	5,65	0,000	0,002	0,000	0,001	**0,003**
18	**6267**	6,27	0,001	0,004	0,000	0,000	**0,006**
19	**6887**	6,89	0,000	0,005	0,000	0,000	**0,005**
20	**7507**	7,51	0,000	0,006	0,000	0,002	**0,007**
21	**8127**	8,13	0,000	0,003	0,000	0,001	**0,005**
22	**8747**	8,75	0,000	0,013	0,000	0,001	**0,014**
23	**9367**	9,37	0,000	0,003	0,000	0,001	**0,004**
24	**9987**	9,99	0,000	0,003	0,000	0,000	**0,003**
25	**10607**	10,61	0,000	0,003	0,000	0,000	**0,003**
26	**11227**	11,23	0,000	0,004	0,000	0,000	**0,004**

***Table 3**: Crack Specific Surface data using Stereology applied to SEM images. Specimen D12-2a.*

Row	Depth(µm)	Depth(mm)	Intergr	Intra-Felsic.	Intra-Mafic.	Pore	Global
1	**310**	0,31	0,000	0,057	0,001	0,000	**0,058**
2	**620**	0,62	0,000	0,050	0,000	0,000	**0,050**
3	**930**	0,93	0,000	0,021	0,008	0,000	**0,030**
4	**1240**	1,24	0,002	0,020	0,001	0,000	**0,023**
5	**1550**	1,55	0,000	0,024	0,003	0,000	**0,027**
6	**1860**	1,86	0,001	0,007	0,008	0,000	**0,016**
7	**2170**	2,17	0,000	0,022	0,003	0,000	**0,025**
8	**2480**	2,48	0,000	0,016	0,001	0,000	**0,017**
9	**2790**	2,79	0,001	0,016	0,000	0,000	**0,017**
10	**3100**	3,1	0,000	0,015	0,000	0,000	**0,015**
11	**3410**	3,41	0,000	0,011	0,002	0,000	**0,013**
12	**3720**	3,72	0,000	0,007	0,000	0,000	**0,007**
13	**4030**	4,03	0,000	0,007	0,000	0,000	**0,007**
14	**4340**	4,34	0,000	0,009	0,000	0,000	**0,009**
15	**4650**	4,65	0,000	0,012	0,000	0,000	**0,012**
16	**4960**	4,96	0,000	0,007	0,000	0,000	**0,007**
17	**5310**	5,31	0,000	0,001	0,000	0,000	**0,001**
18	**5930**	5,93	0,000	0,009	0,000	0,000	**0,009**
19	**6550**	6,55	0,000	0,004	0,000	0,000	**0,004**
20	**7170**	7,17	0,000	0,007	0,000	0,000	**0,007**
21	**7790**	7,79	0,002	0,007	0,001	0,000	**0,010**
22	**8410**	8,41	0,000	0,009	0,000	0,001	**0,009**
23	**9030**	9,03	0,000	0,001	0,001	0,000	**0,001**
24	**9650**	9,65	0,003	0,000	0,002	0,000	**0,005**
25	**10270**	10,27	0,002	0,002	0,005	0,000	**0,009**
26	**10890**	10,89	0,000	0,005	0,000	0,001	**0,005**
27	**11510**	11,51	0,002	0,001	0,000	0,000	**0,003**

***Table 4**: Crack Specific Surface data using Stereology applied to SEM images. Specimen D13-1a.*

Row	Depth(μm)	Depth(mm)	Intergr	Intra-Felsic.	Intra-Mafic.	Pore	Global
1	**310**	0,31	0,000	0,052	0,001	0,000	**0,054**
2	**620**	0,62	0,000	0,032	0,000	0,000	**0,033**
3	**930**	0,93	0,000	0,015	0,008	0,001	**0,024**
4	**1240**	1,24	0,000	0,009	0,006	0,001	**0,016**
5	**1550**	1,55	0,000	0,018	0,000	0,000	**0,018**
6	**1860**	1,86	0,000	0,014	0,000	0,000	**0,014**
7	**2170**	2,17	0,000	0,013	0,000	0,000	**0,013**
8	**2480**	2,48	0,000	0,012	0,000	0,001	**0,013**
9	**2790**	2,79	0,000	0,005	0,000	0,002	**0,006**
10	**3100**	3,1	0,000	0,010	0,000	0,001	**0,011**
11	**3410**	3,41	0,000	0,006	0,000	0,001	**0,007**
12	**3720**	3,72	0,000	0,009	0,000	0,002	**0,011**
13	**4030**	4,03	0,000	0,010	0,000	0,000	**0,010**
14	**4340**	4,34	0,000	0,006	0,001	0,000	**0,006**
15	**4650**	4,65	0,000	0,008	0,000	0,001	**0,009**
16	**4960**	4,96	0,000	0,013	0,000	0,000	**0,013**
17	**5672**	**5,67**	0,004	0,005	0,000	0,000	**0,009**
18	**6292**	**6,29**	0,001	0,003	0,001	0,000	**0,004**
19	**6912**	**6,91**	0,002	0,010	0,000	0,000	**0,012**
20	**7532**	**7,53**	0,000	0,009	0,000	0,000	**0,009**
21	**8152**	**8,15**	0,005	0,007	0,000	0,000	**0,012**
22	**8772**	**8,77**	0,000	0,005	0,000	0,000	**0,005**
23	**9392**	**9,39**	0,000	0,004	0,000	0,000	**0,004**
24	**10012**	**10,01**	0,002	0,001	0,001	0,000	**0,003**
25	**10632**	**10,63**	0,000	0,003	0,000	0,000	**0,003**
26	**11252**	**11,25**	0,000	0,008	0,000	0,000	**0,009**

***Table 5**: Crack Specific Surface data using Stereology applied to SEM images. Specimen D12-2b(1b).*

Row	Depth(µm)	Depth(mm)	Intergr	Intra-Felsic.	Intra-Mafic.	Pore	Global
1	**310**	**0,31**	0,002	0,025	0,006	0,000	**0,034**
2	**620**	**0,62**	0,003	0,015	0,003	0,000	**0,021**
3	**930**	**0,93**	0,000	0,015	0,001	0,001	**0,017**
4	**1240**	**1,24**	0,002	0,013	0,000	0,000	**0,015**
5	**1550**	**1,55**	0,001	0,017	0,003	0,000	**0,021**
6	**1860**	**1,86**	0,001	0,017	0,003	0,000	**0,021**
7	**2170**	**2,17**	0,000	0,011	0,000	0,001	**0,012**
8	**2480**	**2,48**	0,001	0,015	0,001	0,000	**0,017**
9	**2790**	**2,79**	0,001	0,014	0,003	0,000	**0,018**
10	**3100**	**3,10**	0,000	0,024	0,000	0,001	**0,024**
11	**3410**	**3,41**	0,001	0,017	0,000	0,001	**0,018**
12	**3720**	**3,72**	0,001	0,009	0,004	0,001	**0,016**
13	**4030**	**4,03**	0,001	0,009	0,004	0,001	**0,016**
14	**4340**	**4,34**	0,000	0,010	0,003	0,000	**0,013**
15	**4650**	**4,65**	0,000	0,007	0,003	0,000	**0,010**
16	**4960**	**4,96**	0,001	0,009	0,002	0,001	**0,013**
17	**5270**	**5,27**	0,001	0,006	0,001	0,000	**0,008**
18	**5580**	**5,58**	0,001	0,004	0,003	0,000	**0,008**

***Table 6**: Crack Specific Surface data using Stereology applied to SEM images. Specimen D12-1b(1b).*

Row	Depth(µm)	Depth(mm)	Intergr	Intra-Felsic.	Intra-Mafic.	Pore	Global
1	**310**	**0,31**	0,003	0,048	0,042	0,000	**0,094**
2	**620**	**0,62**	0,011	0,038	0,006	0,002	**0,057**
3	**930**	**0,93**	0,002	0,036	0,003	0,003	**0,044**
4	**1240**	**1,24**	0,001	0,028	0,003	0,001	**0,034**
5	**1550**	**1,55**	0,004	0,014	0,016	0,002	**0,035**
6	**1860**	**1,86**	0,002	0,015	0,017	0,000	**0,035**
7	**2170**	**2,17**	0,003	0,011	0,009	0,001	**0,024**
8	**2480**	**2,48**	0,004	0,010	0,013	0,001	**0,028**
9	**2790**	**2,79**	0,002	0,013	0,009	0,000	**0,024**
10	**3100**	**3,10**	0,002	0,017	0,002	0,001	**0,022**
11	**3410**	**3,41**	0,002	0,008	0,001	0,000	**0,012**
12	**3720**	**3,72**	0,001	0,008	0,003	0,000	**0,013**
13	**4030**	**4,03**	0,001	0,007	0,004	0,001	**0,014**
14	**4340**	**4,34**	0,002	0,006	0,007	0,000	**0,015**

***Table** 7: Crack Specific Surface data using Stereology applied to SEM images. Specimen D15-1b(r).*

Row	Depth(µm)	Depth(mm)	Intergr	Intra-Felsic.	Intra-Mafic.	Pore	Global
1	**310**	**0,31**	0,006	0,015	0,027	0,000	**0,047**
2	**620**	**0,62**	0,003	0,022	0,012	0,000	**0,037**
3	**930**	**0,93**	0,001	0,006	0,012	0,000	**0,020**
4	**1240**	**1,24**	0,002	0,004	0,005	0,000	**0,011**
5	**1550**	**1,55**	0,003	0,004	0,013	0,000	**0,020**
6	**1860**	**1,86**	0,001	0,005	0,010	0,001	**0,017**
7	**2170**	**2,17**	0,001	0,003	0,015	0,000	**0,019**
8	**2480**	**2,48**	0,000	0,003	0,016	0,000	**0,019**
9	**2790**	**2,79**	0,000	0,002	0,005	0,002	**0,008**
10	**3100**	**3,1**	0,000	0,002	0,002	0,000	**0,004**
11	**3410**	**3,41**	0,000	0,004	0,000	0,001	**0,004**
12	**3720**	**3,72**	0,001	0,002	0,006	0,001	**0,009**
13	**4030**	**4,03**	0,001	0,006	0,009	0,001	**0,017**
14	**4340**	**4,34**	0,002	0,002	0,009	0,001	**0,014**
15	**4650**	**4,65**	0,002	0,004	0,002	0,000	**0,007**
16	**4960**	**4,96**	0,001	0,002	0,004	0,001	**0,007**
17	**5270**	**5,27**	0,001	0,003	0,004	0,001	**0,008**
18	**5890**	**5,89**	0,000	0,001	0,002	0,001	**0,004**
19	**6510**	**6,51**	0,001	0,001	0,006	0,000	**0,008**
20	**7130**	**7,13**	0,002	0,002	0,001	0,000	**0,006**
21	**7750**	**7,75**	0,001	0,002	0,004	0,000	**0,007**
22	**8370**	**8,37**	0,002	0,003	0,008	0,000	**0,013**
23	**8990**	**8,99**	0,000	0,002	0,008	0,000	**0,009**
24	**9610**	**9,61**	0,000	0,001	0,001	0,001	**0,003**
25	**10230**	**10,23**	0,002	0,001	0,001	0,000	**0,004**
26	**10850**	**10,85**	0,002	0,003	0,002	0,000	**0,006**
27	**11470**	**11,47**	0,001	0,002	0,003	0,000	**0,006**
28	**12090**	**12,09**	0,001	0,001	0,011	0,001	**0,014**
29	**12710**	**12,71**	0,000	0,001	0,004	0,000	**0,005**